



UNIVERSITY COLLEGE LONDON

UCL Research Department of Structural and Molecular Biology

Sequence and structural analysis of
antibodies

Abhinandan K. Raghavan

A dissertation submitted to University College London for the
degree of Doctor of Philosophy

Declaration

I, Abhinandan K. Raghavan, confirm that the work presented in this thesis is my own. Where information has been derived from other sources, I confirm that this has been indicated in the thesis.

A handwritten signature in black ink, reading "Abhinandan K. Raghavan". The signature is written in a cursive style with a horizontal line under the name.

Abhinandan K. Raghavan

April 5, 2009

Abstract

The work presented in this thesis focusses on the sequence and structural analysis of antibodies and has fallen into three main areas.

First I developed a method to assess how typical an antibody sequence is of the expressed human antibody repertoire. My hypothesis was that the more “human-like” an antibody sequence is (in other words how typical it is of the expressed human repertoire), the less likely it is to elicit an immune response when used in vivo in humans. In practice, I found that, while the most and least-human sequences generated the lowest and highest anti-antibody responses in the small available dataset, there was little correlation in between these extremes.

Second, I examined the distribution of the packing angles between V_H and V_L domains of antibodies and whether residues in the interface influence the packing angle. This is an important factor which has essentially been ignored in modelling antibody structures since the packing angle can have a significant effect on the topography of the combining site. Finding out which interface residues have the greatest influence is also important in protocols for ‘humanizing’ mouse

antibodies to make them more suitable for use in therapy in humans.

Third, I developed a method to apply standard Kabat or Chothia numbering schemes to an antibody sequence automatically. In brief, the method uses profiles to identify the ends of the framework regions and then fills in the numbers for each section. Benchmarking the performance of this algorithm against annotations in the Kabat database highlighted several errors in the manual annotations in the Kabat database. Based on structural analysis of insertions and deletions in the framework regions of antibodies, I have extended the Chothia numbering scheme to identify the structurally correct positions of insertions and deletions in the framework regions.

Abbreviations

The following abbreviations have been used in this thesis:

Amino acids

One-letter code	Three-letter code	Amino-acid
A	Ala	Alanine
C	Cys	Cysteine
D	Asp	Aspartic acid
E	Glu	Glutamic acid
F	Phe	Phenylalanine
G	Gly	Glycine
H	His	Histidine
I	Ile	Isoleucine
K	Lys	Lysine
L	Leu	Leucine
M	Met	Methionine
N	Asn	Asparagine
P	Pro	Proline
Q	Gln	Glutamine
R	Arg	Arginine
S	Ser	Serine
T	Thr	Threonine
V	Val	Valine
W	Trp	Tryptophan
Y	Tyr	Tyrosine

Miscellaneous

ANN	Artificial Neural Network
BLAST	Basic Local Alignment and Search Tool
GA	Genetic Algorithm
NH	Number of hidden nodes in neural network
NN	Neural Network
PDB	Protein Data Bank
Rprop	Resilience propogation
SNNS	Stuggart Neural Network Simulator
SRS	Sequence Retrieval Service
SSE	Sum of Square Error
SSEARCH	Sequence Search
SVM	Support Vector Machine

Acknowledgements

At the outset, I would like to thank my supervisor, Dr. Andrew Martin, for the support and patience through what has been a very exciting PhD. I couldn't thank him enough for all the help that he has extended to me.

I'd like to thank members of the group, Anja, Craig, Jacob, Lisa, and Sri for being so nice and helpful throughout and for making the lab such a wonderful place to work in. I would also like to thank my mentor, Prof. Christine Orengo, for her encouragement and help, and the BBSRC and GlaxoSmithKline for funding my PhD. I am very grateful to Tom, Jesse, and Jahid for excellent maintenance of the computers and clusters in the department. I have used the research computing resources at UCL extensively over the last couple of years and the help of all staff who maintain these resources is gratefully acknowledged.

This PhD would never have been possible without the support of my family, particularly my wife Kalyani. I'd like to thank her for being a wonderful partner, teacher, and a pillar of support during exacting phases of my PhD. I would also like to thank my parents, sister, and my wife's family for being extremely supportive

during the last 4 years.

I've made innumerable friends in UCL and in London, each of whom has been very special. Making it this far is unimaginable without them. I'd like to thank them all - Lisa, Andrew, Jacob, Anja, Sri, Craig, Sunita, Roger, Juan, Ali, Sarah, Tom, Jesse, Duncan, Jahid, Kanchan, Ranga, Padu, Natesh, Mark, Sanjay, Anwar, Gillian, Tjelvar, Michael, Antonio, Stefano, Tom, Paul, Dhami, Venu, Pape, Harkamal, Meena, and the CATH team. In particular, I'd like to thank Sunita and Roger for their technical inputs while I was writing grant proposals, Lisa for her limitless patience in answering all my queries and her help, Michael Wright for help with all the paperwork during my trips outside of the UK, Padu for being a wonderful host when I needed a change from my cooking, and my cousin Ranga and his wife Jyothi who made all holidays delightful. I'd also like to thank staff at the numerous restaurants and eateries in London that made my life as a PhD student a lot easier than I could imagine.

Dedication

This work is dedicated to my family, my home India, a country of extraordinary uniqueness, and to London, my second home.

Contents

Declaration	2
Abstract	3
Abbreviations	5
Acknowledgements	7
1 Introduction to immunology	26
1.1 Innate immune system	27
1.2 The Adaptive Immune system	29
1.2.1 B-Lymphocytes	30

1.2.2	T-Lymphocytes	31
1.2.3	MHC molecules	31
1.3	Activation of the adaptive immune system	32
1.3.1	Structure of an antibody	34
1.3.2	Generation of antibody diversity	35
1.3.3	VDJ Recombination	37
1.3.4	B-cell maturation, activation and proliferation	40
1.3.5	B-cell activation	45
1.3.6	B-cell effector-response	48
1.4	T-cell responses and cell-mediated immune system	49
1.4.1	T-cell receptor	49
1.4.2	T-cell maturation	49
1.4.3	T-cell activation	51
1.4.4	T-cell differentiation	52

1.5	Importance of the immune system	53
2	Introduction to computational methods in bioinformatics	55
2.1	An introduction to genetic algorithms	55
2.1.1	Elements of a genetic algorithm	56
2.1.2	GA Operators	57
2.1.3	Encoding a problem	58
2.1.4	Selection methods	59
2.1.5	Replacement strategies	64
2.2	Introduction to artificial neural networks	66
2.2.1	Machine learning approaches	66
2.2.2	Artificial neural networks	67
2.2.3	The process of learning: Learning algorithms	72
2.3	Introduction to protein sequence analysis	76

2.3.1	Pairwise sequence alignment	78
2.3.2	Searches against a database of proteins	81
2.3.3	Profile-based search methods	86
3	Assessing humanness of antibody sequences	88
3.1	Preparation of the dataset	91
3.2	Comparing pairwise identities of human and mouse sequences	91
3.3	A statistic to assess ‘humanness’ of antibody sequences	96
3.3.1	Analysis of pairwise sequence identities	96
3.3.2	Analysis of mean sequence identities	99
3.3.3	Z-Score analysis	101
3.3.4	Assessment of humanized antibodies	105
3.3.5	Analysis of humanness of human immunoglobulin germline genes	106
3.3.6	Correlating immunogenicity with humanness	113

3.4	Assessing humanness of antibody CDRs	118
3.5	Discussions and conclusions	122
4	An automatic method for applying numbering to antibodies: Analysis and applications	128
4.1	An alignment-based method to number antibody sequences	132
4.1.1	An existing tool for numbering	132
4.1.2	Preparation of the test dataset	133
4.1.3	Principle of the algorithm	133
4.1.4	Deriving consensus sequences	136
4.1.5	Identifying chain type using Z-scores	139
4.1.6	How the numbering algorithm works	143
4.1.7	Adjustments to alignments in the L3-LFR4 regions	143
4.1.8	Discussion	149
4.2	A profile-based numbering method	149

4.2.1	Preparation of the dataset	150
4.2.2	Creation of profile sets	150
4.2.3	The numbering algorithm	153
4.2.4	Benchmarking the numbering algorithm	160
4.3	Analysis of errors in the Kabat database	163
4.4	Structural analysis: An alternate structure-based numbering scheme to accommodate indels in the framework regions	172
4.5	Conclusions	174
5	Predicting the V_H/V_L interface angle from interface residues	180
5.1	Preparation of the dataset	182
5.2	Calculation of the packing angle	184
5.3	Identifying interface residues	189
5.4	Predicting packing angle from interface residues	194
5.5	Using a genetic algorithm to sample the interface-residue space . . .	201

5.6	Methods of selection	204
5.7	Problems: Redundancy in individual population and intelligent selection	207
5.8	Scoring the quality of each individual	212
5.9	Results of GA runs	215
5.9.1	Prediction the V_H/V_L packing angle	215
5.9.2	Choosing key framework interface residues	219
5.9.3	Jackknifing and analysis of errors of the best individuals . . .	221
5.10	Discussions and conclusion	225
6	Conclusions	228
6.1	Assessing humanness of antibodies	228
6.2	Analysis of antibody numbering	230
6.3	Analysis of packing angle at the V_H/V_L interface	232
	Bibliography	234

List of Figures

1.1	Activation of the adaptive immune system	33
1.2	Structure of an Immunoglobulin (IgG1) consisting of 12 domains . .	36
1.3	VDJ recombination to produce light chains	38
1.4	VDJ recombination to produce heavy chains	39
1.5	Antigen-independent phase of B-cell maturation	43
1.6	Antigen-dependent phase of B-cell maturation	44
2.1	Schematic representation of a neurode	68
2.2	Plot of induced local field (V_k) vs. the adder function (U_k)	71
2.3	Three-layered architecture of a neural network	73

2.4	Steps involved in FASTA	82
2.5	Extreme-value distribution of amino acid sequences	85
3.1	Algorithm to compute the mean and standard deviation for every antibody sequence in the dataset	93
3.2	Plots of standard deviation vs. the mean percentage identity for mouse and human sequences	95
3.3	Frequency distribution plots human/human and mouse/human pairwise sequence identities in light and heavy chains	97
3.4	Histogram of human/human and mouse/human pairwise sequence identities in lambda and kappa class light chains	98
3.5	Z-score distribution for light and heavy chain sequences	103
3.6	Z-score distribution in the light chain lambda and kappa classes . .	104
3.7	Z-score plots for the human germline genes	108
3.8	Plot of AAR percentages vs. humanness scores for therapeutic antibodies	116

3.9	Variation of AAR percentages against mean, minimum and maximum humanness scores of therapeutic antibodies	117
3.10	Z-score distributions of the lambda class light chain CDRs	119
3.11	Z-score distributions of the kappa class light chain CDRs	120
3.12	Z-score distributions of the heavy chain CDRs	121
3.13	Z-score distribution for the concatenated CDRs	123
4.1	Introduction to numbering	129
4.2	Sequence-alignment-based algorithm for numbering	134
4.3	Original light and heavy chain consensus sequences	135
4.4	Schematic representation of the antibody variable region	137
4.5	Alternate light and heavy chain consensus sequences	138
4.6	Identifying chain-type from Z-scores	142
4.7	Algorithm for alignment-based numbering method	144
4.8	Error in alignment in HFR3–H3–HFR4 region	148

4.9	Isolating the sequence of every region from the best profile assignments	156
4.10	Detection of errors in alignments	157
4.11	Normal numbering	158
4.12	Reverse numbering	159
4.13	Straight numbering	159
4.14	The numbering algorithm	161
4.15	Benchmarking the numbering algorithm	164
4.16	Kabat annotation error in LFR1	167
4.17	Kabat annotation error in CDR-L1	168
4.18	Errors in the Kabat annotation in the regions L1–LFR3	169
4.19	Error in the Kabat annotation in L3–LFR4	170
4.20	Kabat annotation error in H2–HFR3	171
4.21	Rigid body superposition in the light chain framework regions . . .	176
4.22	Rigid body superposition in the heavy chain framework regions . .	177

4.23	Kabat error in HFR3	177
4.24	Alignment showing insert at H72	178
4.25	Spacefilled representation of HFR3	179
5.1	Algorithm to calculate packing angle	185
5.2	Rigid-body superposition of the $C\alpha$ atoms in the light chain variable region	186
5.3	Rigid-body superposition of the $C\alpha$ atoms in the heavy chain variable region	187
5.4	The beta strands at the V_H/V_L interface, best-fit lines, and packing angle	188
5.5	Algorithm to calculate best-fit lines for the light and heavy chain variable regions	190
5.6	Frequency distribution of the packing angle	191
5.7	Extreme packing angles	192
5.8	Frequency distribution of interface residues	193

5.9	Architecture of a fully-connected neural network	198
5.10	Demonstration of an individual in a population	202
5.11	Crossover of two high-scoring individuals A and B	203
5.12	Redundancy of individuals in a GA run	208
5.13	Comparing redundancy in Rank and Intelligent selection	211
5.14	Plot comparing the predicted packing angle vs. the actual packing angle	212
5.15	Performance of the genetic algorithm involving all interface positions	217
5.16	Performance of the GA involving only non-CDR interface positions	220
5.17	Results of jackknifing the best individual from the GA runs	222
5.18	Frequency distribution of the errors in predicting packing angle	223
5.19	Plot of errors in packing angle prediction against the actual packing angle	224

List of Tables

3.1	Number of sequences in the dataset of mouse and human sequences	91
3.2	Mean raw humanness scores	101
3.3	Humanness scores of humanized antibodies in published literature .	106
3.4	Humanness scores for the lambda class germline genes	107
3.5	Humanness scores for the lambda class germline genes	109
3.6	Humanness scores for the heavy chain germline genes	110
3.7	Number of V-region genes in Lambda and Kappa class light chain and heavy chain germline families	111
3.8	Correlations between humanness scores and Anti-antibody response (AAR) of antibodies approved for therapy	112

3.9	Sources of therapeutic antibody sequences	113
3.10	Correlation coefficient between AAR and humanness scores of therapeutic antibodies	115
4.1	Number of sequences in the dataset	133
4.2	Optimal parameters for light and heavy chain sequence alignment .	136
4.3	Numbers of sequences that gave insertions in the consensus alignment	137
4.4	Z-score thresholds for identifying chaintype	141
4.5	Number of complete/truncated light and heavy chain sequences in Kabat	150
4.6	Kabat positions used in the profile definitions	151
4.7	Numbers of sequences that could not be numbered using 3 profiles (Lambda/Kappa/Heavy)	151
4.8	Classification scheme and number of profile sets	152
4.9	Minimum and maximum observed lengths of the 7 regions in the light and heavy chain	154

4.10	Regions in the light and heavy chain and methods that are used to number them	160
4.11	Number of sequences numbered by AbNum that match the Kabat database annotations	163
4.12	Benchmarking the performance of AbNum: comparison with the Kabat database annotations. The percentages reported in the last two columns are estimated error percentages based on the sample set examined manually.	165
4.13	Region-wise distribution of errors in the Kabat database.	166
4.14	Table comparing the Kabat indels with the structurally corrected indels	173
5.1	Numbers representing the amino acid properties	197
5.2	Manual selected sets of interface positions	199
5.3	Results of a 5-fold evaluation over manually-chosen interface positions	200
5.4	Comparing Roulette-wheel and Rank-based selection methods. The table shows the best Pearson's r calculated over 40 generations of a GA run.	206

5.5	Standard parameters for the Neural network and the Genetic algorithm	215
5.6	Best individual involving a GA run with all interface positions . . .	218
5.7	Best individual involving a GA run with non-CDR interface positions	219

Chapter 1

Introduction to immunology

The human body contains a number of microenvironments that provide an ideal niche for the growth and proliferation of several pathogenic and non-pathogenic microorganisms. In order to prevent the entry and survival of pathogens, each of us is equipped with a complex immune system capable of efficiently combating invading microorganisms. The human immune system can be broadly divided into two- the innate immune system and the acquired or adaptive immune system. As the name suggests, innate immunity is the inherent immune system that the organism is born with. The adaptive immune system, on the other hand, is acquired during the lifetime of the organism. The innate adaptive system is well developed even in invertebrates, like the nematode *Caenorhabditis elegans* while the adaptive immune system is a unique feature of higher vertebrates starting from jawed fishes. Referred to as the immunological ‘Big Bang, the evolution of the adaptive immune system conferred many additional advantages to the organisms possessing

them.

1.1 Innate immune system

The innate or the non-adaptive immune system offers the first line of defense and provides a quick and immediate response to invading pathogens. This branch of immunity comprises of several players, which provide a physical barrier to pathogen entry, physiological barrier to their survival, and their elimination by phagocytosis or extracellular killing of these pathogens to eliminate them from circulation.

The skin is often the first barrier encountered by invading pathogens. In addition to being impermeable, the lactic acid and fatty acids in sweat and sebaceous secretions from the skin are maintain a low pH, which is inhibits the survival of most pathogens. Mucous secreting cells and cilia that propel mucous-entrapped pathogens out of the body guard the other openings of the body like the respiratory and urogenital tracts. In addition, many of the secretions of the body, including the tears and saliva contain bactericidal factors like lysozyme, a hydrolytic enzyme that is capable of destroying the bacterial cell wall.

If the microorganism manages to overcome these barriers and enter a tissue, it encounters resident tissue macrophages. These cells are derived from circulating monocytes that exit from circulation and settle down in various tissues. Macrophages are long-lived phagocytic cells that are usually the first cells of the

innate immune system to recognize invading pathogens. They do this using various cell-surface receptors including CD14, a receptor that recognizes bacterial lipopolysaccharide (LPS). Clustering of the receptors upon ligand binding induces phagocytosis of the pathogen into vesicles known as phagosomes inside the macrophage. These phagosomes then fuse with vesicles called lysosomes, which are highly acidic compartments harbouring enzymes that can destroy the internalized pathogen. However, the internalization of pathogens by macrophages results not only in their destruction by active phagocytosis, but also triggers the macrophage to secrete various toxic chemicals like hydrogen peroxide, nitric oxide and superoxide anion into the surrounding tissue. In addition, macrophages also secrete cytokines, which are low molecular weight proteins that regulate the function of immune cells. These cytokines attract another subset of phagocytes—the neutrophils. These are short-lived polymorphonuclear neutrophilic leukocytes that are found in circulation. Local cytokine release induces neutrophils to migrate to the site of injury in large numbers. Just like macrophages, neutrophils are also phagocytic cells that actively engulf the pathogens and participate in the elimination of invading microorganisms.

Cytokines also trigger a local inflammatory response, which serves to not only recruit more cells of the immune system, but also to restrict the area of infection. An inflammatory response is characterized by redness, pain, heat and swelling in the area of infection. The inflammatory mediators induce changes in the local environment i.e. they cause vasodilation of nearby blood vessels and increase the expression of adhesion molecules on the surface of endothelial cells. These steps facilitate the recruitment of circulating neutrophils for increased phagocytosis, monocytes that will mature into more tissue macrophages, as well as mast cells

and eosinophils.

In addition to these cell-mediated innate immune responses, tissue damage also activates several enzymatic systems in the plasma. One of the most important of these is the complement system. Although it was first discovered as a factor that augments the activity of humoral branch of acquired immunity, hence the name complement proteins, it is now clear that it is first activated as part of the innate immunity. The complement system comprises of a series of enzymatically catalyzed reactions whose end products bring about various effector functions. These include the opsonization of antigen to facilitate recognition by macrophages thereby increasing their phagocytosis, promoting the inflammatory response, and the formation of a membrane attack complex that lyses pathogens by forming pores on their surface. The complement system can be activated on microbial surfaces and also by antibodies, hence they participate in both the innate and adaptive immune system.

1.2 The Adaptive Immune system

The most important cells of the adaptive immune system are the lymphocytes. These cells continuously circulate through the blood and the lymph, thus monitoring the status of the body. The two main types of lymphocytes that are involved in the adaptive immune system are the B-lymphocytes and the T-lymphocytes. These cell types differ not only in the surface receptors that they possess, but also their method of recognition of foreign antigen, and their effector mechanisms. The

key players of the adaptive immune system are:

- B-Lymphocytes
- T-Lymphocytes
- MHC molecules

1.2.1 B-Lymphocytes

B-lymphocytes mature in the bone marrow in the adult mammals, and are characterized by the presence of approximately 1.5×10^5 receptor molecules on their cell surface that are actually membrane bound antibody molecules. All such receptor molecules on a single B lymphocyte are specific for one particular antigen. The generation of the enormous diversity of these receptors is brought about by a process termed VDJ recombination—a process whereby the germline encoded gene segments for B lymphocyte receptors are recombined in different ways to give rise to unique combinations of final gene sequence coding for receptor proteins that are capable of recognizing two antigens differing only in one residue. Upon recognition of an antigen by the receptor, these B-lymphocytes eventually differentiate into effector cells called plasma cells, which secrete soluble antibody molecules, and memory B-cells. B-lymphocytes constitute the humoral immune response branch of the adaptive immune system, as they can directly recognize soluble antigens in body fluids (once known as humors). Their only contribution to the adaptive immune system are the antibody molecules.

1.2.2 T-Lymphocytes

T-lymphocytes mature in the thymus and like the B-cells, also possess cell surface receptors for antigen recognition. However, unlike the B cell receptors which are capable of recognizing soluble antigens, T cell receptors can only recognize antigens displayed by special MHC molecules on the surface of antigen-presenting cells, or on self-cells infected with intracellular pathogens like viruses. Hence, T-cells constitute the cell-mediated immune response branch of the adaptive immune system. When a T cell encounters an altered self-cell, it is stimulated to proliferate and differentiate into effector cells and memory T-cells. There are two sub-populations of T-cells – the T helper (T_H) cells and the T cytotoxic (T_C) cells. They differ in the type of additional cell surface glycoprotein molecules (CD4 or CD8) they possess. Generally, cells possessing CD4 function as TH cells while those possessing CD8 function as T_C cells. Recognition of an MHC bound antigenic molecule by TH cells results in their differentiation into effector cells that secrete various cytokines. These cytokines serve as activating signals for B-cells, T_C cells, macrophages and various other cells of the immune system. Activated T_C cells display cytotoxic activity, and they destroy altered self-cells.

1.2.3 MHC molecules

The major histocompatibility complex (MHC) is a cluster of genes on chromosome 6 in humans. It is also known as the HLA complex in humans. The loci constituting the MHC complex are highly polymorphic. Several alleles exist at

each locus, hence providing for a wide range of antigen-binding MHC molecules. The MHC cluster can be subdivided into three regions encoding for three classes of MHC molecules.

1. **Class I MHC genes** encode glycoprotein molecules that are expressed on the surface of nearly all nucleated cells. They are important for displaying peptide antigens on the surface of infected or altered self-cells for recognition by T_C cells.
2. **Class II MHC genes** encode glycoprotein molecules that are mainly expressed on the surface of antigen-presenting cells i.e. dendritic cells, macrophages and B-cells. They are important for displaying peptide antigens for recognition by TH cells.
3. **Class III MHC genes** encode a variety of secreted proteins involved in providing immunity, including some complement proteins, soluble serum proteins etc.

1.3 Activation of the adaptive immune system

The activation of the two branches of adaptive immune system occur in different manner. B-cells can either be activated on their own by some non-protein antigens (e.g. capsular polysaccharides on the surface of certain bacteria), or by interaction with TH cells that recognize the processed antigen-MHC Class II complex on the surface of B-cells. Interactions between specific co-stimulatory molecules

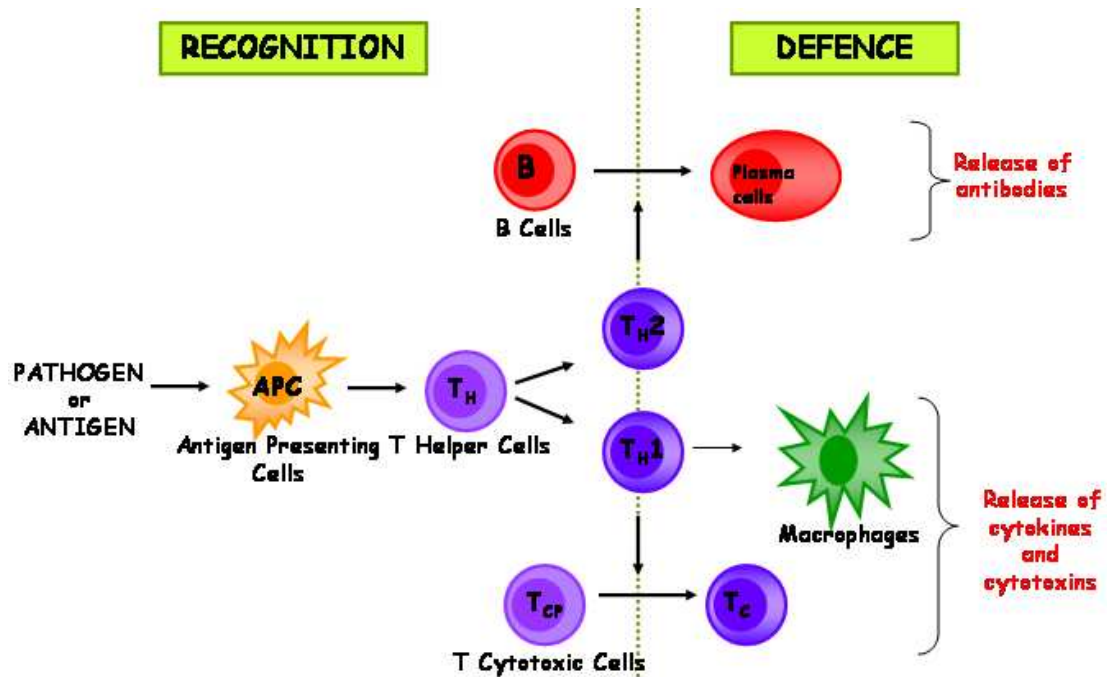


Figure 1.1: Activation of the adaptive immune system

on the TH cells and B-cells, and directed release of cytokines by the TH cells stimulate B cell proliferation and differentiation into antibody secreting plasma cells and memory cells. The activation of the adaptive immune system is shown in Figure 1.3.

The activation of T cell responses requires the interaction of naive T-cells by specialized cells called the *Antigen Presenting Cells (APCs)*. These cells internalize foreign bodies efficiently, either by phagocytosis or endocytosis, and process it intracellularly for display with class II MHC complex on the cell surface. Three types of cells function as professional APCs, namely the *dendritic cells*, *B-cells* and *macrophages*. Dendritic cells are perhaps the most important professional APCs of the immune system. They are phagocytic cells arising from bone marrow precursor cells, from where they migrate and settle down in various tissues. After internalizing a pathogen in the infected tissue, dendritic cells are stimulated to

migrate to a peripheral lymph node or lymphoid organ, where naive T-cells are constantly being circulated. Here, the dendritic cells display the processed antigenic fragments in a complex with MHC Class II molecules on their cell surface. T-lymphocytes possessing the antigen-specific receptor recognizing the displayed antigenic fragment become activated, and they proliferate and give rise to effector and memory cells.

The most important component of the B cell responses are the B-cell receptors and antibodies. B-cell receptors are membrane-bound antibody molecules. Antibodies belong to the immunoglobulin family of proteins, as they possess a characteristic compact structure known as the immunoglobulin fold.

1.3.1 Structure of an antibody

The basic structure of an antibody is shown in Figure 1.3.1. Antibodies are Y-shaped immunoglobulin molecules comprised of two light chains and two heavy chains. Each chain in turn is composed of a variable region at the N-terminus of the protein and a constant region at the C-terminal end of the protein. The original four chain model was proposed by Porter (1959). The constant regions of light chains have either of the two amino acid sequences named kappa (κ) and lambda (λ). The constant regions of the heavy chains have one of five basic amino acid sequences i.e. γ , α , μ , δ , or ϵ . These sequences determine the isotype of the antibody molecules, and based on the isotype of the heavy chain constant region, immunoglobulins adopt one of 5 classes in humans – *IgG*, *IgA*, *IgM*, *IgD* and *IgE*.

The Y-shape of an antibody was first proposed by Valentine and Michael during their studies of an antibody-hapten complex through electron microscopy (Valentine and Green, 1967). The variable region of an antibody (F_v) consists of two identical light and heavy chain components on either arm of the molecule (marked V_L and V_L respectively in Figure 1.3.1). The variable regions of an antibody contain the interaction site of the antibody with the antigen. The virtually infinite sequence diversity of the variable region allows an antibody to bind with a wide range of antigens.

Among the Immunoglobulin isotypes, *IgG* is the most abundant, making up about 75% of all immunoglobulins found in the human serum (Junqueira and Carneiro, 2005). Further, *IgGs* consist of four subtypes: *IgG1*, *IgG2*, *IgG3*, and *IgG4* (GREY and KUNKEL, 1964; Gergely, 1967), in decreasing order of occurrence. These subtypes differ mainly in their amino acid sequences as well as in the number of disulphide bonds between the heavy chains.

1.3.2 Generation of antibody diversity

The ability of the B cell receptors to recognize a wide range of antigens arises from the generation of a diverse set of B-cell receptors specific for almost every possible antigen that the organism might come across during its lifetime. Instead of loading the genome with genes encoding for each specific B cell receptor, the adaptive immune system evolved to generate diversity from a handful of gene segments by the simple process of recombination.

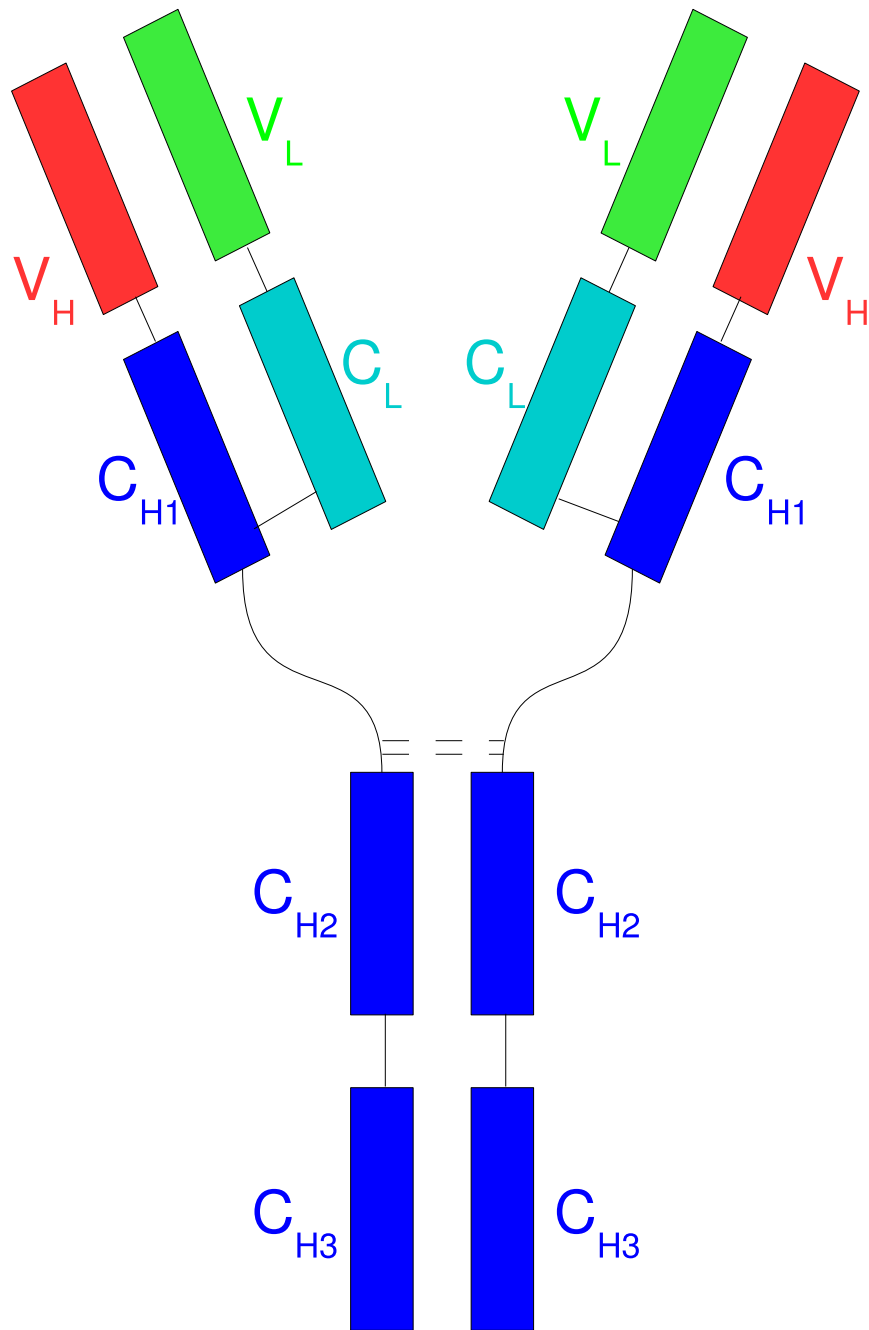


Figure 1.2: Structure of an Immunoglobulin (IgG1) consisting of 12 domains

The gene families encoding for B cell receptors are present on three chromosomes in humans. The multigene families encoding for the κ and λ light chains are present on chromosomes 2 and 22 respectively, while those encoding for the heavy chains are present on chromosome 14. The germline sequences of these multigenic families consist of a number of coding sequences called gene segments. It is these gene segments that are rearranged during B cell maturation to give rise to various combinations of sequences. The κ and λ light chain gene families consist of multiple V and J gene segments and a single C gene segment. The heavy chain locus consists of multiple V, D and J gene segments, as well as multiple C gene segments. The rearranged V(D)J gene segments codes for the variable region of antibodies, while the C region codes for the constant region.

1.3.3 VDJ Recombination

Recombination of the V, D and J gene segments is carried out with the help of lymphoid cell specific recombinase enzymes RAG-1 (Recombination Activating Genes) and RAG-2. These enzymes recognize unique sequences flanking the V, D and J segments called the Recombination Signal Sequence (RSS). The RSSs are made up of a conserved heptameric sequence (5' CACAGTG 3') on one end, a conserved nonameric sequence (5' ACAAAAACC 3') on the other end, and a spacer region in between containing 12 or 23 base pairs. An RSS containing a 12 base spacer can only join to another gene segment possessing 23 base pair spacer, a rule known as the 12/23 rule. Each V gene segment has an RSS on its 3' end, each J gene segment on its 5' end and each D gene segment has an RSS on both sides. The nature of the spacer in the RSS of the V, D and J gene segments ensures that a V gene

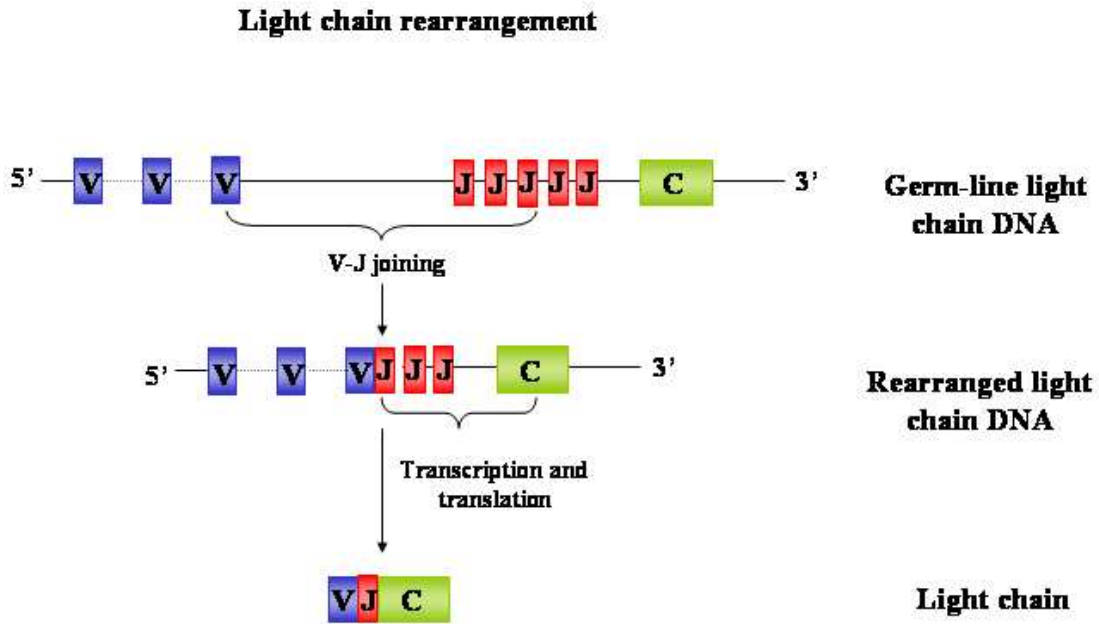


Figure 1.3: VDJ recombination to produce light chains

segment joins only to a J and not to another V gene segment, and likewise, for the J gene segments. The presence of different copies of each gene segment generates a combinatorial diversity that is a major contributing factor towards generating B cell receptor diversity. Apart from this, several other mechanisms also add to the existing diversity. In addition, the diversity of antibodies is enhanced by combinatorial association between the light and heavy chain. The VDJ recombination for light and heavy chains is shown in Figures 1.3 and 1.4 respectively.

Junctional flexibility

During the process of VDJ recombination, the joining of the gene segments is often imprecise, leading to differences in the final coding sequence for each recombination event. This junctional diversity has been shown to occur within the

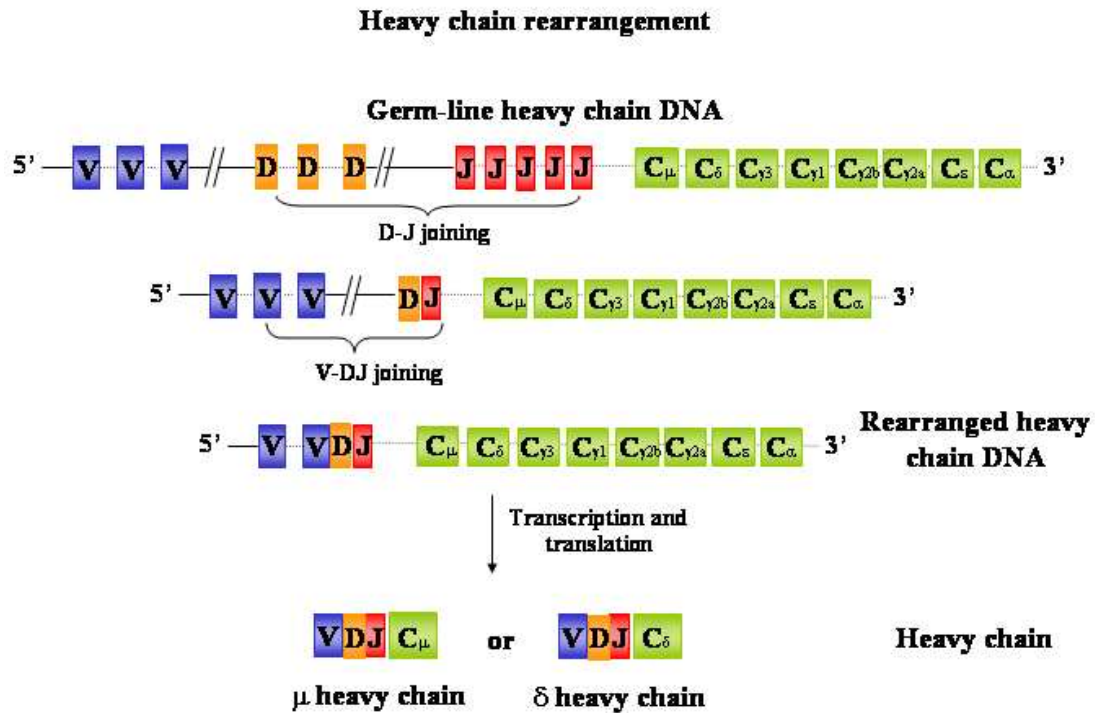


Figure 1.4: VDJ recombination to produce heavy chains

third hypervariable region (CDR3) of the heavy and light chain. Since CDR3 is a region important for antigen recognition, this process further increases the range of epitopes that can be recognized by antibodies.

P-Nucleotide and N-nucleotide addition

During the process of recombination, the 3-OH end of the strand cleaved by RAG enzymes forms a hairpin connecting it to the opposite DNA strand. This hairpin is cut, sometimes resulting in a short single stranded region referred to as the P-nucleotides. This is because addition of complementary nucleotides to fill up the gap results in the generation of palindromic sequences. N-nucleotide addition refers to the addition of nucleotides by the enzyme terminal deoxynucleotidyl

transferase (TdT). Upto 20 nucleotides can be added. N-nucleotides are found in V-D and D-J gene junctions of assembled heavy chains as the enzyme TdT is expressed exclusively at the time of heavy chain rearrangement and not during light chain rearrangement. These nucleotides are not encoded by the V, D or J gene segments and thus lead to additional diversity of the antibody sequence.

Somatic hypermutation

There exists another mechanism that acts post gene rearrangements of the heavy and light chains to generate more antibody diversity. Nucleotides in the V region of the antibody chain are replaced by alternate nucleotides in a nearly random manner. These mutations occur at a much greater frequency as compared to normal mutations, hence it is called hypermutation. It aids in generating B cell receptor sequences that may bind more strongly to antigens. Such a B- cell is then selected for rapid proliferation in a process termed affinity maturation.

1.3.4 B-cell maturation, activation and proliferation

B-cell maturation

B-cells maturation begins in the embryo in the fetal liver, fetal bone marrow and the yolk sac, and continues during adulthood in the bone marrow. The maturation process involves two distinct phases - antigen-independent phase and antigen-dependent phase.

Antigen-independent phase This phase occurs in the bone marrow in the absence of exposure to any antigen, and leads to the generation of naive B-cells that then enter into circulation. Lymphoid stem cells give rise to the first B-cell lineage cells- the progenitor B-cells (pro-B cell). In the niche provided by the bone marrow stromal cells, these pro-B-cells differentiate into precursor B-cells (pre-B-cells). This occurs by the close association between pro-B-cells and stromal cells which is mediated by cell-cell adhesion molecules expressed on the pro-B cell and the corresponding receptor present on the bone marrow stromal cells. Initial contact is mediated by molecules like VLA-4 expressed on the pro-B-cells that recognize and bind to its ligand VCAM-1 on the stromal cell. This is followed by the activation of c-Kit receptors on the pro-B-cells by stromal cell surface molecules. By virtue of its tyrosine kinase activity, c-Kit kick-starts a series of events that lead to the proliferation and differentiation of pro-B-cells into pre-B-cells. Cytokines like IL-7 secreted by the stromal cells further contributes to the maturation process and also leads to the detachment of pre-B-cells from stromal cells.

The maturation of pro-B-cells involves Ig-Gene rearrangements. These occur in a fixed order. First the heavy chain gene rearrangement takes place. The DH - J H joint is formed, followed by the VH - DH J H rearrangement to give rise to a productive gene arrangement. At this stage, the B-cell is termed pre-B cell. The subsequent productive rearrangement of the light chain gene gives rise to an immature B cell that expresses IgM on its cell surface. The transition of immature B-cells to mature B-cells proceeds with the expression of IgD isotype of the B cell receptor in addition to the IgM isotype.

Before mature B-cells enter into circulation, they are tested for specificity to self-antigens. Since the entry into circulation of B-cells reactive to self-antigens can be fatal, this process of negative selection plays an important role. About 5×10^7 B-cells are produced per day by the bone marrow, and only about 10% of these enter into circulation. Recognition of a self-antigen by an immature B-cell leads to the crosslinking of membrane IgM molecules and subsequent death. However, in many cases, following self-antigen recognition, the immature B-cell quickly edits its light chain in an attempt to generate B-cell receptors that are no more specific towards the self-antigen. The antigen-independent phase of maturation is shown in Figure 1.3.4.

Antigen-dependent phase Mature B-cells that enter circulation survive only for a few weeks unless activated by an antigen against which their receptor displays specificity. Antigens can trigger different routes of B cell activation depending on their nature. Some antigens can directly activate B-cells by binding to the B cell receptor, while others stimulate B cell activation via a special class of T-cells called helper T-cells (TH cells). Therefore, antigens stimulating B-cells can be classified as thymus-independent (TI) and thymus-dependent (TD) respectively. The antigen-dependent phase of maturation is shown in Figure 1.3.4.

Thymus-independent antigens can be of two types:

- Type-I TI antigens e.g. gram-negative bacterial cell wall component lipopolysaccharides, which is capable to non-specifically activating B-cells when present in high concentrations. These are truly thymus-independent antigens as they stimulate B-cell response even in nude mice, which lack a thymus and hence cannot produce T-cells. B-cell

Antigen-independent phase (Bone marrow)

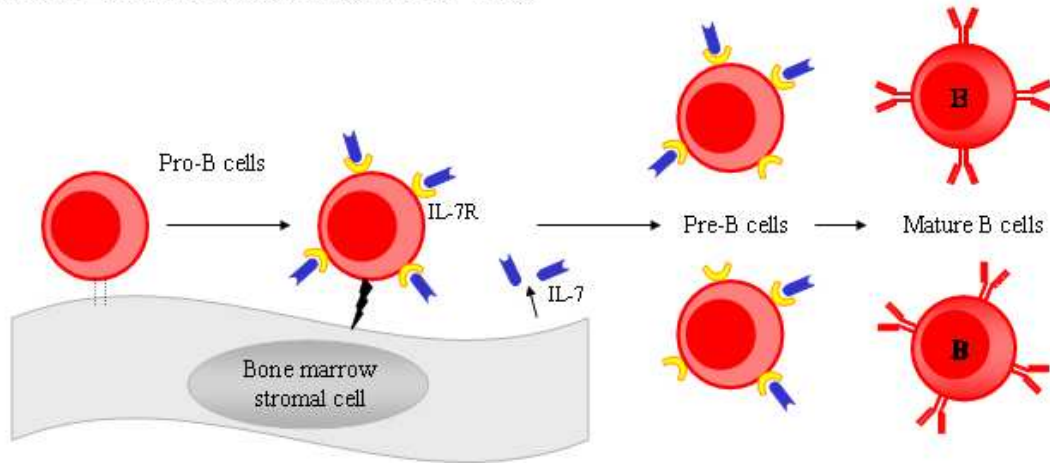


Figure 1.5: Antigen-independent phase of B-cell maturation

response to these antigens is not accompanied by isotype switching, affinity maturation or generation of memory cells.

- Type-II TI antigens e.g. bacterial cell wall polysaccharides. These are usually highly repetitive molecules that lead to cross-linking of mIgM molecules on the B-cell surface and subsequent activation of the B-cell. The complete activation of B-cells by these type of antigens also require cytokines secreted by TH cells. Affinity maturation or generation of memory cells does not accompany b-cell response to these antigens. However, there is some limited isotype switching involved.

Thymus-dependent antigens require the direct involvement of helper T cells for activation of the humoral response. These are soluble protein antigens that cannot give rise to effective activation of B cells on their own. The steps of activation by TD antigens are more complicated, but they result in isotype switching, affinity maturation and generation of memory cells.

Antigen-dependent phase (Peripheral lymphoid organ)

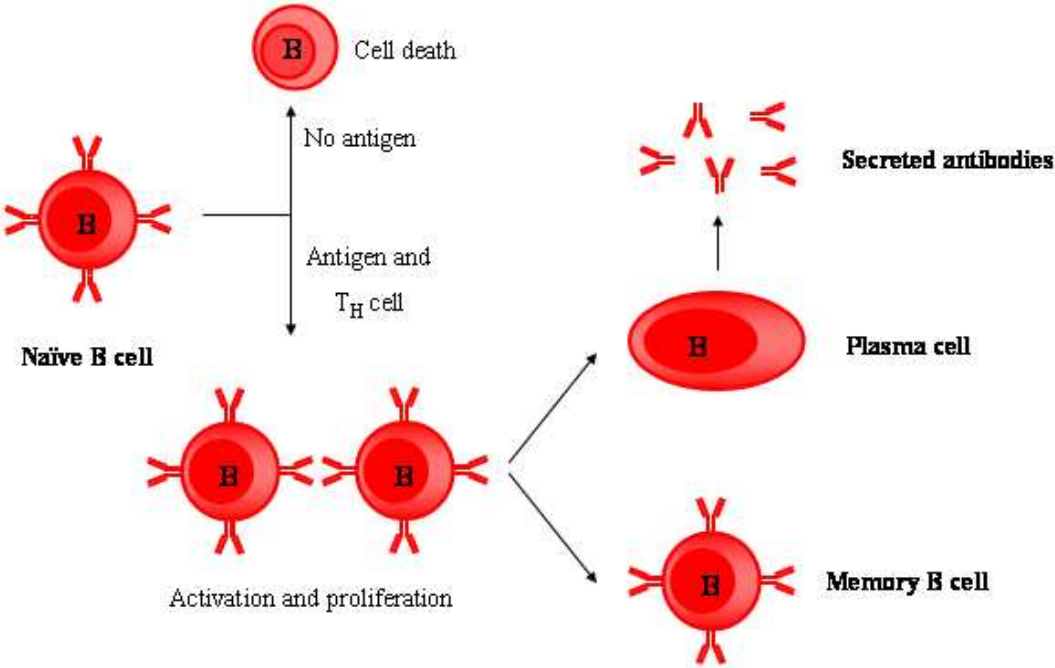


Figure 1.6: Antigen-dependent phase of B-cell maturation

1.3.5 B-cell activation

When activated by an antigen, naive B-cells are stimulated to exit from the G0 or resting phase of the cell cycle and begin replication and differentiation. This activation involves two steps that require two types of signals:

- Competence signals, which stimulate naive B-cells to exit from G0 and enter the G1 phase of the cell-cycle. Two signals (signal 1 and 2) contribute to the competence signals.
- Progression signals, which drive the cell from G1 to the S phase of the cell cycle, and ultimately to the replication and differentiation of B cells.

These two signals mediate their effects by activating signal transduction pathways downstream of the B-cell receptors. The mIgM and mIgD have short cytoplasmic tails that are insufficient for efficient signal transduction. To overcome this shortcoming, mIgs associate with a disulfide-linked heterodimer Ig- α /Ig- β to form the complete B-cell receptor (BCR). The cytoplasmic tails of Ig- α /Ig- β contain a sequence motif of 18 residues called the Immunoreceptor Tyrosine-based Activation Motif (ITAM) which can associate with several downstream intracellular signal transducers like the Src and Syk tyrosine kinases when activated by crosslinking of mIgs. This leads to the phosphorylation of tyrosine residues in the Ig- α /Ig- β cytoplasmic tails and the activation of multiple downstream signaling pathways. The end result of these events is the transcriptional activation of several specific genes that are further needed for B-cell response to antigens.

B-cell activation by thymus-dependent antigens

TD-antigens are not competent enough to induce activation of B-cells on their own. They are instead internalized by B-cells that recognize them and are displayed on the cell surface in conjugation with MHC-II molecules. The antigenic peptide-MHC-II complex is recognized by TH-cells and this interaction leads to the formation of T-B conjugates. This conjugate formation is accompanied by polarized intracellular rearrangement of the golgi and the microtubule-organizing center towards the site of T cell-B cell interaction. This is believed to aid in the directed release of cytokines for B-cell activation. MIgM cross-linking and interaction of specific ligand-receptor molecules on the T cell and B-cell surface provides the competence signal needed to drive the B-cell from G0 to G1 phase. This signal enables B-cells to express cytokine receptors on their cell surface. Cytokines (IL-2, IL-4 and IL-5) released from the TH-cells in a directed manner bind to these receptors and provide the progression signal, leading to the proliferation of these activated B-cells. Subsequently, these B-cells undergo differentiation.

B-cell differentiation

B-cell activation and differentiation takes place in peripheral lymphoid organs like the lymph nodes. These are specialized organs that trap antigens circulating through the lymphatic system. These are also organs through which T-lymphocytes and B-lymphocytes constantly re-circulate. Antigens that enter the body are processed by professional antigen-presenting cells and brought to the T-cell zone of local peripheral lymph nodes. Circulating naive T-lymphocytes are

exposed to the antigen and those displaying specific recognition for the antigen are trapped and activated to become TH cells. Circulating B-cells enter lymph nodes and most B-cells quickly pass through the T-cell zone to enter the B-cell zone (the primary follicle). However, those B-cells possessing B-cell receptors that specifically bind the antigen are trapped within the T-cell zone. The interaction between activated TH cells and B-cells leads to the formation of a primary focus of clonal expansion of both lymphocytes for several days. . This constitutes the first phase of the primary humoral immune response. Many of the cells in the primary focus die by apoptosis at the end of the first phase. Those that survive can have either of two fates. Some B-cells differentiate into plasma cells capable of antibody secretion and migrate to the medulla of lymph nodes. Antibodies secreted from these plasma cells provide immediate protection to the individual.

Some of the remaining B-cells and T-cells migrate to the primary follicles where they proliferate and form a germinal center. Events that transpire in germinal centers serve to provide effective later response in case of re-infection. B-cells undergo a number of differentiation events in germinal centers including somatic hypermutation, affinity maturation and isotype switching. This serves to select for B-cells displaying increased affinity for the antigen and enables these selected B cells to perform various effector functions depending on the isotype. These B-cells can now differentiate further into plasma cells and memory cells. Plasma cells are terminally differentiated non-dividing cells that secrete antibodies at a high rate. They migrate to the bone marrow where the bone marrow cells provide survival signals to plasma cells. These plasma cells serve as a long-lasting source of high-affinity antibodies. Memory cells are long-lived cells that provide long-term immunological memory.

1.3.6 B-cell effector-response

The first encounter with an antigen leads to a primary humoral response (described above) that culminates in the production of plasma cells and memory cells. The primary humoral response is characterized by a lag phase, which is the time required for clonal selection, proliferation and differentiation of naive B-cells. Memory B-cells that arise from the primary humoral response are key to initiating the secondary humoral response in case of re-infection by the same antigen. The secondary response is characterized by a much shorter lag period and an immune response of greater magnitude as compared to the primary response.

Antibodies synthesized in response to an infection effectively eliminate antigens by a variety of means including:

1. Acting as opsonins, thus enabling easy recognition by antigen-presenting cells.
2. Activating the complement system to bring about lysis of infecting cells.
3. Binding to target cells and facilitation recognition by cytotoxic T-cells, thus leading to antibody-dependent cell-mediated cytotoxicity (ADCC).
4. Binding and neutralizing bacterial toxins

The large number of antibody molecules secreted by plasma ensures that the invading pathogen is effectively eliminated.

1.4 T-cell responses and cell-mediated immune system

1.4.1 T-cell receptor

T-cell receptors are heterodimers composed of either $\alpha\beta$ chains or $\gamma\delta$ chains. Like B-cell receptors, the diversity of T-cell receptors is generated by gene rearrangements. The T-cell receptor is also associated with a signal-transducing complex CD3 which functions in a similar way to the Ig- α /Ig- β complex in the B-cell receptor. The cytoplasmic tail of CD3 possesses the immunoreceptor tyrosine-based activation motif (ITAM) by which it can interact with downstream kinases and activate downstream signal transduction kinases in response to T-cell receptor activation. The T-cell receptor recognizes an antigen only in a complex with MHC molecules. While the variable region of the T-cell receptor binds to the peptide fragment in the peptide-MHC complex, the extracellular domains of coreceptors CD4 and CD8 mediate interaction of the T-cell with the MHC molecule in the peptide-MHC complex.

1.4.2 T-cell maturation

T-lymphocytes originate in the bone marrow, but subsequently migrate to the thymus for development in the eighth or ninth week of gestation in humans. Similar to B-cell development, T-cells also undergo a series of gene rearrangements

that give rise to cells expressing different cell surface molecules. T-cell maturation starts with the expression of a pre-T cell receptor lacking surface CD4 and CD8 (referred to as the **double-negative** state) consisting of the CD3 protein, the β -chain of the TCR and a pre-T α . First the TCR β -chain gene rearrangement takes place following which the expression of CD4 and CD8 is induced. These thymocytes are now called double-positive or CD4⁺8⁺ T-cells possessing identical β -chain sequence. It is only when these double-positive T-cells stop proliferating that the TCR α -chain gene rearrangements take place. T-cells that fail to make a productive gene rearrangement do not mature and they die by apoptosis. Those T-cells that survive are subjected to the next phase of selection termed thymic-selection. This step is important in ensuring that only those T-cells that recognize self-MHC molecules in conjunction with foreign antigens are released into circulation. Thymic-selection occurs in two phases:

1. Positive selection of T-cells capable of recognizing self-MHC molecules thus resulting in MHC restriction. This is brought about by an interaction with thymic epithelial cells. During this selection, α -chain gene rearrangements continues to take place and those T-cells that fail to express $\alpha\beta$ -TCR with self-MHC recognition die by apoptosis in 3-4 days.
2. Negative selection of T-cells possessing high-affinity receptors for self-antigens displayed by self-MHC molecules, or to self-MHC molecules alone, resulting in self-tolerance. Positively selected T-cells interact with dendritic cells and macrophages bearing class I and class II MHC molecules and self-reactive T-cells are eliminated by apoptosis.

At the end of thymic-selection, only those T-cells capable of recognizing altered-self cells are able to survive and mature. By the time these mature T-cells are released into the periphery, they are either single-positive CD4+ thymocytes or single-positive CD8+ thymocytes. These T-cells that have not yet been activated by an antigen are termed naive T-cells.

1.4.3 T-cell activation

Naive T-cells that exit from the thymus continuously circulate between the blood and lymphatic system. This includes a passage through the various lymph nodes, where the chance of encountering an antigen or an antigen-presenting cell displaying an antigenic peptide is very high. Upon infection by an antigen, professional antigen presenting cells ingest, process and display antigenic fragments on their cell surface. These antigen-presenting cells then migrate to the nearby lymph node where they are sampled by circulating naive T-cells. The most potent activator of naive T-cells are dendritic cells. T-cells that are not specific for a particular MHC-peptide complex quickly re-enter circulation, while those displaying specificity to the complex are efficiently retained in the lymph node. Interaction of the TCR with the peptide-MHC complex initiates a series of events in the naive T-cell leading to its exit from the resting G0 phase and entry into the cell cycle. This is accompanied by the expression of several genes whose products enable the naive T-cell to proliferate, differentiate, and stimulate effector functions.

The interaction between TCR and CD4/CD8 on the T-cell and the peptide-MHC complex on the antigen presenting cell alone is not sufficient to induce activa-

tion of nave T-cells. Accompanying this interaction is an antigen-nonspecific co-stimulatory signal provided by the interaction between CD28 molecule on the T-cell and B7 molecule on the antigen-presenting cell. Co-stimulation of the T-cell leads to the increased production of the cytokine interleukin-2 (IL-2) and its receptor (IL-2R) by the activated T-cell, stimulating it's own proliferation and differentiation.

1.4.4 T-cell differentiation

The initial proliferative phase of T-cell activation lasts for about 4-5 days ,after which activated T-cells differentiate into armed effector T-cells and memory T-cells. Differentiated T-cells do not need stringent conditions for stimulation and therefore, any subsequent encounter with the peptide-MHC complex leads to a rapid response. For example, armed effector T-cells no longer need a co-stimulatory signal for their activation. Armed T-cells are capable of synthesizing all the effector molecules needed to bring about an effective cell-mediated immune response. CD4⁺ T cells differentiate into armed effector TH (T helper) cells while CD8⁺ T cells differentiate into armed effector TC (T cytotoxic) cells.

CD4⁺ T cells are capable of differentiating into either of two subsets, which differ in the cytokines they produce and also their effector functions:

- **T_H1** subset which activates the cell-mediated functions of the immune system including activation of cytotoxic T-lymphocytes. This subset of CD4⁺ T-cells secretes cytokines like IL-2, IFN- γ and TNF- β .

- T_H2 which functions as a helper cell for B-cell activation and secretes IL-4, IL-5, IL-6 and IL-10.

Activated $CD8^+$ T cells enter into circulation and recognize and actively kill infected cells by two major pathways:

1. The release of cytotoxic proteins like perforins and granzymes. Perforins are pore-forming proteins and they lead to cell death by virtue of disrupting the membrane integrity of target cells. Granzymes are lytic enzymes that are believed to trigger a cascade leading to DNA fragmentation of target cell and its apoptosis.
2. The activation of apoptosis in target cells by engaging Fas ligand on cytotoxic T-cells with Fas receptor on target cell surface.

1.5 Importance of the immune system

Each and every player of the immune system is essential for effectively preventing infections and diseases. This is highlighted by the manifestations of immunodeficiency diseases. These diseases can arise from a defect in any or several components of the immune system e.g. defects in the phagocytic system, complement system, cell-mediated immune system or humoral system. Immunodeficiencies affecting the humoral immune system can arise from defects in B-cell maturation, defects in mature B cells, ineffective TH cell activation or inappropriate T cell suppression. Examples of such diseases include X-linked hyper-IgM syndrome, common

variable immunodeficiency etc. Cell-mediated immunodeficiencies can arise from defects in T cell maturation for example DiGeorge syndrome. One of the most severe immunodeficiencies arises due to defects in the humoral and cell-mediated branch of the immune system. For example, defective T and B-cell maturation gives rise to Severe Combined Immunodeficiency Disease (SCID) while failure to express MHC molecules gives rise to the Bare-Lymphocyte Syndrome. Such severe disorders usually result in an early death unless an effective treatment to replace the defective immune cells is given.

Chapter 2

Introduction to computational methods in bioinformatics

2.1 An introduction to genetic algorithms

The principles of biological evolution have inspired many developments in the field of computer science. Genetic algorithms (GAs) are search algorithms that mimic principles of natural selection and natural genetics to find the best possible solution in a search space that is large and complex.

Genetic algorithms, together with Evolution strategies (Rechenberg, 1965; Rechenberg, 1973) and Evolutionary programming (Fogel *et al.*, 1966) comprise a field termed as *Evolutionary computation*. GAs were originally developed by John Holland and colleagues (1975) with the following aims:

- To synopsise the processes involved in evolution and natural selection.
- To design computational methods that would be based on the principle of natural selection.

The core theme behind GAs has been searching for optimal solutions in large and complex search spaces with reduced cost and extended functionality for artificial systems. The capabilities of GAs in finding optimal solutions have been established in numerous papers (e.g. Axelrod (1984), Axelrod and Dion (1988)) and the themes of adaptation and evolution appeal naturally as potential ways of finding solutions to complex problems where the search space is enormous. GAs incorporate these philosophies through *crossover* and *mutation*. In addition, the fundamentally parallel nature of GAs makes it possible to examine large populations of candidate solutions to problems simultaneously.

2.1.1 Elements of a genetic algorithm

The technical terms used in describing genetic algorithms bear close semblance to scientific terms in biology. Understanding the biological terms is therefore a useful step in understanding the basic components of a genetic algorithm. The following biological terms constitute the basic terms of a GA:

Chromosome The term *Chromosome* in biology used to denote strings of DNA.

A chromosome in a GA is used to refer to a potential solution to the problem

being addressed and is usually encoded as a bit string (i.e. a set of boolean values) (See Section 2.1.3).

Gene In biology, the term *Gene* refers to a block of genomic sequence which performs a specific function. In GAs, a gene is either a single bit or short blocks of adjacent bits in a chromosome that correspond to a specific characteristic of a chromosome.

Allele The biological meaning of the term *Allele* is a member of one of several forms of a gene. Each allele of a gene encodes for a specific trait or function. In a GA, an allele represents all the possible combinations of values at every position (generally a 0 or 1).

2.1.2 GA Operators

Further, two commonly used terms in GAs are *parent* and *child* populations of chromosomes. The *parent* population of chromosomes is initially created by randomly assembling strings with combinations of alleles (0 and 1 in GAs). The quality of every chromosome is evaluated to select parents and a new population of *child* chromosomes is created by *Crossover* and *Mutation*. These steps are described below and are commonly referred to as GA *operators*:

1. Selection: This term is used to describe the process of choosing parent chromosomes for reproduction. Parent chromosomes are evaluated for their quality and assigned scores and selection for reproduction is biased towards parents that have good scores. There are several methods of selecting parent

chromosomes which are described in the following sections.

2. Crossover: Once two parent chromosomes have been selected for reproduction, a random locus is chosen and the parent substrings are spliced together to form a new chromosome.
3. Mutation: Once parent substrings have been spliced together to form a new chromosome, some alleles in the new chromosome are changed randomly and this operation is known as *Mutation*.

2.1.3 Encoding a problem

The process of representing a problem to the computer is termed as *encoding* the problem. Optimal encoding of problems for genetic algorithms is central to their success. Most genetic algorithms are encoded as fixed length chromosomes. However, the encoding scheme is largely problem-specific and a number of encoding schemes have been devised for GAs. Some of the most prominent encoding schemes are:

1. Binary encoding: This is the most common encoding method for a GA and traces its history back to the time when genetic algorithms were first described by John Holland and colleagues (Holland, 1975). Binary strings are used to encode potential solutions to the problem at hand with each position containing one of two possible alleles: 0 or 1. Holland and colleagues established that the binary scheme has an inherently parallel nature compared with shorter strings that have more than two possible alleles at every

position. However, for some problems such as evolving weights in a neural network, the binary encoding scheme is not the best option.

2. Many-character and real-valued encoding: There are some problems for which a simple binary encoding will not be adequate. For example, when one of the inputs to a genetic algorithm is the torsion angle of a specific residue in a protein, it would be more convenient to have a real-valued encoding scheme where each position in the string is represented by numbers between 0 and 9. However, there are no established standards on the best encoding scheme and while a real-valued encoding is useful in one problem, a simple binary encoding scheme might suffice for another. The encoding scheme will depend on the problem being addressed in the genetic algorithm.
3. Tree encoding: In this scheme, every chromosome is represented as a tree of objects. This scheme is most suited for evolving rules or programs. It has an open-ended limit on the search space. However, there are no standard benchmarks for the efficacy of this encoding method, as development efforts for this scheme of encoding are currently at a very nascent stage (O' Relilly and Oppacher, 1995; Tackett, 1994).

2.1.4 Selection methods

The process of selection in a GA implies the selection of parent chromosomes to create a new chromosome. All selection methods are biased towards the selection of parents that have very high scores. There are many different selection methods and their applicability depends on the nature of the problem. The following are

examples of the most commonly used selection methods:

Roulette wheel selection

This is fitness-proportionate selection method where the likelihood of a particular parent being selected is given by the fitness of the parent divided by the average fitness of the entire population of chromosomes. The steps involved in this algorithm are detailed below. These steps are typically used to select 2 parents which are then crossed over to create a new chromosome.

- Sort the fitnesses of the parent chromosomes in ascending order.
- For the population of parent chromosomes, calculate the total fitness T .
- Select a random value r between 0 and T .
- The chromosome whose fitness puts the sum (when summed in ascending order of fitnesses) above the randomly chosen value r is chosen for crossover.

One problem with Roulette wheel selection is premature convergence of the population of chromosomes. Initially, the population is quite diverse. Some parents that score significantly better than others are selected frequently and, when crossed over, result in the same set of child chromosomes being created. This can cause the population to converge in a local minimum and become saturated.

Sigma selection

Several techniques have been developed to overcome the problem of premature convergence of the chromosome population. One such strategy is Sigma selection (Forrest, 1985). In this selection method, the use of the raw scores of the chromosomes is avoided. Instead, an *expected value* is calculated for each chromosome, the value of which depends on the score of the chromosome, the mean score for the population and the standard deviation in the score of the population. The expected value is calculated as:

$$e(i, t) = \begin{cases} 1 + \frac{f(i) - \bar{f}(t)}{2\sigma(t)} & \text{if } \sigma(t) \neq 0 \\ 1 & \text{if } \sigma(t) = 0 \end{cases} \quad (2.1)$$

where $e(i, t)$ is the expected value for chromosome i at time t , $f(i)$ is the fitness (or score) of chromosome i , $\bar{f}(t)$ is the average fitness of the population at time t and $\sigma(t)$ is the standard deviation of the population fitness at time t (Mitchell, 1996).

Melanie Mitchell reasons that, at the beginning of the GA when the fitness scores are fairly divergent, the expectation value for chromosomes with high scores will not be much higher than the average score of the population ($\bar{f}(t)$). However, after several time steps of the GA when the population starts to converge, the standard deviation in fitness levels ($\sigma(t)$) is small, and the chromosomes with high scores will stand out.

Boltzmann selection

Boltzmann selection is only slightly different from Sigma selection in that a ‘temperature’ component is involved while calculating the expectation value for every chromosome. A high temperature factor ensures that all genes have roughly equal chances of being selected for crossover. At the beginning of the GA run, the population of chromosomes is likely to be more diverse and therefore the variance in their scores is also high. In order to boost variability in the population at the earlier stages of the GA, a high temperature factor is applied in calculating the expectation factor. However, as convergence occurs, the variance in scores reduces and the temperature factor is also reduced.

The expectation value for every chromosome is calculated as follows:

$$e(i, t) = \frac{e^{\frac{f(i)}{T}}}{\mu(e^{\frac{f(i)}{T}})} \quad (2.2)$$

where $f(i)$ is the score of chromosome i , T is the temperature, $\mu(e^{\frac{f(i)}{T}})$ denotes the average score of the entire population at time t .

Rank selection

This scheme was originally developed by Baker (1985) in which every chromosome is assigned a rank depending on its score. Assuming a population of N chromo-

somes which are all distinct, the highest-scoring chromosome is assigned a rank of N and the lowest-scoring chromosome is assigned a rank of 1. In this way, the need for absolute scores is eliminated.

The procedure of selecting two parents for crossover is similar to Roulette-wheel selection with the difference being that scores are replaced by ranks. Every chromosome in the population is assigned a rank between 1 and N – the chromosome with the lowest score is given a rank of 1 and the chromosome with the highest score is given a rank of N . The following steps are performed twice to select two parents for crossover.

- Sort the parent chromosomes in ascending rank order.
- For the population of parent chromosomes, calculate the total rank T .
- Select a random value r between 0 and T .
- The chromosome whose rank puts the sum (when summed in ascending order of ranks) above the randomly chosen value r is chosen for crossover.

Tournament selection

Several of the selection methods described above employ time-consuming computations to calculate the probability of selection of every chromosome in a population. For example, in Rank-based selection, chromosomes are required to be sorted in increasing order of their scores so that selection can be biased towards chromosomes that have high scores and therefore low ranks. Similarly in Sigma selection,

one round of calculations is used to calculate the mean score of the population and another to calculate the probability of selection for each chromosome in the population.

Tournament selection avoids these problems by employing simple selection procedures. The selection of chromosomes for crossover are performed as follows:

- Select N chromosomes at random from the population.
- Choose a random number r between 0 and 1.
- If r is less than k (a user-defined parameter of the algorithm), then the most fit of the N chromosomes is chosen. Otherwise, one of the remaining chromosomes is chosen at random.

2.1.5 Replacement strategies

Once child chromosomes have been created after crossover of parent chromosomes, the process by which the parent and child chromosomes are combined to yield a new population is termed as replacement. The two most common replacement strategies are:

Generational replacement

This is the oldest replacement strategy and came into existence when genetic algorithms were originally developed. This method mimics the biological model in which a whole population of parents are replaced by children. In this method, the population of parent chromosomes is completely replaced by a population of child chromosomes.

Steady State Replacement

The Steady State Replacement strategy is a slight variation of generational replacement. In this method, only a few individuals from the parent population are replaced by individuals from the child population. The replaced individuals are usually the least-fit parents. This method is used in systems where incremental learning is important and members of a population collectively represent the solution to a problem (See Sywerda (1989), Sywerda (1991), Whitley *et al.* (1989), De Jong and Sharma (1993)).

Elitist replacement

This method is a slight variation of the Steady State Replacement method in which the best genes from the common pool of child and parent chromosomes are retained. The principle behind this replacement strategy is to retain the best chromosomes from every generation so that they are not lost in future generations

during crossover and mutation to create new populations. This method has been shown to be very effective in significantly improving the performance of a GA (De Jong, 1975).

2.2 Introduction to artificial neural networks

2.2.1 Machine learning approaches

Machine learning approaches were developed with the aim of identifying patterns in data where they cannot be easily described by a set of mathematical rules. However, the field of machine learning is vast considering that learning can be applied to several types of problems such as image recognition, classification problems, natural language processing and robotics, to name but a few. In my PhD, I have used artificial neural networks along with genetic algorithms to predict the packing angle at the interface of the light chain and heavy chain variable region from the nature of residues in the interface (See Chapter 5).

The most prominent machine learning techniques are:

Support vector machines (SVMs) Support Vector Machines are based on Vapnik's statistical learning theory (Vapnik, 2000). SVMs are principally binary classifiers i.e. they classify a result as belonging to one of two possible outcome sets. SVMs are therefore not suitable for the prediction of the packing angle.

Decision trees (DTs) Decision trees are usually used to create a set of rules from which a classification can be made. They accept a set of properties as input and output a series of yes/no decisions (Russell and Norvig, 1995) and are therefore not suitable for the prediction of packing angle. DTs are most often used in data mining applications and in classification problems.

Bayesian networks (BNets) Bayesian networks are based on the Bayes theorem (Bayes, 1763) and are amongst the most powerful machine learning techniques. However, a requirement for the use of BNets is that the data to be predicted must resemble a normal distribution. As will become clear from Section 5.1 in Chapter 5, the packing angle distribution is indeed normal. The use of BNets for the prediction of packing angle was therefore a possibility.

Artificial neural networks (ANNs) Artificial neural networks assume no prior distribution of data and can be applied to learn any type of data. I decided to use ANNs to predict the packing angle as there was more technical expertise in the group for ANNs compared with BNets.

2.2.2 Artificial neural networks

An *Artificial neural network* (referred to as just *Neural network*) is a system inspired by the working of the neural system. The biological nervous system can be imagined as consisting of *neurons* (nerve cells) which are connected to one another through connections or *synapses*. Similarly, artificial neural networks are made of *neurodes* which are the basic functional units. The schematic representation for a

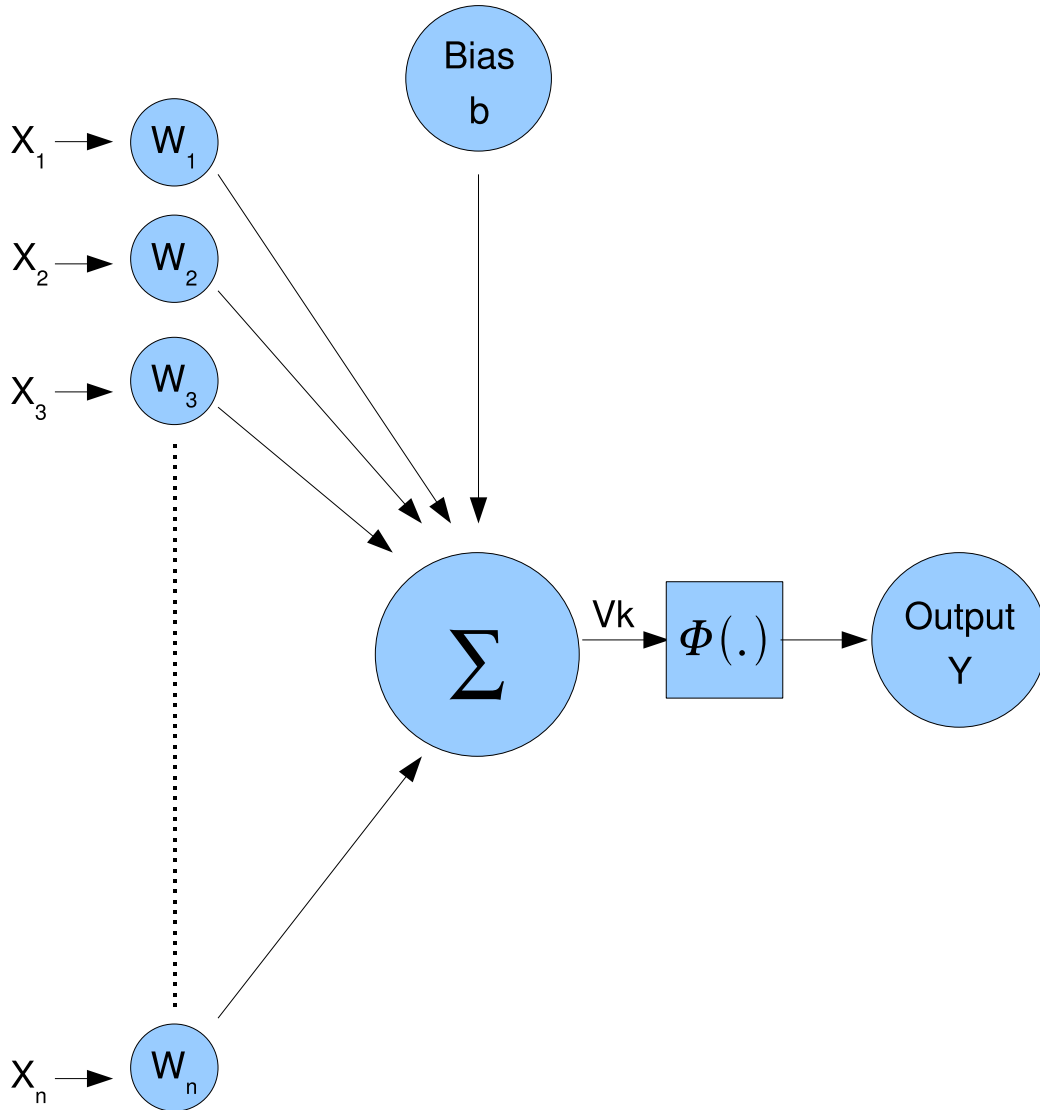


Figure 2.1: Schematic representation of a neurode in an artificial neural network. Figure shows the inputs to the neurode $X_1, X_2, X_3 \dots X_n$, weights of synapses $W_1, W_2, W_3 \dots W_n$, summation function σ , bias b , activation function ϕ and output Y .

neurode in an artificial neural network (*ANN*) is shown in Figure 2.1. The main components of an artificial neural network are:

1. Synapses: Synapses form the interconnects between neurodes. Each synapse that connects a certain input to the neurode is characterised by a weight. For example, in Figure 2.1, the weight for the synapse that links the second input to the synapse (X_2) is represented as W_2 . For every neurode, the input signal X_i is multiplied with the corresponding synaptic weight W_i . These quantities are summed up for all the inputs and together with the bias function b will determine the output of the neurode. It must be emphasised that the synaptic weight may be a positive or negative value.
2. Adder: An adder adds the product of all the input signals and the corresponding synaptic weights. In Figure 2.1, this is represented as Σ .
3. Bias function: This function is capable of increasing or reducing the input to the activation function. The bias function is shown as b in Figure 2.1.
4. Activation function: This function limits the output amplitude of a neurode and is shown as $\phi(.)$ in Figure 2.1.

Consider for example the neurode k^{th} in an artificial neural network. The input to the neural network as summed by the adder (u_k) is given by:

$$u_k = \sum_{j=1}^m w_{kj}x_j \quad (2.3)$$

Further, the output of the neurode is given by y_k :

$$y_k = \phi(v_k) \tag{2.4}$$

where v_k is referred to as the *induced local field* or the *activation potential*. v_k generally contains a bias function such that:

$$v_k = u_k + b_k \tag{2.5}$$

The bias function in Equation 2.5 has the effect of applying an affine transformation to the additive input to the neurode u_k . It must be noted that the bias function is a parameter that is external to the neurode and may be either a positive or a negative value. Depending on the value of the bias function b_k , the plot of v_k vs. u_k may not pass through the origin (Figure 2.2).

In the actual implementation of an artificial neural network, the bias function b_k of a neurode k is fed as an input signal x_0 which is given by:

$$x_0 = +1 \tag{2.6}$$

and the weight of the synaptic connection for this input is:

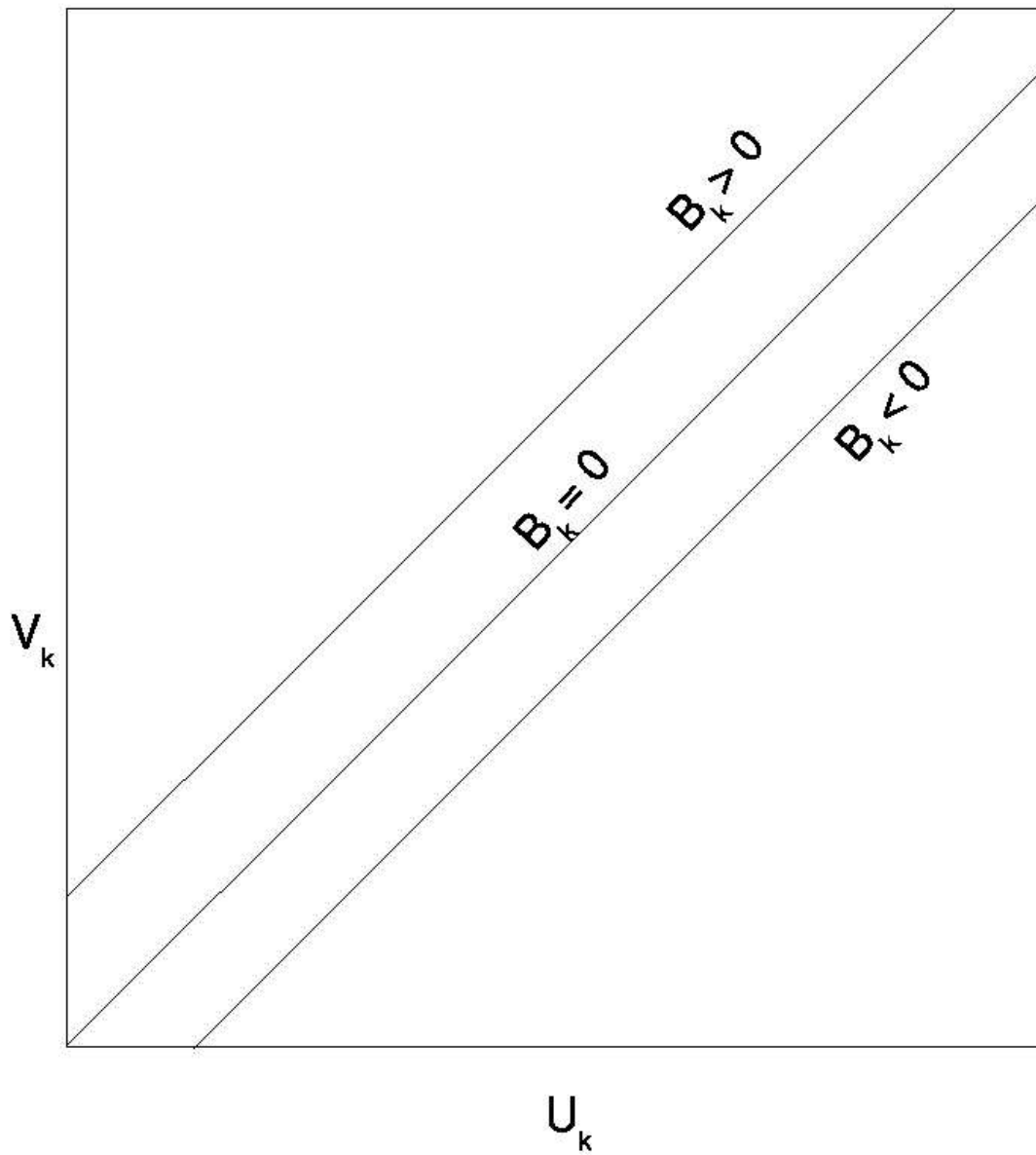


Figure 2.2: Plot of induced local field (V_k) vs. the adder function (U_k)

$$w_0 = b_k \tag{2.7}$$

The induced potential v_k and output y_k of a neurode k may be reformulated as:

$$v_k = \sum_{j=0}^m w_{kj} x_j \tag{2.8}$$

$$y_k = \phi(v_k) \tag{2.9}$$

A neural network typically consists of a three-layered architecture as shown in Figure 2.3: the Input layer, Hidden layer, and the Output layer. Each layer consists of a set of neurodes with interconnects between the neurodes in every level. The interconnects that link the neurodes are the synaptic connections and are characterised by weights described above. Neural networks *learn* by adjusting the weights of the synaptic links between the neurodes in each layer.

2.2.3 The process of learning: Learning algorithms

There are primarily two types of signals in *fully-connected* neural networks (such as that shown in Figure 2.3) (Parker, 1987):

- Functional signal: A functional signal is one that enters the artificial neural

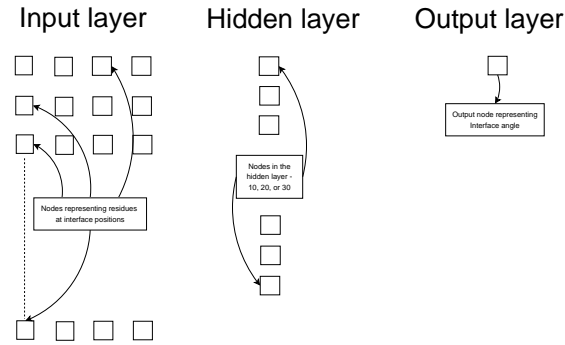


Figure 2.3: Three-layered architecture of a neural network. Each neurode of the input layer is connected to each neurode in the hidden layer which in turn is connected to each neurode in the output layer.

network through the input layer, propagates through the hidden layer and emerges as the output at the output layer. The output from every neurode is characterised by the inputs applied to the neurode and the synaptic weights that lead to the neurode. These signals are called functional because they form the output signal, in addition to determining the output from every neurode in the neural network.

- Error signal: An error signal is the opposite of a functional signal. It is used to refine errors made during the learning process. Error signals originate in the output layer and back-propagate to the input layer. They are so called because calculation of the error signal at every neurode involves computation of an error function in some form.

The process of learning in an artificial neural network involves adjusting the synaptic weights for inputs to every neurode. One of the most common learning techniques is called *Back-propagate* as it involves the adjustments starting in the last layer of the neural network. The following equation summarises the total weight change in the artificial neural network:

$$\Delta w_{ji}(n) = \eta \delta_j(n) y_i(n) \quad (2.10)$$

The notations used in the equation are as follows:

1. n indicates the time step and usually implies a specific training cycle.
2. i and j indicate neurodes in the network such that neurode j is in a layer to the right of neurode i .
3. $\Delta w_{ji}(n)$ is the change in weight (or correction) applied to the weight $w_{ji}(n)$ (weight of the synaptic connection that links neurodes i and j).
4. η is the learning-rate constant of the back-propagate algorithm.
5. $\delta_j(n)$ is the error introduced by neurode j at time step n .
6. $y_i(n)$ is the output of neurode i at time step n .

Updates to the weights are carried out using steepest descent minimisation through the following formula (Rumelhart *et al.*, 1986):

$$w_{ji}(n+1) = w_{ji}(n) - \eta \Delta E(w(n)) \quad (2.11)$$

where $w_{ji}(n+1)$ is the weight at time step $n+1$, $w_{ji}(n)$ is the weight at time step n , η is the learning constant, and $\Delta E(w(n))$ is the sum of square errors in the

weights at time step n . For quick convergence, the rate constant η is usually set to a value between 0 and 1. However, it is known that this method is very slow.

A modification to the Back-propagate algorithm, *Resilient propagate*, was proposed by Riedmiller and Braun (Riedmiller and Braun, 1993) in 1993. Unlike Back-propagate, Resilient propagate (*Rprop*) implements dynamic learning-rate constants during neural network training. Rprop has been shown to be far superior to other learning algorithms in terms of both speed and quality of learning (Schiffmann *et al.*, 1993).

A problem that has often been cited for the Back-propagate algorithm is that it gets stuck in local minima. Small changes to the synaptic weight could cause an overall increase in the cost function (here, the negative overall error rate). However, there may also exist another set of synaptic weights where the overall error rate is lower, causing the algorithm to be caught in local minima. This problem has been overcome in Resilient propagate wherein the size of the weight change is determined by a weight-specific update value, given by:

$$\Delta w_{ij}^{(n)} = \begin{cases} -\Delta_{ij}(n), & \text{if } \delta E(n)/\delta w_{ij} > 0 \\ +\Delta_{ij}(n), & \text{if } \delta E(n)/\delta w_{ij} < 0 \\ 0; & \text{otherwise} \end{cases} \quad (2.12)$$

where $\delta E(n)/\delta w_{ij}$ denotes the partial derivative of the sum-of-square error with respect to the weight of the synaptic link connecting neurodes i and j . Updates to the weights are carried out using the formula:

$$\Delta w_{ij}^{(n)} = \begin{cases} \eta^+ \Delta_{ij}(n); & \text{if } \frac{\delta E(n-1)}{\delta w_{ij}} \cdot \frac{\delta E(n-1)}{\delta w_{ij}} > 0 \\ \eta^- \Delta_{ij}(n); & \text{if } \frac{\delta E(n-1)}{\delta w_{ij}} \cdot \frac{\delta E(n-1)}{\delta w_{ij}} < 0 \\ \Delta_{ij}(n-1); & \text{otherwise} \end{cases} \quad (2.13)$$

Therefore every time the sign of the partial derivative of the weight (w_{ij}) changes (implying that the last update was too big and the algorithm crossed a local minimum value), the update-value $\Delta_{ij}(n)$ is decreased by the value η^- . On the other hand, if the sign of the derivative is retained, then the update value is increased to accelerate convergence.

RProp requires the following parameters to be set:

1. Increase factor η^+ (Default) = 1.2.
2. Decrease factor η^- (Default) = 0.5.
3. Initial update value Δ_0 (Default) = 0.1.
4. Maximum weight step used to prevent the weight from becoming too large Δ_{max} (Default) = 50 (Riedmiller and Braun, 1993).

2.3 Introduction to protein sequence analysis

After the completion of several genome sequencing projects, sequences of nearly 6.5 million proteins are available (<http://www.ncbi.nlm.nih.gov/RefSeq/>). The

most thorough way of annotating protein function is using biochemical analysis. However, this is impossible on a genomic scale considering the costs involved in annotating the function of nearly 6.5 million proteins.

Proteins that show significant amino acid sequence similarity tend to be homologous and have similar or related function. Sequence analysis tools have been developed with the goal of helping to identify homologous proteins. Some of the applications of sequence analysis tools include:

- Comparing protein sequences to identify homologous proteins.
- Tracing the evolution of a protein.
- Identifying conserved regions in the sequence of a protein.

An important focus in Bioinformatics has been the development of protein sequence comparison methods. These may be broadly classified into one of three types:

- Pairwise sequence alignment methods to compare two protein sequences.
- Fast heuristic alignment methods that compare a protein sequence with a database of protein sequences.
- Profile-based search methods to compare a protein sequence with a database of protein sequences.
- Multiple sequence alignment methods to identify regions of conservation in the sequences of homologous proteins.

2.3.1 Pairwise sequence alignment

Considering that there are only 20 amino acids, it is possible that two randomly chosen proteins would have a certain number of similar sets of residues entirely by chance. These statistics must be employed to identify significant relationships. A requirement in establishing regions of similarity between two proteins is to allow insertions or deletions in the sequences, commonly referred to as indels. However, the task of identifying indels to align two protein sequences optimally is difficult. This is particularly the case when the two proteins are remotely related and have very low sequence similarity.

Needleman and Wunsch (1970) developed an algorithm using dynamic programming to align two protein sequences automatically. The procedure uses an $n \times m$ matrix to score the identities, or similarities, of residues being compared, where n and m are the number of amino acids in the two protein sequences. The main steps involved in the Needleman and Wunsch algorithm are described below (Orengo *et al.*, 2003):

1. Scoring the matrix – The 2-dimensional matrix is initially populated with a set of scores to represent the identities or similarities of residues associated with each position in the matrix. In the simplest case, this can be either 1 or 0 where 1 would indicate identical residues (and therefore include all residues on the diagonal) and 0 otherwise. Another way of populating the scores is by using a substitution matrix such as the BLOSUM (Henikoff and Henikoff, 1992) or Dayhoff matrix (Dayhoff *et al.*, 1978). These indicate

the probability of one residue substituting for another residue in a protein over time.

2. Accumulating the matrix – Once the score for each cell in the 2D matrix has been computed, the scores are accumulated from the bottom right corner of the matrix. The best score for a cell represented by the coordinates (i,j) is selected using the equation:

$$S_{i,j} = S_{i,j} + \max \begin{cases} S_{i+1,j+1} \\ S_{i+m,j+1} - g \\ S_{i+1,j+m} - g \end{cases} \quad (2.14)$$

where $S_{i+1,j+1}$ indicates the score of a diagonal move from cell $i + 1, j + 1$, $S_{i+m,j+1}$ is the score of a move from the $j + 1^{th}$ row, and $S_{i+1,j+m}$ is the score of a move from the $i + 1^{th}$ column.

An off-diagonal move from either the $j + 1^{th}$ row or $i + 1^{th}$ column, implies the introduction of a gap in one of the sequences. Adding a gap to the alignment is penalised by imposing a gap penalty score of the form:

$$g = o + ne \quad (2.15)$$

where o is the gap opening penalty, e is the gap extension penalty, and n is the length of the gap.

3. Tracing the highest scoring path – Once the score for every cell in the matrix has been calculated, a trace-back is performed to find the optimal alignment between the two sequences. This is done by starting with the highest-scoring cell near the top left corner and tracing the path through which the score

was accumulated towards the bottom right corner of the matrix. An off-diagonal move implies the introduction of a gap in the alignment of one of the sequences. This is in turn equivalent to an insertion in the other sequence.

While the original dynamic programming method can be slow while aligning long sequences, the process may be speeded up by using a window for the matrix. This implies that the score accumulation and traceback is performed only within the window and the length of insertions or deletions is restricted by the size of the window.

Smith and Waterman (1981) developed an alternative algorithm which identifies a local region of similarity (local alignment) between two protein sequences. The score for each cell in the matrix when aligning sequence a and b is calculated by:

$$S_{i,j} = \max \begin{cases} S_{i+1,j+1} + S(i,j) \\ \max(S_{i+k,j}) - g \\ \max(S_{i,j+1}) - g \\ 0 \end{cases} \quad (2.16)$$

where S , i , j , k , m , and g have the same meaning as in the Needleman-Wunsch algorithm. When the score of a cell becomes negative, then a score of zero is assigned. The traceback step starts at the cell in the matrix with the highest score and is terminated when the cumulative score falls to zero. While the highest score in the Needleman-Wunsch algorithm is always on the outside the matrix, in

the Smith-Waterman algorithm, it can appear anywhere in the matrix.

2.3.2 Searches against a database of proteins

While dynamic programming results in the most reliable alignment, the algorithms are computationally expensive and are not practical when trying to align a protein sequence with sequences in a large database with the aim of identifying homologues or finding regions of local alignment. Alternative methods have been developed using heuristics with the aim of improving the speed of searches against large databases and identifying homologues. These methods help in the identification of putative homologues by assigning statistical scores. The two main heuristic-driven approaches to search against databases of proteins are *FASTA* (Pearson and Lipman, 1988) and *BLAST* (Altschul *et al.*, 1990).

FASTA and BLAST

The FASTA program developed by Pearson and Lipman (1988) is used to compare a protein sequence with a database of protein sequences. It uses the concept of words (or tuples) to identify regions of similarity between two proteins.

The working of the FASTA program is shown in Figure 2.4. FASTA uses the concept of words where a word represents a set of contiguous residues in a sequence. Normally, a word length of 2 residues is used for proteins. The sequence *A* to be compared against a database of sequences is first split into words. In addition,

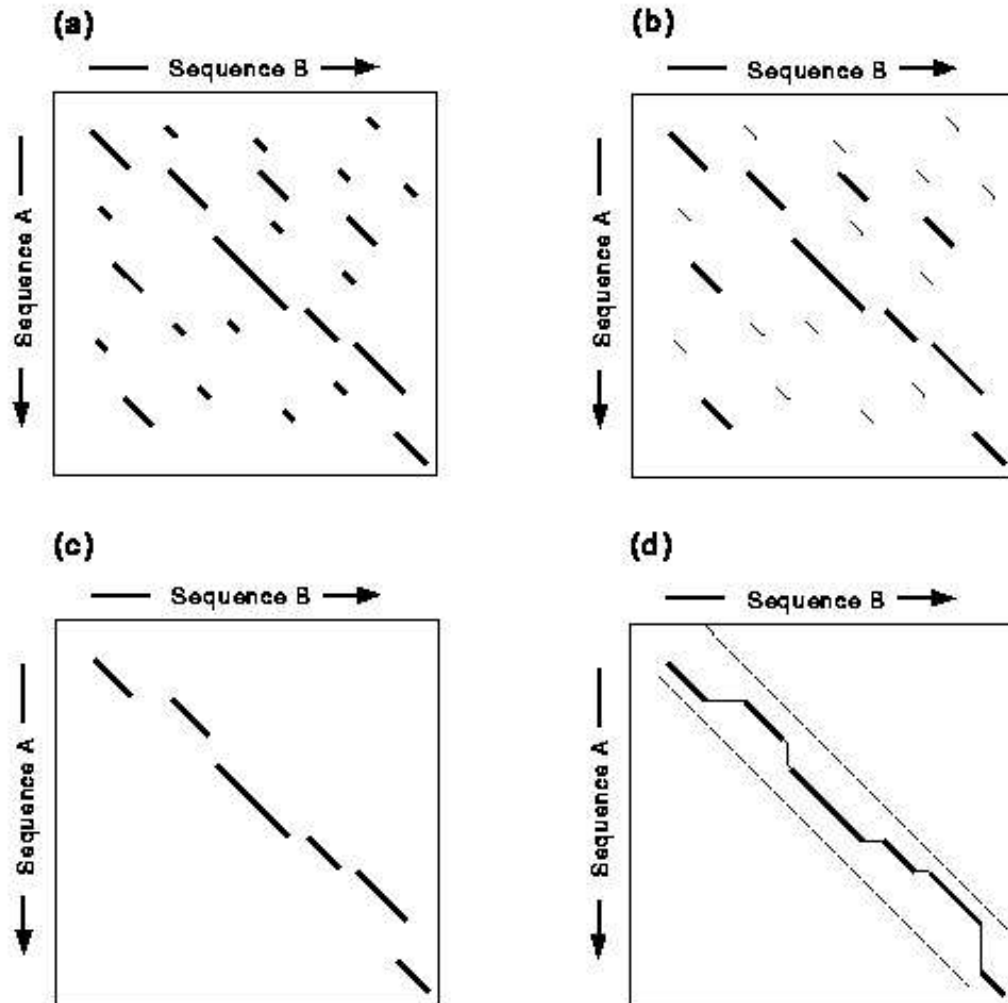


Figure 2.4: Steps involved in the FASTA search program: (a) Find all identical words in the query sequence (A) and sequence in the database (B) (b) All the identical words are scored using a substitution matrix (c) Identical words with a score above a threshold value are joined together using gaps and (d) The two sequences are aligned using the Smith-Waterman algorithm to obtain optimal alignment. Diagram taken from http://www.cbi.pku.edu.cn/images/fasta_algorithm.gif.

to facilitate the comparison of the query sequence with every sequence in the database, the following steps are performed:

1. Every sequence B in the database is split into its constituent words.
2. The words in A and B are compared and all identical words between the two sequences are identified and joined into contiguous stretches
3. The best stretches are scored using a substitution matrix (such as PAM) and words with a score below a threshold value are rejected.
4. All identical words with scores above the threshold value are joined together using gaps.
5. Smith-Waterman dynamic programming is used to perform a local alignment between the sequences using a narrow window around the diagonal identified in the previous steps. This provides an optimised score.

The use of dynamic programming allows the calculation of the overall similarity measure between the two protein sequences. The significance of the similarity measure is estimated by assessing how frequently the similarity score is observed when comparing the query sequence against a database of unrelated sequences.

BLAST

BLAST (or gapped BLAST) (Altschul *et al.*, 1990) performs similar steps to identify homologues of a query sequence in a database. For a word of length 3, all possible words that score above a threshold value are found and these words are

then identified in a database. The regions spanning the words are extended without introducing gaps while the score remains above a threshold value. If sufficiently good hits are found, then a Smith-Waterman alignment is performed. The main practical difference between BLAST and FASTA is that BLAST requires the database to be indexed prior to searching. This is done to increase the speed of searches.

Statistical methods to assess significance of a match

Sequence identity alone cannot establish whether a hit is a true homologue of a query protein. For example, it has been established that in the twilight zone of 25% sequence identity or lower, it is impossible to tell from sequence identity alone whether a hit is a remote homologue, or not a relative at all. This has led to the development of statistical measures to assess the significance of a match during a database search.

An assumption in the early versions of FASTA was that the distribution of pairwise identities between unrelated sequences was normal. Hence, initial versions of FASTA used Z-scores to report the likelihood of a match between two sequences. A Z-score gives the number of standard deviations of a certain value from the mean of a normal distribution. A high Z-score value (e.g. 15) implied a high probability of the hit being a homologue of the query protein. However, subsequent work showed that the distribution of pairwise identities between unrelated sequences is an extreme value distribution (Mott, 1992; Altschul and Gish, 1996) (See Figure 2.5 taken from Hobohm and Sander (1994)). The tail of the extreme

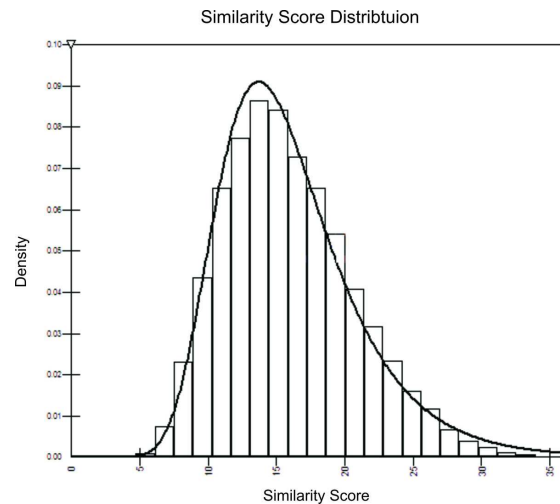


Figure 2.5: Extreme value distribution of 200000 sequences with less than 25% sequence identity randomly chosen from the PDB. Image taken from <http://www.biomedcentral.com/1471-2105/8/388/figure/F9> (Dundas *et al.*, 2007).

value distribution tapers more slowly compared with a normal distribution and is directly proportional to the log of the frequency with which a pairwise sequence identity score is observed. The frequency information can be used to estimate the probability of a hit being a true homologue of the query protein. This is reported by the *P-value*. For example, a *P-value* of 0.0001 implies that 1 in 10000 sequences giving this score or above would be an incorrect hit and not a true homologue of the query sequence. This statistic is extended to give an *E-value* (the expected number of hits with a given score or above in a given database) which is calculated by integrating the linear transformation of the tail of the extreme value distribution curve. In general, low *E-values* (typically less than 0.01) indicate an evolutionary relationship between a hit and the query protein (Pearson, 1998).

2.3.3 Profile-based search methods

A profile is a mathematical representation of a set of related sequences. For every position in the alignment of a set of proteins, a profile contains the probability of each amino acid occurring at that position.

A profile is constructed from a multiple sequence alignment of three or more related proteins. Profiles help in identifying the evolutionary conservation of residues with specific properties at different positions in the sequence. If a specific amino acid is highly conserved at a certain position, then the amino acid receives a high score for that position. At positions that are not well conserved, all amino acids receive low scores. In addition to profiles, there are other mathematical representations to score the conservation of residues. These include motifs (regular expressions that represent patterns of a sequence. e.g. *Prosite* (Hulo *et al.*, 2008)), and Hidden Markov models (Schneider *et al.*, 1986; Gribskov *et al.*, 1987; Staden, 1988; Tatusov *et al.*, 1994; Yi and Lander, 1994; Bucher *et al.*, 1996; Altschul *et al.*, 1997; Durbin, 1998).

An important profile-based database search procedure is the Position-Specific Iterative Basic Local Alignment and Search Tool (PSI-BLAST). This program was created by Altschul and colleagues (Altschul *et al.*, 1997) as an extension to the BLAST program. The steps involved in PSI-BLAST are as follows:

- A protein sequence (P) of interest is compared with a database of sequences by performing a BLAST search between P and every sequence in the database.

- All hits with an E-value below a certain threshold are multiply aligned and a profile is constructed from the multiple alignment.
- In the next iteration, the profile is used to search the database and identify new homologues.
- After each iteration when a new homologue is identified, a new profile is constructed and further iterations are performed using the modified profiles.
- The iterations are terminated when no new homologues are identified or a specified limit is reached.

In Chapter 3, pairwise sequence alignments have been performed using the program *ssearch33* to estimate the degree of humanness of antibodies. Chapter 4 describes a profile-based method to identify the start and end of framework regions of antibodies and apply numbering to antibody sequences. Finally, Chapter 5 describes a method using artificial neural networks using to predict the packing angle at the interface of the light chain-heavy chain variable region from a description of the interface residues. However, since the available training data are limited compared with the number of potential interface residues, a genetic algorithm is used to pick the a subset of interface residues in which the penalty function is the performance of the neural network, in order to select an optimal set of interface residues.

Chapter 3

Assessing humanness of antibody sequences

Rodent (particularly mouse) monoclonal antibodies are widely used in engineering antibodies for the treatment of human disease because they may be produced with high binding affinity to a wide range of antigens. The use of mouse monoclonal antibodies in the human system gives enormous scope for the treatment and diagnosis of several diseases (Glennie and Johnson, 2000). For example, Dyer *et al.* (1989) have reported the effectiveness of treating patients with Chronic Lymphocytic Leukaemia (CLL) with a rat antibody, CAMPATH-1G. The administration of the antibody led to a significant clearance of tumour cells in patients. However, the promulgation of therapy using monoclonal antibodies from other species (typically mouse or rat) for human disease has been slow owing to some important problems. First, in most cases, the original effector function of the rodent

antibody is not retained after introduction into the human system (Clark *et al.*, 1983) and second, rodent antibodies are immunogenic in the human system.

This Human Anti-Mouse Antibody (HAMA) response (Schroff *et al.*, 1985; Shawler *et al.*, 1985) or Anti-Antibody response (Glennie and Johnson, 2000) prevents repetitive administration of the antibody for treatment and may lead to anaphylactic shock. There are two main ways in which one can approach this problem - one could use fully human antibodies produced in phage libraries (Winter *et al.*, 1994; Low *et al.*, 1996) or transgenic mice (Brüggemann *et al.*, 1991; Mendez *et al.*, 1997; Vaughan *et al.*, 1998), or one could engineer rodent antibodies so that they appear more human.

Several strategies now exist which permit antibodies to be engineered in a way such that they retain the specificity of the rodent antibodies while seeming less alien to the human immune system. They may broadly be classified as chimerization (Neuberger *et al.*, 1984; Boulianne *et al.*, 1984) and humanization (Jones *et al.*, 1986; Riechmann *et al.*, 1988).

Chimerization involves grafting the F_v region of a rodent antibody onto the constant region of a human antibody. However, chimeric antibodies still contain a substantial rodent component and may still lead to a HAMA response. In humanization, the rodent content is minimised by grafting only the CDRs from the rodent antibody onto a human framework. Generally a small number of other framework residues need to be changed to the equivalent rodent residue in order to restore binding. Roguska *et al.* (1994) proposed an alternative technique of 'resurfacing' where they replace solvent accessible residues in chimeric antibodies

with human residues.

Clark (2000) has also questioned the value of more elaborate humanization protocols over chimerics. Data on approval rates for monoclonal antibodies (Reichert, 2001) show that 74% of chimerics have completed Phase III trials with 24% of these gaining FDA approval. In contrast, only 34% of humanized antibodies have completed Phase III trials with 25% gaining FDA approval. Thus, overall, chimerics have been at least as successful at getting into the clinic as humanized antibodies and a metric for assessing humanness may be of help in selecting rodent variable domains that could be used effectively as chimerics without the additional effort of humanization (also a patent minefield). It may also be valuable in selecting human frameworks for use in humanization. One can ask whether some rodent variable domains are more human-like than others, and indeed, whether they may be more typically human than some unusual human antibodies. In one case, a murine antibody has been approved for therapy (Orthoclone (OKT3), *Ortho Biotech* (Glennie and Johnson, 2000)).

The general question, therefore, is how typical an antibody sequence is of the expressed human repertoire. To answer this question, I have derived a ‘humanness’ statistic. In the first part, the mean and standard deviation of human and mouse sequences are compared. Further, a Z-score statistic, to assess how typically human an antibody sequence is of the expressed human repertoire, is described. Human and mouse variable regions have been compared with the use of this statistic and the analysis has been extended to the CDRs of light and heavy chains. Part of the work described in this chapter has been published in Abhinandan and Martin (2007).

Type of database	Number of sequences	
	Mouse	Human
Lambda class	62	1003
Kappa class	1292	645
Heavy chain	1562	1847

Table 3.1: Number of sequences in each dataset extracted from Kabat database.

3.1 Preparation of the dataset

Sequences of antibody variable regions were extracted from the last public release of the Kabat database (July 2000) using **KabatMan** (Martin, 1996). Sequences were separated on the basis of chain (light and heavy chain), class (lambda and kappa class for light chains) and species (mouse and human). Table 3.1 gives the number of sequences used in the analysis. The program *ssearch33* from the FASTA package (Pearson and Lipman, 1988) was used to extract pairwise identities between the antibody sequences. Graphs were plotted using *GNUPLOT* (<http://www.gnuplot.org/>) and *GRACE* (<http://plasma-gate.weizmann.ac.il/Grace/>).

3.2 Comparing pairwise identities of human and mouse sequences

The mean pairwise identity \bar{x}_i for sequence i in a database of m sequences is calculated as:

$$\bar{x}_i = \frac{\sum_{j=1, j \neq i}^m x_{ij}}{m-1} \tag{3.1}$$

where x_{ij} is the pairwise identity between sequence i and j . The standard deviation σ_i for sequence i in a database of m sequences is calculated as:

$$\sigma_i = \sqrt{\frac{\sum_{j=1, j \neq i}^m (x_{ij} - \bar{x}_i)^2}{m - 1}} \quad (3.2)$$

x_{ij} is the pairwise sequence identity between sequence i and j , \bar{x}_i is the mean pairwise identity for sequence i , and m is the number of human sequences in the dataset.

In the first step, I wanted to compare the diversity of mouse and human antibody sequences. In order to do this, I plotted the mean and standard deviation of every mouse and human sequence when aligned with every other mouse and human sequence in the dataset respectively. By comparing the mean and standard deviation of mouse and human sequences, I wanted to see if the points would cluster together depending on species and further, whether there were any common characteristics between mouse and human antibodies. The algorithm for this is shown in Figure 3.1.

Every mouse sequence from a specific dataset was taken and queried against the database of mouse sequences using *ssearch33*. A very high e-value cutoff of 100000 was used to ensure that pairwise identities between every pair of sequences were returned by *ssearch33* and considered in the calculations. From the set of pairwise identities, a mean pairwise identity was calculated as shown in equation 3.1. From the individual pairwise identities and mean sequence identity, a standard deviation

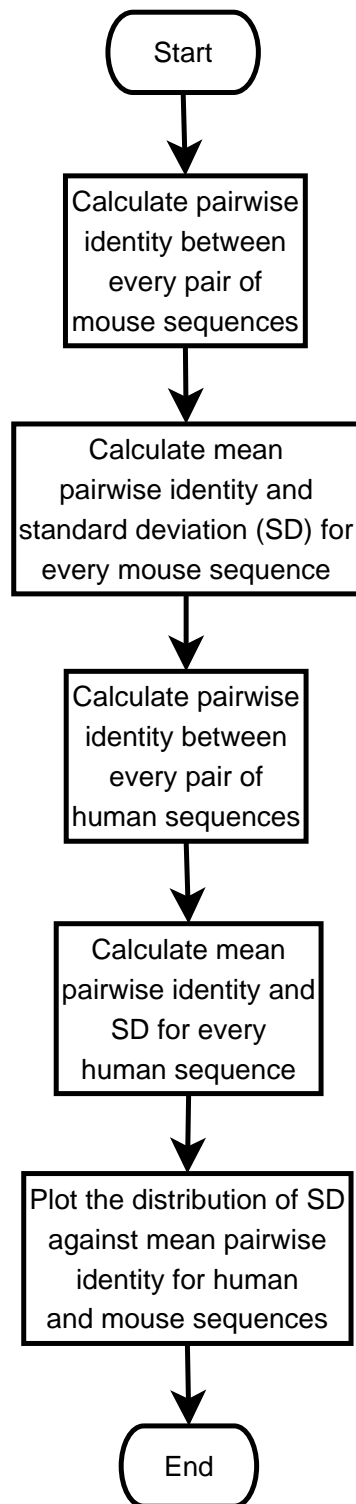
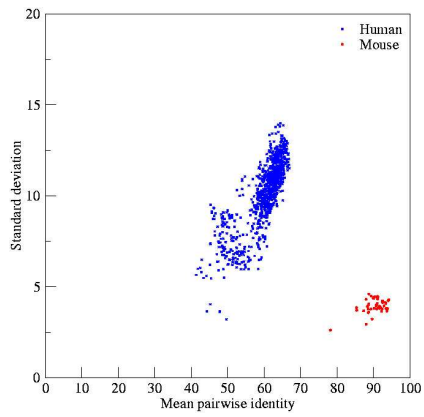


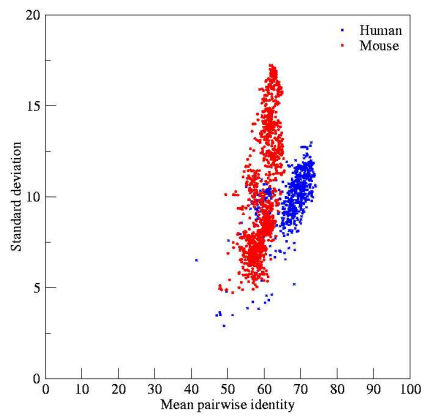
Figure 3.1: Algorithm to compute the mean and standard deviation for every sequence in the dataset (Table 3.1).

was calculated as shown in equation 3.2. All the above steps were repeated for the human sequences and the distribution of standard deviation against the mean percentage identity for the mouse and human sequences were plotted separately. These distributions were plotted for each dataset (heavy chain and lambda and kappa class for the light chain).

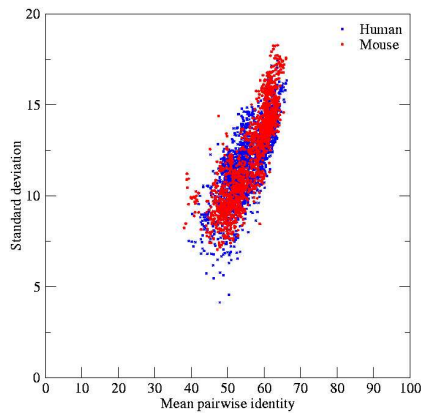
Figure 3.2 gives the plot of standard deviation vs. mean pairwise identity for the mouse and human antibody sequences. It is clear from the graphs that the data points for the human and mouse antibodies form distinct clusters. In the case of lambda class light chains, there is a clear separation between the mouse and the human plots. While the human antibodies tend to have a mean percentage identity between 40 and 70% and a wide range of standard deviations, the plot for the mouse sequences shows that the mouse lambda light chains have high mean percentage identity while showing lesser sequence diversity. The graph for kappa class light chains shows that although the data points for the mouse and human sequences are distinct, a few points overlap. It may also be observed from the plot that the mouse sequences are more diverse than the human sequences which is in slight contrast with the lambda class where the human antibodies are more diverse than their murine counterparts. The graph for the heavy chains shows a virtually complete overlap of both murine and human antibodies. This also establishes that both human and murine heavy chains are equally diverse.



(a)



(b)



(c)

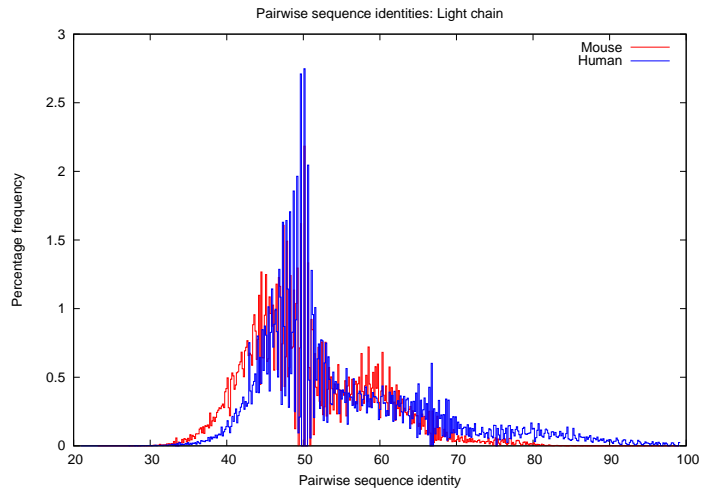
Figure 3.2: Plot of the standard deviation vs. the mean percentage identity of mouse and human sequences in (a) Light chain lambda class (b) Light chain kappa class and (c) Heavy chain.

3.3 A statistic to assess ‘humanness’ of antibody sequences

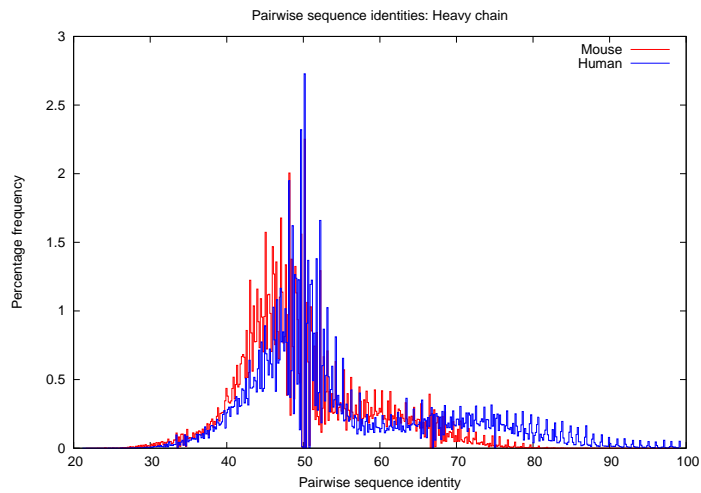
In the next section, I analysed sequences of antibodies belonging to various chains/classes in human and mouse to create a Z-score metric based on percentage sequence identity between antibody sequences. This shows distinct differences between human and mouse sequences. Based on mean sequence identity and standard deviation, I have calculated Z-scores for datasets of antibody sequences extracted from the Kabat database. I have applied the analysis to a set of humanized and chimeric antibodies including a number of sequences where data are available on anti-antibody responses, and to human germline sequences. The aim was to see whether this approach may aid in the selection of more suitable mouse variable domains for antibody engineering to render them more human.

3.3.1 Analysis of pairwise sequence identities

Initially, every human variable domain sequence was taken and compared with the variable domain of every other human antibody in the respective dataset (light or heavy chain, lambda or kappa class in the case of light chain sequences). The program *ssearch33* was used to generate pairwise alignments and the pairwise sequence identities were recorded. The same procedure was repeated for the mouse sequences i.e. every mouse sequence was compared with every human sequence in the respective dataset and the pairwise identities were recorded. The frequency distribution of the pairwise identities of the human and mouse sequences were

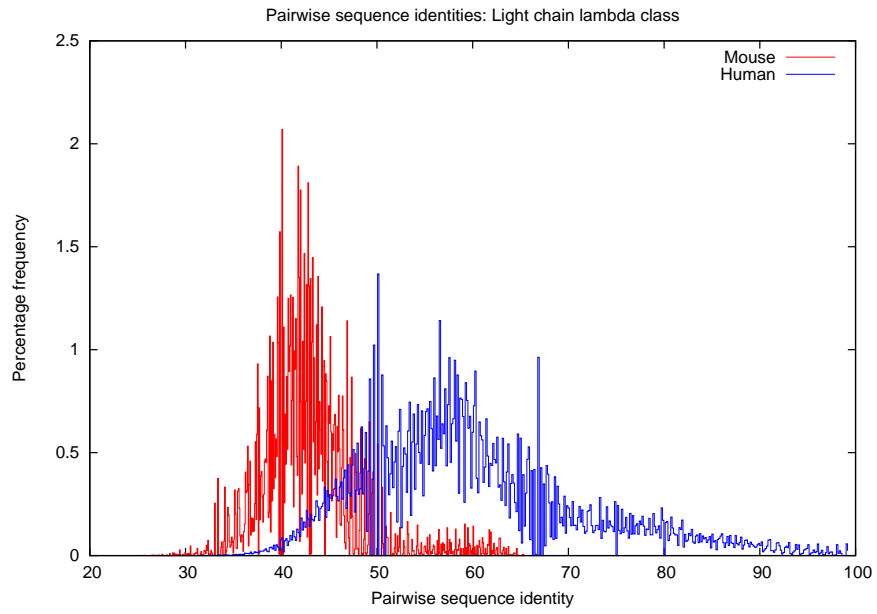


(a) Light

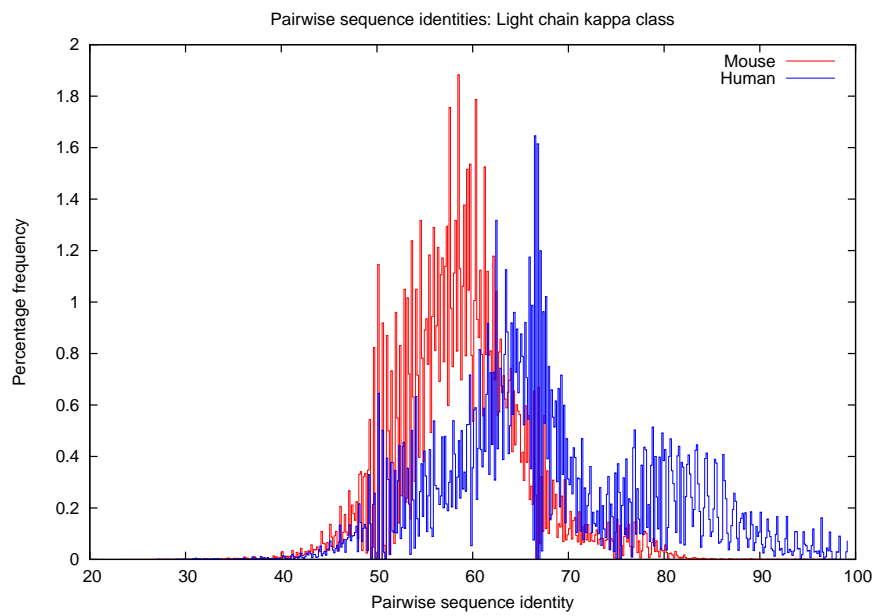


(b) Heavy

Figure 3.3: Histogram of human/human and mouse/human pairwise sequence identities in (a) light and (b) heavy chains.



(a) Lambda



(b) Kappa

Figure 3.4: Histogram of human/human and mouse/human pairwise sequence identities in a) lambda and b) kappa class light chains.

then plotted together. It must be noted that there are significant differences between the number of murine and human antibodies in the dataset for lambda and kappa class light chains. It was therefore decided to use the normalised percentage frequency. The normalised frequency is calculated by dividing the frequency by the total number of pairwise identities for the respective comparison. Figure 3.3 shows the frequency distribution of pairwise identities for human/human and mouse/human between the mouse and human light/heavy chain sequences. The graphs show that both mouse and human distributions are near-normal and they share peaks around 50% sequence identity when compared with human sequences.

Similarly, a graph was plotted to examine the lambda and kappa light chain classes separately (Figure 3.4). These plots separate the light chain classes with a more clear distinction between the mouse and human distributions. The histograms are near normal distributions with the human kappa light chains (Figure 3.4b) appearing to show two overlapping sub-classes. The human lambda class sequences as seen in Figure 3.4a have several peaks. However, the lowest human peak, which occurs at about 50% sequence identity, is still considerably higher than the murine peak, which occurs at about 41% sequence identity.

3.3.2 Analysis of mean sequence identities

This initial analysis provides a histogram of sequence identities for each antibody analysed. In the second stage, I replaced this with a mean sequence identity such that each antibody was represented by a single value. All antibody sequences

belonging to a given dataset were aligned with human sequences of the corresponding chain/class as above. The pairwise identity between every non-identical pair of sequences was then obtained. By calculating the mean sequence identity of a sequence scored against the set of human sequences, I obtain a value which represents how typical a sequence is of the human repertoire. I call this the ‘raw humanness’.

For each mouse antibody sequence, i , the mean is calculated as:

$$\mu_i = \sum_{j=1}^N P_{ij}/N \quad (3.3)$$

while the mean sequence identity for every human antibody is calculated as:

$$\mu_i = \sum_{j=1, j \neq i}^N P_{ij}/(N - 1) \quad (3.4)$$

where N is the number of sequences in the respective human dataset and P_{ij} is the pairwise sequence identity between the i 'th and the j 'th sequence in the query and target dataset respectively. The second equation uses $N - 1$ since both query and target database are the same and the human probe sequence is not compared against itself.

A ‘mean raw humanness’ ($\bar{\mu}$) can be calculated for each dataset:

Organism	Light chain	Heavy chain	Light chain lambda class	Light chain kappa class
Mouse	50.61	49.85	42.79	58.84
Human	55.21	55.01	59.93	67.57

Table 3.2: Mean raw humanness ($\bar{\mu}$) for each dataset.

$$\bar{\mu} = \sum_{i=1}^M \mu_i / M \quad (3.5)$$

where M is the number of sequences in the probe dataset (mouse or human).

Table 3.2 lists the calculated means for each dataset of sequences for human and mouse with respect to human. As expected, there are marked differences between the human and murine antibody datasets: the human sequences show higher average sequence identity than the murine sequences.

3.3.3 Z-Score analysis

Having obtained individual raw humanness scores (μ_i) and mean scores for each human dataset (human $\bar{\mu}$, Table 3.2), Z-scores were calculated as a form of normalisation. A Z-score indicates how many standard deviations above or below the mean a certain value is. Z-scores for both the mouse and human sequences were calculated with respect to the appropriate human distribution to assess the degree of divergence of each sequence from the human average. For the human sequences, these Z-scores are approximately normally distributed with a mean of zero. The Z-score was defined as the final measure of how typical a sequence is of the human repertoire. For simplicity, this was termed the ‘humanness’ (although

every human sequence is clearly 100% human). Thus a Z-score of zero represents a sequence which shows average similarity to the repertoire of human sequences. Positive Z-scores represent sequences which, on average, show higher sequence identity with other human sequences and negative Z-scores represent sequences with less typically human character.

The standard deviation, σ is calculated as:

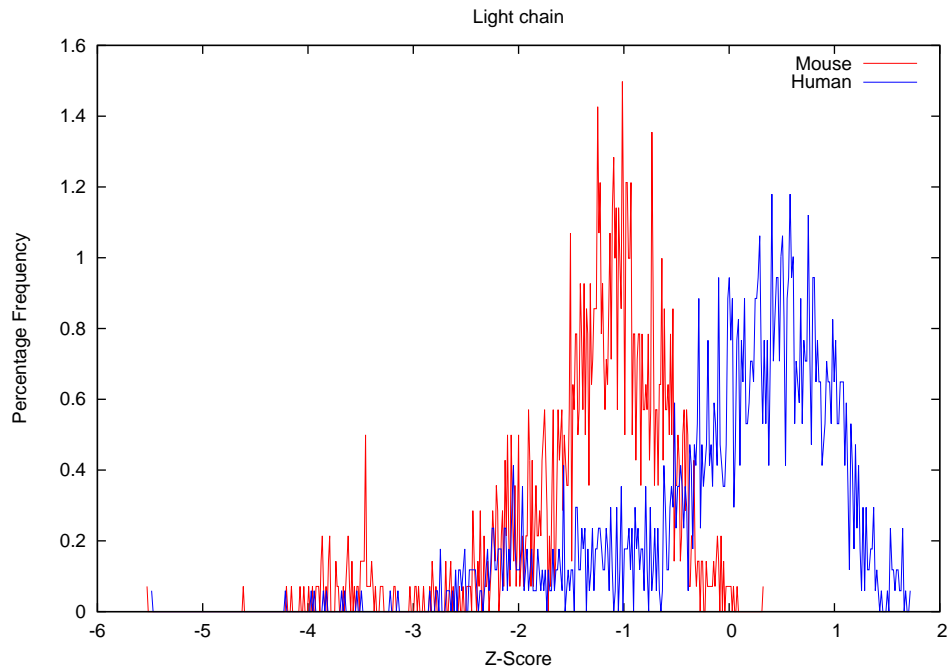
$$\sigma = \sqrt{\sum_{i=1}^M (\mu_i - \bar{\mu})^2 / M} \quad (3.6)$$

where μ_i is the ‘raw humanness’ of an individual sequence and $\bar{\mu}$ is the mean raw humanness of the human dataset.

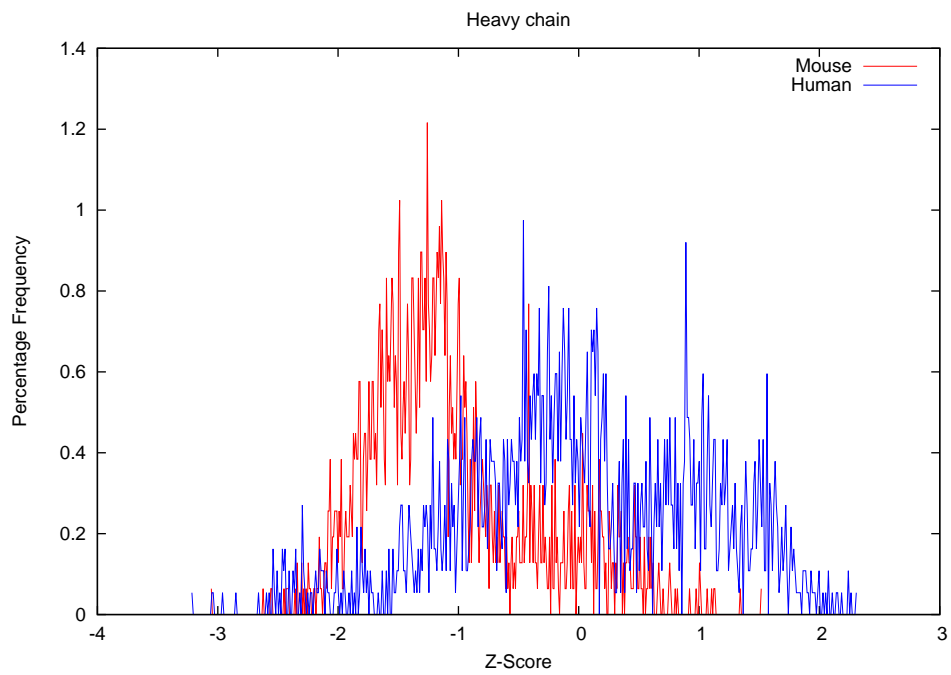
Finally, the Z-score of each sequence was calculated as:

$$Z_i = (\mu_i - \bar{\mu}) / \sigma \quad (3.7)$$

Z-scores were calculated for every dataset of the mouse and human sequences and the frequency distribution of the two were overlaid, as shown in Figures 3.5 and 3.6. The two plots show distinct differences between the mouse and the human distributions. Figure 3.6a appears slightly skewed as the number of mouse lambda class sequences is less than 10% of the number of human lambda class sequences (see Table 3.1). Although the mouse lambda class sequences are typically non-

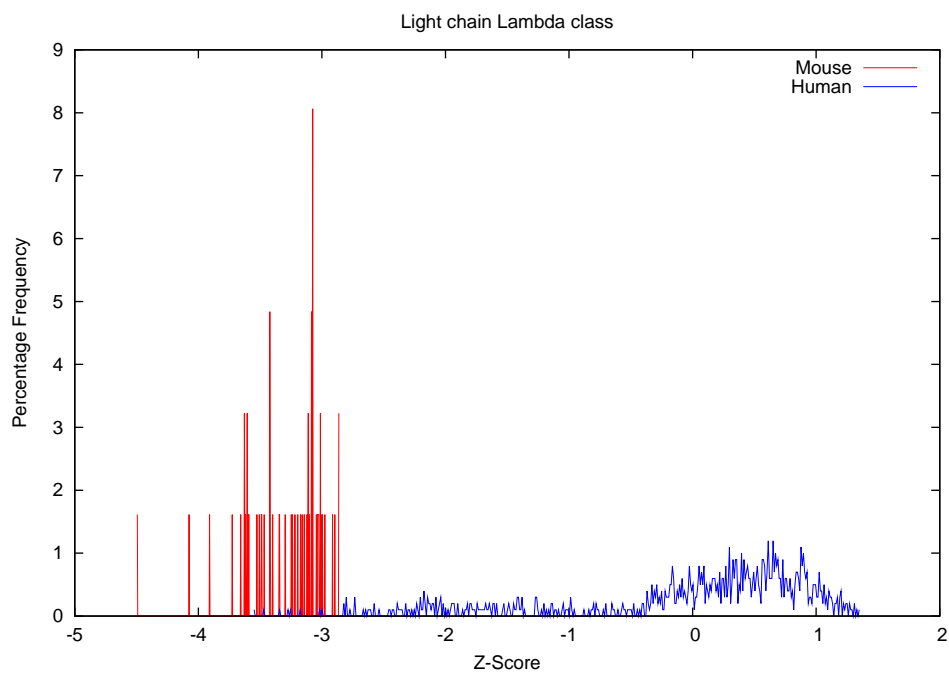


(a) Light chain

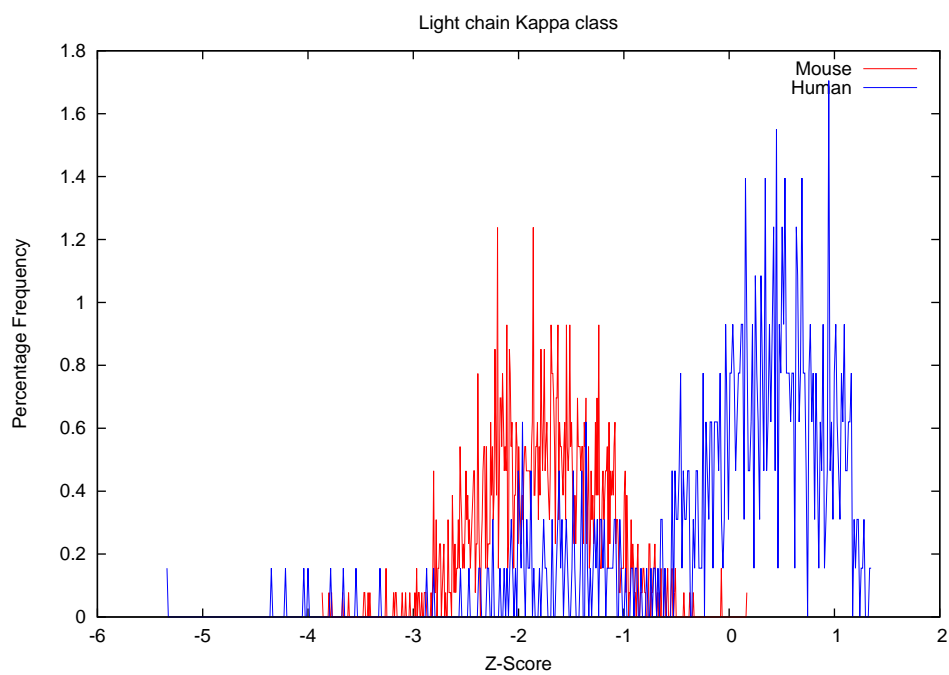


(b) Heavy chain

Figure 3.5: Z-score distribution for (a) Light chain (b) Heavy chain sequences.



(a) Lambda class



(b) Kappa class

Figure 3.6: Z-score distribution for (a) Light chain Lambda class and (b) Light chain Kappa class.

human, it can be seen that in general, there are significant overlaps between the mouse and the human plots. This indicates that many mouse sequences are more typically human than some human sequences.

3.3.4 Assessment of humanized antibodies

The methodology was applied to a small selection of humanized antibodies. Two papers reporting humanization of murine antibodies were identified from literature (Yazaki *et al.*, 2004; Roguska *et al.*, 1994). The humanness of the original murine antibody and the humanized antibody were calculated and compared.

Yazaki *et al.* (2004) have reported the humanization of *T84.66*, a murine antibody that binds with high affinity to the carcinoembryonic antigen (CEA) (Wagener *et al.*, 1983). They made two humanized antibodies *M5A* and *M5B* differing only in the sequence of the heavy chain. Roguska *et al.* (1994) have employed a technique called resurfacing where human surface residues are grafted onto a murine variable domain. Two ‘resurfaced’ antibodies *N901* and *B4* have been made using this procedure.

Table 3.3 gives the humanness scores for the original murine and the humanized antibodies. From the table, it can be observed that the humanness values for the humanized antibodies are clearly higher than those of the original murine donor antibodies. It must also be highlighted that in the case of *N901* produced by resurfacing, only two residues in the murine antibodies were replaced with their human counterparts in the light chain. Despite this, there is a small, yet

		Humanness Z-score (σ)		
		Murine	Humanized	Human
T84.66	Light	-1.847	-1.152	
	Heavy	-1.161	0.836(M5A) 0.464(M5B)	
N901*	Light	-1.929	-1.775	
	Heavy	0.110	0.728	
B4*	Light	-2.055	-1.762	
	Heavy	-1.686	-1.420	
HPC4 [†]	Light	-2.246	0.187	1.390
	Heavy	-2.413	0.135	1.875

Table 3.3: Results of applying the Z-score analysis to humanized antibodies. All light chain scores are in comparison with human light chain kappa class sequences. *Antibodies humanized by the resurfacing method of Roguska *et al.* (1994). [†]The human light chain sequence was the consensus for light chain κ subgroup I and the heavy chain was the consensus for human heavy chain subgroup III.

appreciable increase in the humanness score establishing the method's sensitivity even to small changes in sequence. This also shows that the human residues chosen by Roguska are generally typical of human antibodies and not just a small subset of human sequences. It must however be noted that the humanness scores of the humanized *T82.66* are higher than those of the resurfaced antibodies as the resurfaced antibodies are based on chimeric rodent variable domains rather than human variable domains.

3.3.5 Analysis of humanness of human immunoglobulin germline genes

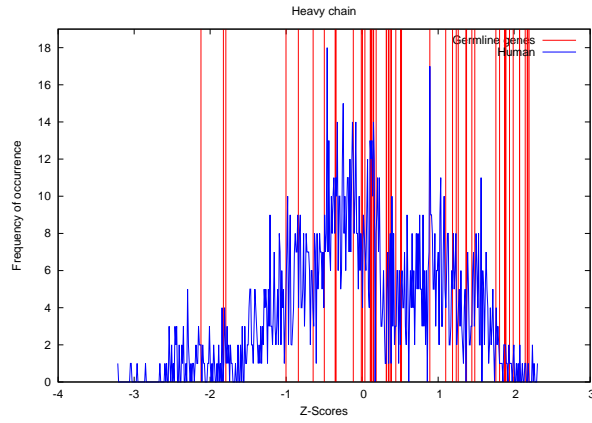
The method is also capable of identifying that humanized antibodies are 'less human' than the original human acceptor sequence. O'Connor *et al.* (1998) have reported the use of consensus sequences as human acceptors, selecting a consensus

Family	VBase Gene name	Humanness	Family	VBase Gene name	Humanness
V λ 1	13-7(A) 1a	0.40	V λ 3	11-7 3e	-0.17
V λ 1	14-7(A) 1e	1.17	V λ 3	11-7 3m	0.50
V λ 1	13-7(A) 1c	0.90	V λ 3	11-7 2-19	0.32
V λ 1	13-7(A) 1g	0.89	V λ 4	12-11 4c	-3.27
V λ 1	13-7(A) 1b	0.92	V λ 4	12-11 4a	-2.28
V λ 2	14-7(A) 2c	1.09	V λ 4	12-11 4b	-2.62
V λ 2	14-7(A) 2e	1.27	V λ 5	14-11 5e	-1.70
V λ 2	14-7(A) 2a2	1.02	V λ 5	14-11 5c	-1.91
V λ 2	14-7(A) 2d	1.24	V λ 5	14-11 5b	-2.38
V λ 2	14-7(A) 2b2	0.92	V λ 6	13-7(B) 6a	-0.34
V λ 3	11-7 3r	0.67	V λ 7	14-7(B) 7a	-2.39
V λ 3	11-7 3j	0.46	V λ 7	14-7(B) 7b	-2.26
V λ 3	11-7 3p	0.44	V λ 8	14-7(B) 8a	-1.27
V λ 3	11-7 3a	0.04	V λ 9	12-12 9a	-3.28
V λ 3	11-7 3l	0.19	V λ 10	13-7(C) 10a	-1.19
V λ 3	11-7 3h	0.42			

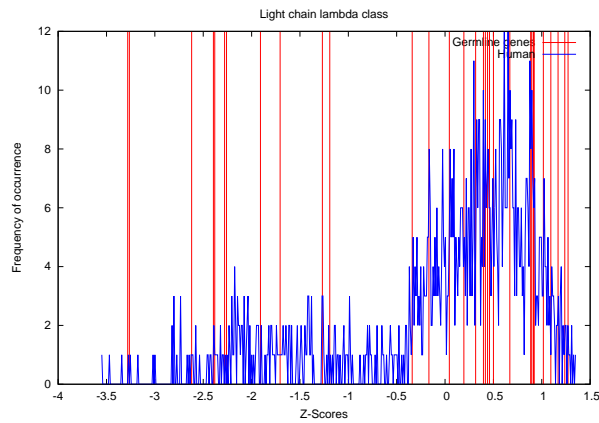
Table 3.4: Humanness scores for the lambda class germline genes.

human subgroup V κ I light chain and VH-III family heavy chain. Similarly, Hwang *et al.* (2005) selected germline-expressed sequences most similar to the mouse sequence, the rationale being that germline sequences would be expected to be non-immunogenic.

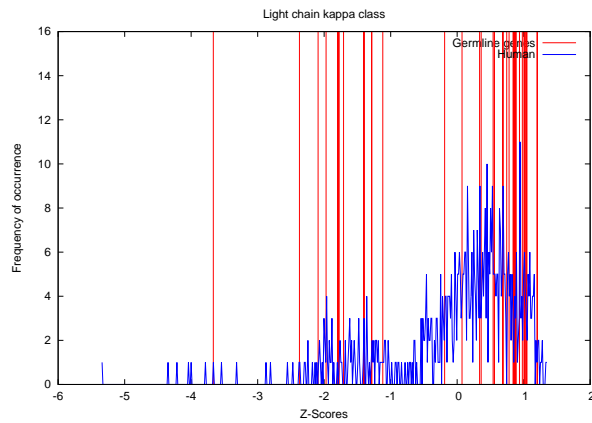
It is clear that some germline sequences tend to be used more frequently than others so, it was decided to examine the ‘humanness’ of human germline sequences. The amino-acid sequences of human V-region germline genes were extracted from VBase (<http://vbase.mrc-cpe.cam.ac.uk/>) and were queried against the database of expressed human antibodies to obtain their humanness scores. Table 3.7 gives the number of germline genes for λ and κ light chains, and heavy chain germline families. Figure 3.7 gives the plot of humanness score distributions of the germline genes shown as vertical lines. The humanness scores of individual germline genes are given in Tables 3.4–3.6.



(a) Heavy chain



(b) Light chain lambda class



(c) Light chain kappa class

Figure 3.7: Results of the Z-score analysis for human germline sequences. The germline sequences are indicated by vertical lines overlaid on the distribution of humanness scores for expressed human sequences.

Family	VBase	Gene name	Humanness	Family	VBase	Gene name	Humanness
V κ I	2-1-(1)	O12	1.20	V κ II	3-1-(1)	O1	-1.79
V κ I	2-1-(1)	O2	1.20	V κ II	4-1-(1)	A17	-1.97
V κ I	2-1-(1)	O18	0.56	V κ II	4-1-(1)	A1	-2.09
V κ I	2-1-(1)	O8	0.56	V κ II	4-1-(1)	A18	-1.71
V κ I	2-1-(U)	A20	0.78	V κ II	4-1-(1)	A2	-1.77
V κ I	2-1-(1)	A30	0.34	V κ II	4-1-(1)	A19	-1.40
V κ I	2-1-(1)	L14	-0.19	V κ II	4-1-(1)	A3	-1.40
V κ I	2-1-(1)	L1	0.89	V κ II	4-1-(1)	A23	-2.37
V κ I	2-1-(1)	L15	0.75	V κ III	6-1-(1)	A27	1.05
V κ I	2-1-(1)	L4	1.02	V κ III	6-1-(1)	A11	0.87
V κ I	2-1-(1)	L18	1.02	V κ III	2-1-(1)	L2	0.94
V κ I	2-1-(1)	L5	0.84	V κ III	2-1-(1)	L16	0.94
V κ I	2-1-(1)	L19	0.84	V κ III	2-1-(1)	L6	1.04
V κ I	2-1-(1)	L8	0.86	V κ III	2-1-(U)	L20	0.98
V κ I	2-1-(1)	L23	0.36	V κ III	6-1-(1)	L25	1.00
V κ I	2-1-(1)	L9	0.69	V κ IV	3-1-(1)	B3	0.07
V κ I	U-1-(1)	L24	0.54	V κ V	2-1-(1)	B2	-3.67
V κ I	2-1-(1)	L11	0.68	V κ VI	2-1-(1)	A26	-1.28
V κ I	2-1-(U)	L12	1.04	V κ VI	2-1-(1)	A10	-1.28
V κ II	3-1-(1)	O11	-1.79	V κ VI	2-1-(1)	A14	-1.12

Table 3.5: Humanness scores for the lambda class germline genes

In general, it can be seen that the germline genes correspond to peaks in the distributions. Some germline genes are more typical of the expressed human repertoire than some others. Each germline falls within a cluster of humanness scores reflecting the relative frequency with which they are used in the expressed human repertoire; some families are also seen to overlap. The VH-III, V κ III (and some of V κ I) and V λ 2 (and some V λ 1) are families that have very high Z-scores and thus are likely to be the germline families from which the high-scoring expressed human sequences are derived.

Choosing germline sequences as the basis for humanization from one of the high-scoring sequences is likely to be more effective than choosing germline sequences from one of the low scoring sequences. This is because a large number of expressed

Family	VBase Gene name	Humanness	Family	VBase Gene name	Humanness
VH-I	1-3 1-02	0.04	VH-III	1-3 3-43	1.44
VH-I	1-3 1-03	0.12	VH-III	1-3 3-48	1.81
VH-I	1-3 1-08	-0.34	VH-III	1-U 3-49	0.89
VH-I	1-2 1-18	0.00	VH-III	1-1 3-53	1.87
VH-I	1-U 1-24	-0.50	VH-III	1-3 3-64	1.76
VH-I	1-3 1-45	-0.84	VH-III	1-1 3-66	2.18
VH-I	1-3 1-46	0.38	VH-III	1-4 3-72	1.19
VH-I	1-3 1-58	-0.64	VH-III	1-4 3-73	1.10
VH-I	1-2 1-69	0.15	VH-III	1-3 3-74	1.94
VH-I	1-2 1-e	0.32	VH-III	1-6 3-d	1.24
VH-I	1-2 1-f	-0.36	VH-IV	2-1/1-1 4-04	0.44
VH-II	3-1/2-1 2-05	-2.12	VH-IV	2-1 4-28	0.14
VH-II	3-1 2-26	-1.83	VH-IV	3-1 4-30.1	0.35
VH-II	3-1 2-70	-1.79	VH-IV	3-1 4-30.2	0.11
VH-III	1-3 3-07	1.88	VH-IV	3-1 4-30.4	0.38
VH-III	1-3 3-09	1.36	VH-IV	3-1 4-31	0.35
VH-III	1-3 3-11	1.99	VH-IV	1-1 4-34	-0.01
VH-III	1-1 3-13	1.26	VH-IV	3-1 4-39	0.12
VH-III	1-U 3-15	1.48	VH-IV	1-1 4-59	0.52
VH-III	1-3 3-20	1.37	VH-IV	3-1 4-61	0.38
VH-III	1-3 3-21	1.89	VH-IV	2-1 4-b	0.50
VH-III	1-3 3-23	2.17	VH-V	1-2 5-51	0.18
VH-III	1-3 3-30	2.07	VH-V	1-2 5-a	0.32
VH-III	1-3 3-30.3	2.20	VH-VI	3-5 6-01	-1.00
VH-III	1-3 3-30.5	2.07	VH-VII	1-2 7-4.1	-0.12
VH-III	1-3 3-33	2.15			

Table 3.6: Humanness scores for the heavy chain germline genes.

VBase Gene Family	Number
<hr/> Light chain – λ class <hr/>	
VL1	5
VL2	5
VL3	9
VL4	3
VL5	3
VL6	1
VL7	2
VL8	1
VL9	1
VL10	1
<hr/> Light chain – κ class <hr/>	
VK1	19
VK2	9
VK3	7
VK4	1
VK5	1
VK6	3
<hr/> Heavy chain <hr/>	
VH1	11
VH2	3
VH3	22
VH4	11
VH5	2
VH6	1
VH7	1

Table 3.7: Number of V-region genes in Lambda and Kappa class light chain and heavy chain germline families.

Antibody	AAR	Light chain	Heavy chain	Notes
Humanized				
Zenapax	34%	-0.129	-0.136	Immuno-suppressant action
HuBrE-3	14%	-1.811	0.252	Patients may be immuno-suppressed
Synagis	1%	-0.497	-1.708	Neonatal
Herceptin	0.1%	0.462	0.965	Patients may be immuno-suppressed
Hu-A33	17%	-0.401	0.850	Patients may be immuno-suppressed
Xolair	0.1%	0.309	0.657	
Campath-1H	1.9%	-0.009	-0.564	Patients may be immuno-suppressed
Chimeric				
Infliximab	61%	-2.237	-0.684	Immuno-suppressant action
Rituximab	0%	-1.813	-1.350	Patients may be immuno-suppressed
ch14.18	0%	-1.829	-1.605	Patients may be immuno-suppressed
U36	40%	0.135	1.308	Patients may be immuno-suppressed
Fully human				
Humira	12%	0.874	0.886	Immuno-suppressant action

Table 3.8: Anti-antibody response (AAR, expressed as a percentage of patients who showed a response — data taken from Hwang and Foote (2005) and from full prescribing information of antibodies approved for therapy) and humanness scores for seven humanized and four chimeric antibodies. All light chains were of the κ class.

sequences similar to the high-scoring germlines is observed in the human repertoire and these may be less likely to be immunogenic. Highly used frameworks will have been ‘seen’ by the immune system in the context of different CDR regions (after somatic hypermutation). This will make it likely that peptides derived from these antibodies have previously been seen and tolerated by the immune system. It is not known why some germline sequences are used more frequently than others, but one possibility is that variations on the less commonly observed germlines leads to higher immunogenicity and B-cells producing these antibodies are rapidly eliminated from the body.

Antibody name	Reference for sequence
Infliximab	USP 6284471
Rituximab	2B8
ch14.18	USP 6969517
Re-labelled Chimeric U36	USP 6972324
Zenapax	(Queen <i>et al.</i> , 1989)
Hu-BrE-3	(Couto <i>et al.</i> , 1994)
Synagis	(Johnson <i>et al.</i> , 1997)
Herceptin	(Carter <i>et al.</i> , 1992)
Humira	USP 6509015
Campath-1H	(James <i>et al.</i> , 1999)
Hu-A33	USP 5773001

Table 3.9: Table listing clinical antibodies and the references containing their sequence. Abbreviation *USP* stands for US Patent.

3.3.6 Correlating immunogenicity with humanness

I further investigated the potential of the humanness score as a predictor of anti-antibody response (AAR). Recently, Hwang and Foote (2005) reviewed reported AAR data against murine, chimeric and humanized antibodies and classified the responses as *negligible* ($< 2\%$), *tolerable* (2–15%) and *marked* ($> 15\%$). As expected, they found that the change from mouse to chimeric antibodies leads to the greatest reduction in immunogenicity, while humanization leads to a further decrease. Their paper provides a summary table which reports the percentage of patients suffering an anti-antibody response. I attempted to obtain sequence data for the antibodies described. Despite searches of the original literature and patent data (both from the original patents and the patent sequence data available through the SRS server at the EBI, <http://srs.ebi.ac.uk/>, and the IMGT list of monoclonal antibodies with clinical indications, <http://imgt.cines.fr/textes/IMGTrepertoire/GenesClinical/monoclonalantibodies/>), it proved dif-

difficult to obtain sequence data for more than a handful of the antibodies. A list of clinical antibodies and the source of their sequences is shown in Table 3.9.

These sequences were tested using the humanness assessment and humanness scores are listed in Table 3.8. The results are very difficult to interpret as there are a number of other factors that may contribute to the AAR. In particular, as shown in the table, patients may be immuno-compromised as the result of other treatments (many of the antibodies are used in cancer therapy) and the antibody itself may have an immuno-suppressant action. Nonetheless, in the case of the humanized antibodies it can be seen that the sequence with the best humanness scores (Herceptin) results in virtually no AAR while the worst individual humanness score (Infliximab) results in the worst AAR. To investigate the relationship between humanness and AAR further, I decided to plot the variation of AAR against the following variables:

- Light chain humanness score.
- Heavy chain humanness score.
- Mean humanness score of the light and heavy chain.
- Maximum humanness score between the light and heavy chain.
- Minimum humanness score between the light and heavy chain.

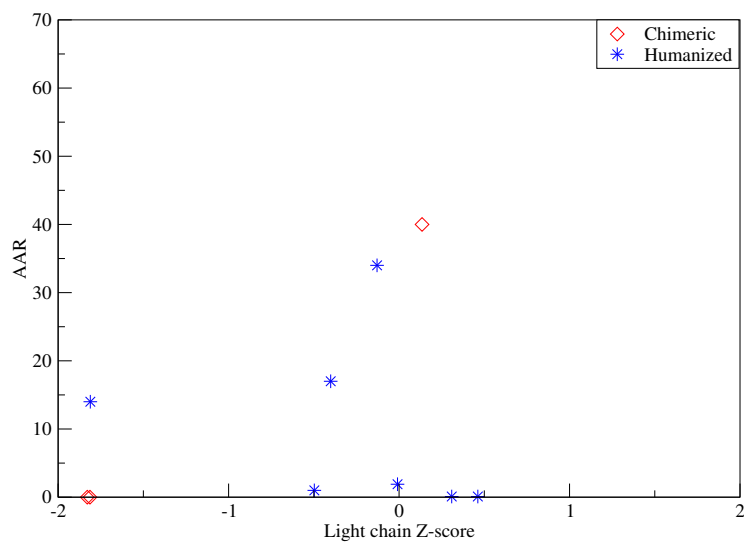
The graphs for these variations are shown in Figures 3.8 and 3.9. Averaging the humanness scores for light and heavy chains for each humanized antibody and calculating the Pearson's correlation coefficient with AAR values showed no

Type	Pearson's correlation coefficient (r)	
	Humanized	Chimeric
Light	-0.290	0.144
Heavy	0.105	0.576
Mean	-0.090	0.408
Min	-0.029	0.144
Max	-0.169	0.577

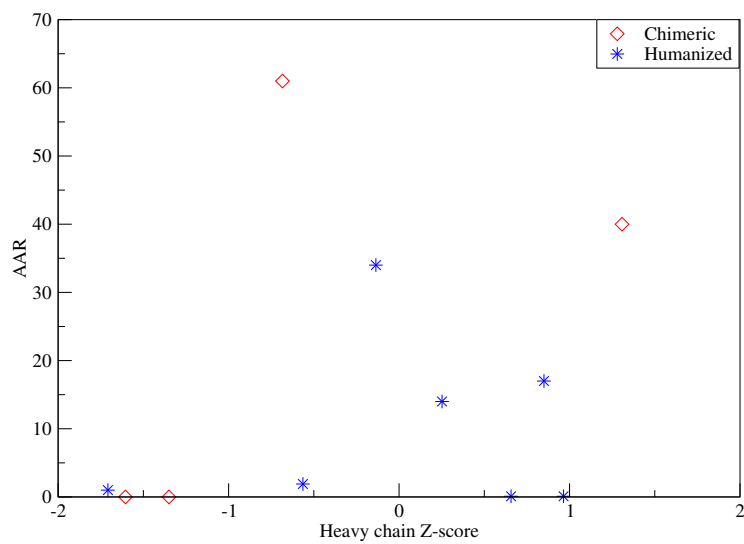
Table 3.10: Correlation coefficient between the AAR and humanness scores of the antibodies approved for therapy. A negative correlation coefficient implies that the AAR decreases as the humanness score increases.

significant correlation ($R=-0.09$). In contrast, amongst the chimeric antibodies, the most typically human antibody, U36 (an anti-CD44 v6-domain antibody) leads to the second highest AAR and surprisingly, there is a positive correlation ($r = 0.50$). Table 3.10 summarises the correlation coefficients between AAR and the different categories of Z-scores described earlier. Clearly there is a very limited amount of data and the interpretation of the data is complex. From preliminary investigations, there does not appear to be a direct relationship between AAR and Humanness scores of the therapeutic antibodies (Table 3.8).

Surprisingly Humira, the first ‘fully human’ antibody (generated by phage display) to be approved for use in therapy is not any less immunogenic than the humanized antibodies. Immunogenicity data indicate that 12% (Hwang and Foote, 2005) of people who were repeatedly injected with the drug without an adjuvant developed neutralising antibodies. This was lower (1%) when Humira was administered with Methotrexate. Humanness scores for Humira were 0.874 (Light chain Kappa class) and 0.886 (Heavy chain). While these scores are quite high, there are similar (and in some cases higher) scores amongst the humanized and chimeric antibodies.

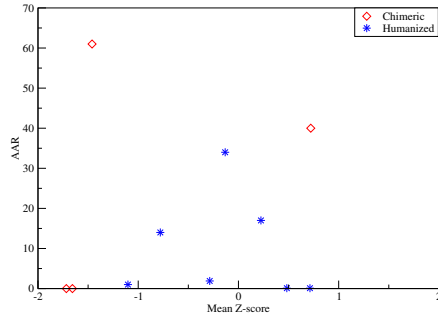


(a)

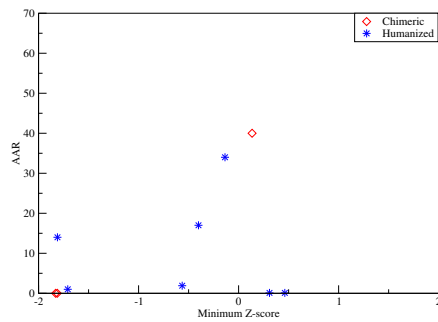


(b)

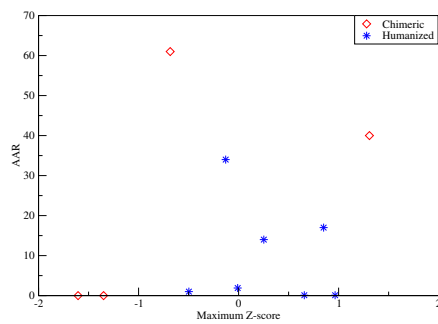
Figure 3.8: Figure showing the variation of AAR percentages for the chimeric and humanized antibodies against (a) light chain and (b) heavy chain humanness scores.



(a)



(b)



(c)

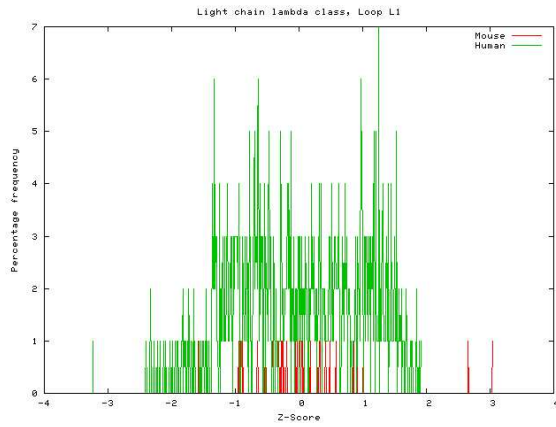
Figure 3.9: Variation of AAR percentages for chimeric and humanized antibodies against (a) Mean (b) Minimum and (c) Maximum humanness scores.

In conclusion, while (with the limited data available) there does not appear to be a correlation between humanness and AAR, as stated above, it is worth noting that the least human individual chain also led to the worst AAR while the antibody with the highest humanness led to the lowest AAR.

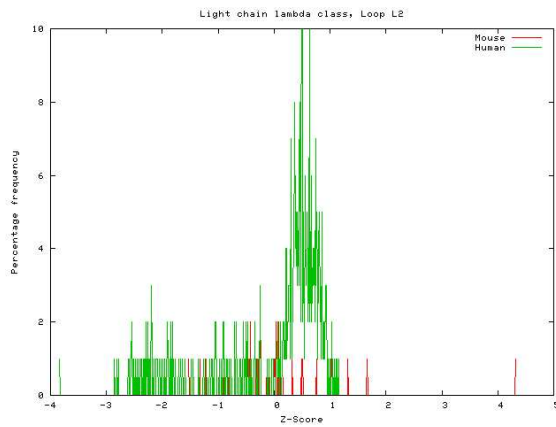
3.4 Assessing humanness of antibody CDRs

While it is largely assumed that human antibodies are not immunogenic, it has been shown that this is not necessarily the case (Macias *et al.*, 1999). As Clark (2000) points out, every antibody has a unique idiootype encoded by the hypervariable regions and even fully human antibodies may elicit an immune response. This ‘HAHA’ (Human Anti-Human Antibody) response is a concept familiar to immunologists as the ‘network hypothesis’ in which every antibody provokes another anti-idiotypic antibody to regulate the immune response (Jerne, 1974).

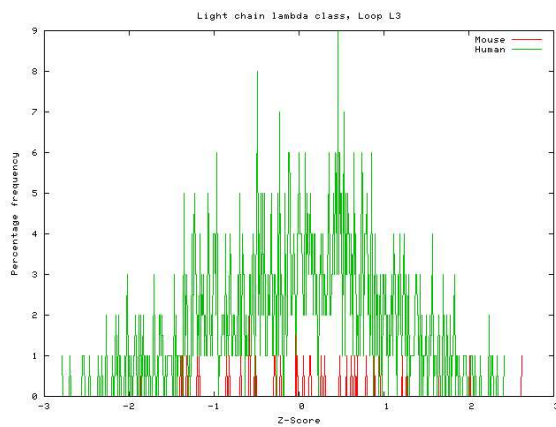
Based on this assumption, I decided to investigate the humanness of the CDRs alone in a similar way (the work described above included both the framework regions and the CDRs). Sequences of antibody CDRs were extracted from the July 2000 release of the Kabat database using *KabatMan* and the sequences were split into 3 sets based on chain/class (heavy, lambda, and kappa) and species (murine and human). Humanness of the CDRs was evaluated in two ways: first, the individual CDRs of murine and human antibodies were compared. In the second stage, the three CDRs for each dataset were concatenated and compared together using *ssearch33* as above to calculate pairwise identities.



(a) CDR-L1

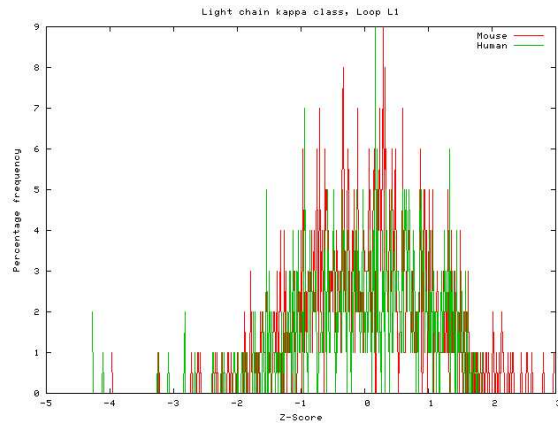


(b) CDR-L2

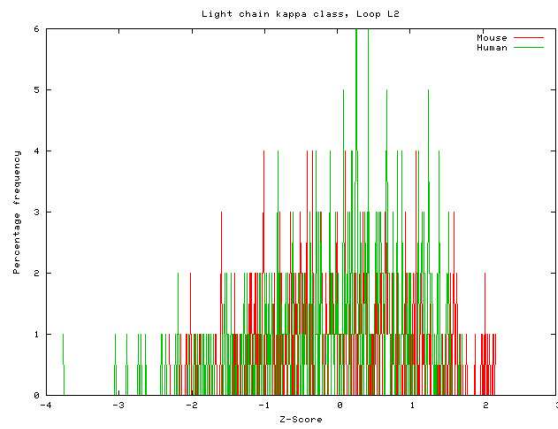


(c) CDR-L3

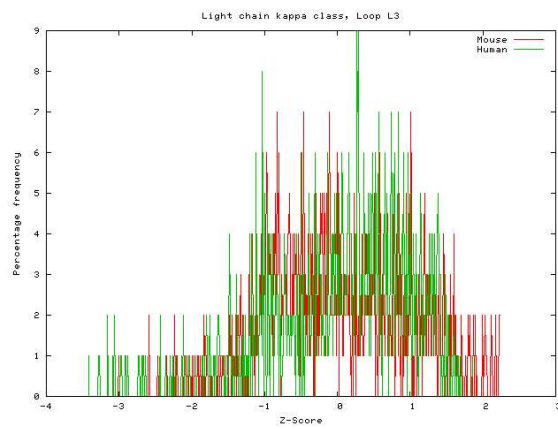
Figure 3.10: Z-score distribution for CDRs in the lambda class light chain (a) CDR-L1 (b) CDR-L2 (c) CDR-L3.



(a) CDR-L1

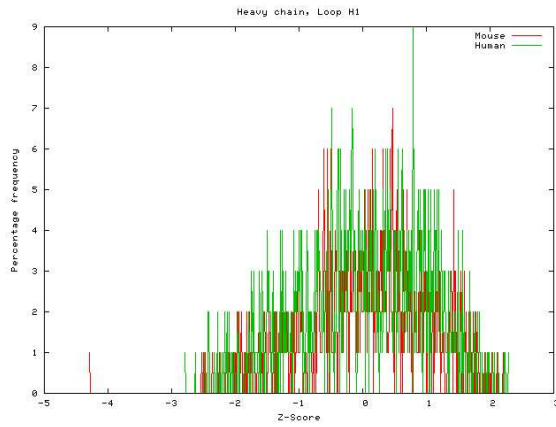


(b) CDR-L2

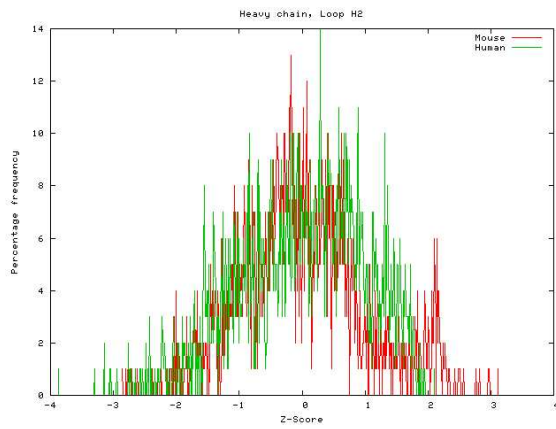


(c) CDR-L3

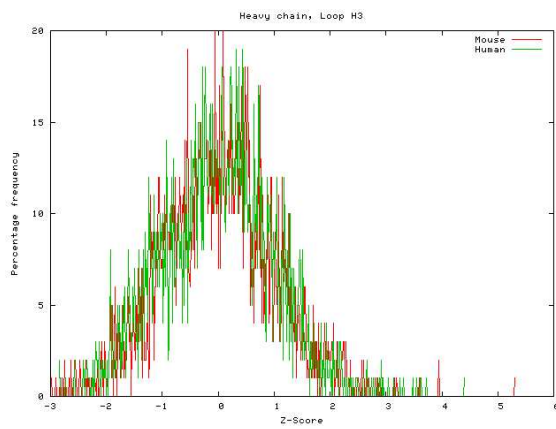
Figure 3.11: Z-score distribution for CDRs in the kappa class light chain (a) CDR-L1 (b) CDR-L2 (c) CDR-L3.



(a) CDR-L1



(b) CDR-H2



(c) CDR-H3

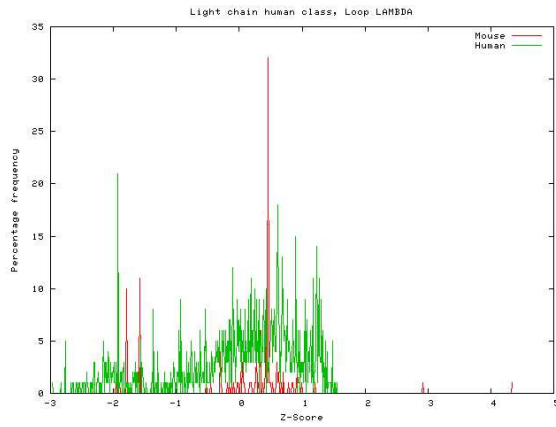
Figure 3.12: Z-score distribution for CDRs in the heavy chains. (a) CDR-H1 (b) CDR-H2 (c) CDR-H3.

The plots comparing the Z-Scores of the individual murine CDRs with the human CDRs are shown in Figures 3.10, 3.11 and 3.12 for the light chain lambda and kappa classes and the heavy chain respectively. It may be seen that the human and mouse plots overlap almost completely in all the CDRs suggesting that they are very similar in both species. While calculating humanness, percentage identity must be calculated over long stretches of sequence as short sequence alignments may be incorrect and skew the measure of percentage identity. As CDRs vary considerably in length (see Table 4.9 on page 154) and it was therefore decided that humanness of the CDRs would be reassessed by concatenating their sequences instead of treating them independently.

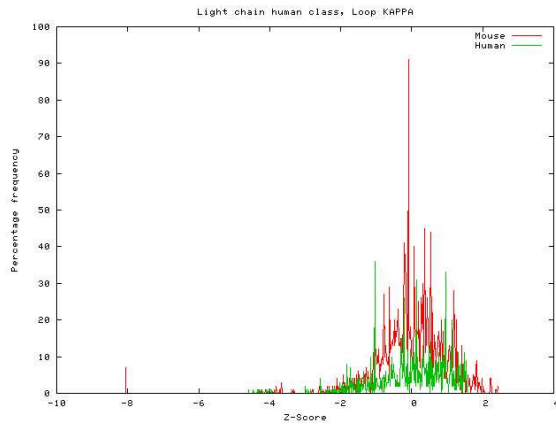
The plots for the concatenated CDRs for each dataset are shown in Figure 3.13. From the plots, it is clear that there is almost a complete overlap between the mouse and human plots. From the individual CDR plots and the concatenated plots, it can be seen that the mouse and human CDRs are not very different and that the main differences appear to be encoded in the framework regions.

3.5 Discussions and conclusions

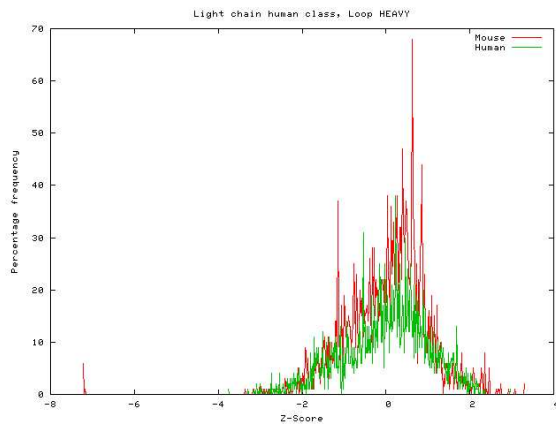
The use of Z-scores allows a normalised ‘humanness’ score to be assigned to an antibody sequence. While, by definition, it is the case that every human sequence is 100% human, this analysis shows very clearly that some human sequences are more typical of the human repertoire (as sampled in the Kabat database) than other sequences. The fact that differences in ‘humanness’ can be detected between



(a) Lambda class light chain



(b) Kappa class light chain



(c) Heavy chain

Figure 3.13: Z-score distribution for the concatenated CDRs (a) Lambda class light chain (b) Kappa class light chain (c) Heavy chains.

humanized antibodies and the human acceptor sequences used in the humanization indicates that the CDRs play an important role in the overall humanness score. Nonetheless, looking at the CDRs out of context of the framework shows little difference in humanness of mouse and human CDRs.

Of course there are many other factors that may contribute to immunogenicity. For example, the nature of the target, whether it is endocytosed or not, the aggregation state and formulation of the antibody, the patient's genetic background, disease state, etc. However, the notion of typically human antibodies has been exploited elsewhere. As described above, an approach to humanization had been described by Hwang *et al.* (2005) which involves selecting germline-expressed sequences most similar to a human germline sequence. Using the repertoire of expressed sequences rather than the germline provides a more realistic sample of circulating antibodies.

Thus while there may be no means to abolish an anti-idiotypic anti-antibody response completely (given that mouse and human CDRs are very similar), measures can be taken to minimise the likelihood of the framework leading to a response. It is reasonable to assume that an antibody which is more typical of the human repertoire will be less likely to be immunogenic than a sequence which is less typical. Analysis indicates that a significant number of mouse antibodies are more human-like than many human antibodies.

In a recent Phase I drug trial, six healthy volunteers were injected with a humanized anti-CD28 antibody, TGN1412 (Hopkin, 2006). This led to a massive and life-threatening immune response in all six subjects. Initially it was not known whether this was the result of severe anaphylactic shock induced by TGN1412 it-

self, or whether the mode of action of the antibody in binding to CD28 induced a ‘cytokine storm’. The TGN1412 sequence was obtained from US Patent Application 20060008457 and showed humanness scores of 0.48 (light) and -0.85 (heavy). The light chain has a similar humanness score to the best humanized antibody shown in Table 3.8 (Herceptin), while the heavy chain is much higher than the score for Synagis. Both of these antibodies are very well tolerated. Thus, before more information on the mode of action of TGN1412 became available, we were able to conclude that it was unlikely that the immune response seen in the six volunteers was a reaction to the humanized antibody itself.

Our analysis of correlations between humanness scores and anti-antibody responses (Table 3.8) was very limited because finding sequence data for antibodies where AAR data are available was a near-impossible task. While the small sample is probably statistically insignificant, it appears that humanness score does show some correlation with reduced AAR amongst the humanized antibodies, but not amongst the chimerics. Clearly there is a lot more involved in immunogenicity than the simple similarity to the human repertoire and it seems likely that there are specific features within some mouse sequences that render them visible to the human immune system. I therefore analysed all the sequences in Table 3.8 with the T-cell epitope prediction server, SYFPEITHI (Rammensee *et al.*, 1999), to discover whether antibodies leading to a marked anti-antibody response showed a higher concentration of likely T-cell epitopes. In fact, no differences were found between the immunogenic and non-immunogenic antibodies.

The process of humanization has usually involved the selection of a human antibody that has a high sequence identity with the murine donor antibody from

which the CDR sequences are taken (Queen *et al.*, 1989). This is done to maximise the chances of obtaining good binding. However, in some cases, such humanized antibodies still show significant AAR. As described above, an alternative strategy has been to use germline sequences (Hwang *et al.*, 2005), or consensus sequences derived from germline sequences (1998; 1992) as the human acceptors. The efficacy of using consensus human sequences in obtaining good binding has been compared with selecting the most similar human sequence (Kolbinger *et al.*, 1993; Sato *et al.*, 1994) and these studies show that, while both methods give similar results, the use of the human acceptor sequence with the best sequence identity gives somewhat better binding. There has been no direct comparison of the efficacy of the methods in avoiding AAR. The strategy of using (consensus) germline sequences as acceptors is designed to maximise the human nature of the acceptor sequence in the hope that this will be less likely to elicit an anti-antibody response, even if more mouse donor residues need to be introduced into the framework to obtain good binding. Our analysis of germline sequences indicates that certain germline families and specific genes within these families give higher humanness scores and are therefore more representative of observed expressed antibodies.

As described above, selecting a human acceptor framework on the basis of sequence similarity with the mouse donor may give better binding than selecting a (consensus) germline sequence. Of course, there is a trade-off between good binding and AAR. Poorer binding may mean that more antibody has to be administered thus increasing the amount of AAR. Germline, or expressed, human antibodies with high positive Z-scores may be good candidates for use as acceptor sequences in humanization to minimise the chance of AAR. It may be possible to select human acceptor sequences which balance sequence identity with the mouse

donor (to optimise binding) and the humanness score (to reduce AAR).

One possible problem with the method is that humanness has been evaluated based on average similarity to the human repertoire as sampled by the Kabat database. It could therefore be biased simply by the selection of sequences which appear in the database, or by the frequency of occurrence of particular antigens. However, the fact that the consensus human sequences used by O'Connor *et al.* (1998), and certain germ-line sequences, obtain very high humanness scores suggests that bias in the selection of antibodies in Kabat is not a problem.

Recent work by an undergraduate project student (Michael Eckett) using IMGT sequence data suggests that bias in the smaller Kabat dataset is not a problem.

In conclusion, the method I propose allows antibodies from any species to be screened for their similarity to the expressed human repertoire (their 'humanness'). This gives us a tool which may be used to investigate the importance of humanness in triggering an anti-antibody response. The method suggests a modified strategy for selecting human frameworks for humanization and may contribute towards predicting chimeric antibodies with low antigenicity.

Chapter 4

An automatic method for applying numbering to antibodies: Analysis and applications

In the analysis of protein sequence and structure, having a standardised numbering scheme allows comparison of features without explicit alignment. A numbering scheme defines standard positions in the sequence and possibly in relation to structure. Numbering of antibodies was first established by Kabat and Wu (1983) who analysed antibodies for variability of residues at various positions in the sequence (Wu and Kabat, 1970). They established that certain regions in the antibody sequence are more variable than others and termed these hypervariable regions as

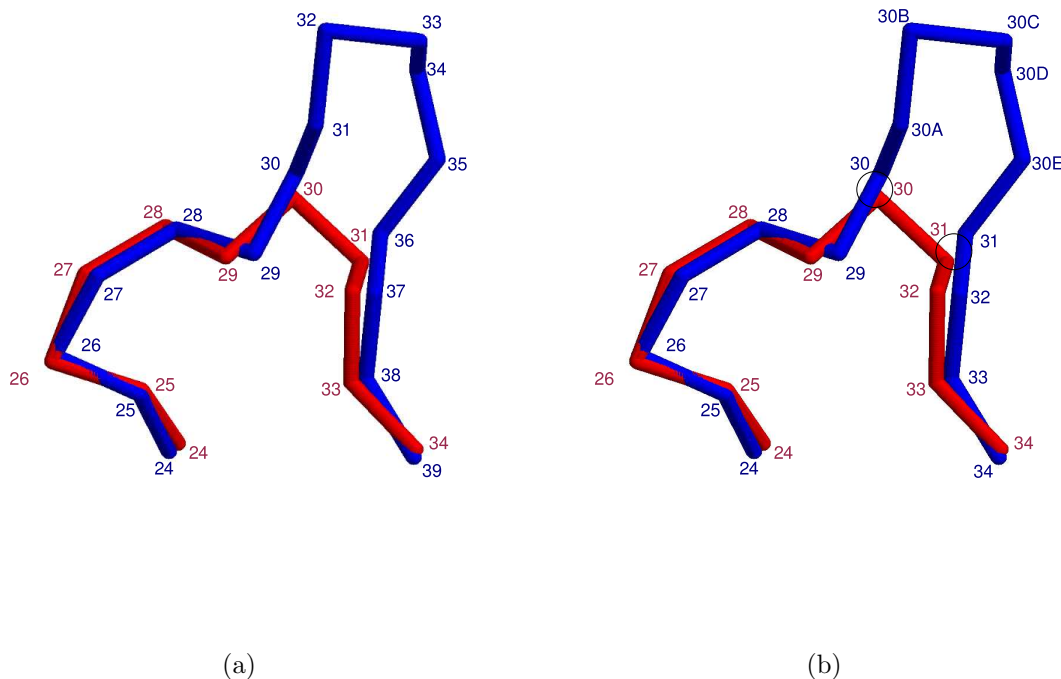


Figure 4.1: Two CDR-L1 loops fitted using rigid body superposition. The short loop (in red) is 11 residues long while the long loop (in blue) is 16 residues. (a) The numbers give the sequential numbering of residues in the loops (24-34 for the short loop, 24-39 for the long loop) (b) The two CDR-L1 loops numbered so that structurally equivalent residues have the same number.

‘Complementarity Determining Regions’ (or CDRs) which they predicted would interact with the antigen.

This initial analysis has been expanded by other groups leading to the development of several numbering schemes. Figure 4.1 explains the concept of numbering in antibodies. The figure shows CDR-L1 from the light chains of two different antibodies structurally fitted to one another. The shorter loop (coloured in red) is 11 residues long while the longer loop (in blue) is 16 residues long. If the residues are numbered sequentially, then the numbering is as indicated in the Figure 4.1a.

However, from Figure 4.1b, it can be seen that the residues highlighted by the grey circles are structurally equivalent and it would be appropriate to assign the same number to such residues. Therefore in a structurally correct numbering scheme, the protrusion in the longer loop is regarded as an insertion at position L30 and residues in this protrusion are numbered L30A, L30B, L30C, L30D, and L30E. (The prefix L is used to indicate the light chain.)

As stated above, a standardized numbering scheme for antibodies was first introduced by Wu and Kabat (1970). This numbering scheme was derived on the basis of sequence alignments when no structural information for antibodies was available. Chothia and Lesk (1987) examined the structures of antibody variable domains and showed that the sites of insertions and deletions (indels) in CDRs L1 and H1 suggested by Kabat on the basis of sequence were not structurally correct leading to the introduction of the Chothia numbering scheme. Unfortunately in 1989 (Chothia *et al.*, 1989), the numbering scheme was erroneously changed but in 1997 (Al-Lazikani *et al.*, 1997), the structurally correct numbering scheme originally proposed in 1987 was reintroduced. Since then, two further schemes have been introduced. The IMGT numbering scheme (Lefranc *et al.*, 2003) tries to unify numbering for antibody light and heavy chains with T-cell receptor α and β chains. However, since IMGT is predominantly a DNA database, the numbering stops at the end of the region encoded by the V-gene segment. The AHo numbering scheme (Honegger and Plückthun, 2001) extends the IMGT numbering scheme into CDR-3 and framework 4 in the antibody variable region. Both IMGT and AHo schemes accommodate indels by allowing sufficiently long gaps so that all known sequences may be numbered without insertion letters (e.g.: 30A). Nonetheless, it is possible in future that unusual antibodies with extremely long

insertions will be identified which cannot be numbered using these schemes. While a common scheme for light and heavy chains and T-cell receptors has a certain elegance, the practical applications are less obvious. It remains true that immunologists tend to continue to use the Kabat scheme while those interested in structural analysis use the Chothia scheme.

Thus far however, there has been no resource whereby numbering of an antibody sequence can be performed automatically and accurately. In this chapter, two methods to number antibody sequences automatically are described. Section 4.1 describes a method that uses pairwise sequence alignments to number an antibody sequence. This was a refinement of a method previously developed by Dr. A. C. R. Martin. The target antibody sequence is aligned with a sequence representing the consensus pattern of an antibody sequence and based on the alignment, the target antibody sequence is numbered. Section 4.2 describes a more rigorous and accurate method that uses profiles to fix anchor points in the antibody sequence and then numbers the framework regions and the loops independently. A web-server for this program has also been made available via the webpage at <http://www.bioinf.org.uk/abs/abnum/>.

I assessed the performance of the numbering method (Section 4.3) by comparison with numbering annotations in the last publicly available release of the Kabat database (July 2000) (Johnson and Wu, 2001). From this analysis, several significant errors have been identified in the manual Kabat annotations and this automated numbering method can be used to rectify these errors. A further interesting outcome of this analysis has been the correction of insertion and deletion positions in the framework regions of the antibody. While Chothia *et al.* (1989)

corrected the positions of indels in the CDRs of the Kabat numbering scheme based on structural information, the framework regions were not included in their analysis. In Section 4.4 of this chapter, I suggest corrections to the Chothia numbering scheme for the positions of indels in the framework regions. Some of the work presented in this chapter has been published in Abhinandan and Martin (2008).

4.1 An alignment-based method to number antibody sequences

4.1.1 An existing tool for numbering

Martin (1996) has described a method automatically to apply numbering to an antibody sequence by performing a global alignment of the sequence with a consensus pattern. However, this method fails to number a sequence accurately under the following conditions:

- When a leader sequence precedes the N-terminal end.
- When there are truncations to the sequence.
- When there are unusual insertions or deletions which tend to distort the alignment thereby introducing mistakes into the numbering.

Type of dataset	Number of sequences
Lambda class	1525
Kappa class	2453
Heavy chain	4724

Table 4.1: The number of sequences in each dataset extracted from the Kabat database.

As an improvement to this method, it was decided that refinements to this program could be developed to correct the errors introduced for the above reasons.

4.1.2 Preparation of the test dataset

Using KabatMan (Martin, 1996) a test dataset was prepared by extracting sequences of the variable region of antibodies from the most recent public release of the Kabat database (July 2000) (Johnson and Wu, 2001). These sequences were filtered by KabatMan for 100% sequence identity and were grouped on the basis of chain (light and heavy chain) and class (Lambda and Kappa in the case of light chain sequences). Table 4.1 gives the number of sequences that populated each dataset.

4.1.3 Principle of the algorithm

The program was written in the C programming language and a simplified version of the algorithm is as shown in Figure 4.2.

The first step in the procedure was deriving a consensus pattern to represent a

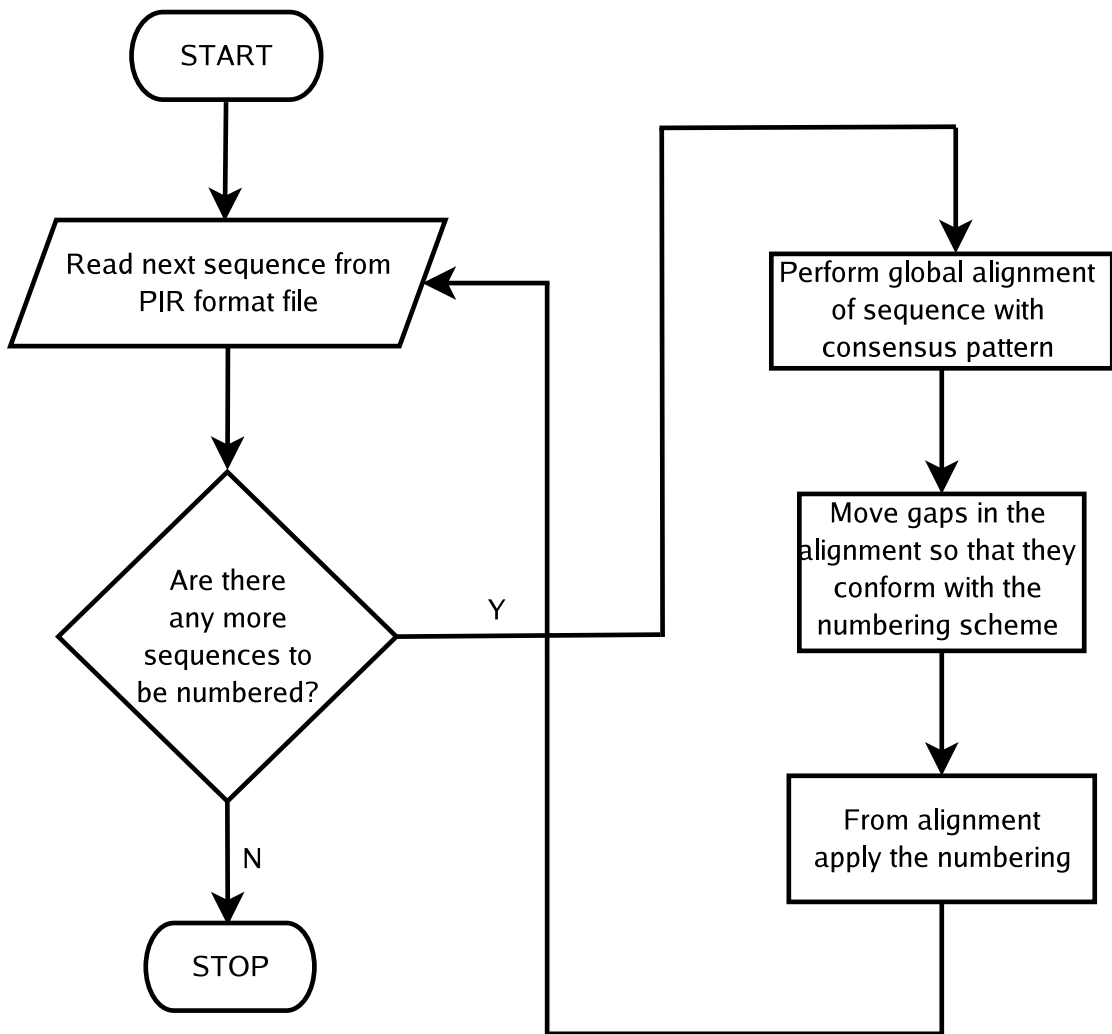


Figure 4.2: Numbering algorithm based on pairwise sequence alignment.

Light chain:

LFR1 (Framework 1): ~AVLTQPPXS!%!S!GXXVTI%C
L1 (Loop 1): XXSXXXXXXXXXXXXX!X
LFR2 (Framework 2): WYQQKXGXXPK!LIY
L2 (Loop 2): XX%XXXS
LFR3 (Framework 3): GVPXRFGS!SGTXX%LXISX!XXEDX!XY#C
L3 (Loop 3): XXXXXXXXXXXXXXXX
LFR4 (Framework 4): FGXGTKLEIXKRA

Heavy chain:

HFR1 (Framework 1): XVQLXXSGXXL!XPGXS!\$!SCX!SG#%F%
H1 (Loop 1): XXXXXXX
HFR2 (Framework 2): WV\$QXPG\$XLEW!!
H2 (Loop 2): XIXXXXXXGXXXYYYYXXK!
HFR3 (Framework 3): \$XX!%XDXSXX%!YXXXXSLXXED%AXYYCXX
H3 (Loop 3): XXXXXXXXXXXXXXXXXXXXXXXXXXXXX
HFR4 (Framework 4): WGQGTXTVTVSS

The following symbols represent groups of amino acids of a specific nature:

~: Acidic
!: Hydrophobic
#: Aromatic
\$: Basic
%: Hydroxyl containing

Figure 4.3: Light and Heavy chain consensus sequences derived from the multiple alignment of 48 structures from the PDB (described in <http://www.bioinf.org.uk/abs/seqmethod.html>).

light and heavy chain. Martin (1996) describes deriving a consensus pattern from the multiple alignment of light and heavy chain sequences from 49 structures. (see <http://www.bioinf.org.uk/abs/seqmethod.html>). Figure 4.3 gives the original consensus sequences derived for the light and heavy chain.

The *nw* program developed by Dr. A. C. R. Martin that implements the Needleman and Wunsch method for global pairwise alignment (Needleman and Wunsch,

Type of chain	Gap insertion penalty	Gap extension penalty	Type of matrix
Light	10	1	BLOSUM62
Heavy	15	1	Normalized MDM78

Table 4.2: Optimal parameters for alignment of light and heavy chain sequence alignment.

1970) was used to perform alignment between the antibody and the consensus sequence. Since the numbering scheme depends on the alignment, it is imperative to ensure correct alignment so that residues are numbered correctly. In order to ensure correct alignment, the following alignment parameters were varied:

1. Substitution matrix - PET, BLOSUM62, Normalized MDM-78.
2. Gap insertion penalty - 10, 15, and 5.
3. Gap extension penalty - 0, 1, 2, 3, and 5.

After manual examination of several pairwise alignments, the parameters shown in Table 4.2 were chosen as they gave the most correct alignments of the antibody sequences with the consensus sequences.

4.1.4 Deriving consensus sequences

An antibody variable region sequence consists of 7 regions, as shown in Figure 4.4. For unusually long antibody sequences, the pairwise alignment with the consensus sequence could be incorrect. To resolve this problem, it was decided to derive

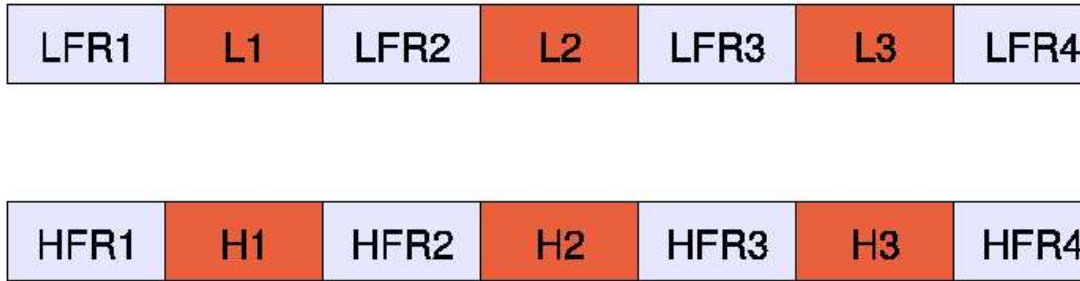


Figure 4.4: Schematic representation of the seven regions of the antibody variable region. The prefix L or H indicate light or heavy chain respectively. LFR1, HFR1, LFR2, HFR2, LFR3, HFR3, LFR4, HFR4 - Light or Heavy chain framework regions. L1, H1, L2, H2, L3, H3 - Complementarity Determining Regions (CDRs) or loops.

Chain/Class	FR1	Loop1	FR2	Loop2	FR3	Loop3	FR4
Lambda	0	0	62	119	132	0	0
Kappa	4	0	3	13	19	1	0
Heavy	1	0	18	3	3	0	3

Table 4.3: Numbers of sequences that gave insertions in the consensus alignment. FR = framework region

alternate consensus sequences for the unusual cases. Having fixed the optimal alignment parameters, all alignments between the antibody sequence and the original consensus sequence (Figure 4.3) were examined. Sequences that gave gaps in the consensus sequence alignment were isolated and clustered based on regions where they have more residues than the consensus sequence. These sequences were multiply aligned using *MUSCLE* (Edgar, 2004) and an alternate consensus sequence was derived on the basis of sequence conservation. The alternate consensus sequences are shown in Figure 4.5.

Table 4.3 shows the number of sequences that were clustered based on the region of insertion in the original consensus sequence.

LFR1: ~AVLTQPPXS!%!S!GXXVTI%C
 L1: XXSXXXXXXXXXXXXXXXXX!X
 LFR2: WYQQKSPGSAPVTVIY
 L2: X%DSDXXXXGS
 LFR3: GVPXRFSGS\$D!SGTXX%LXISX!XXEDX!XY#C
 L3: XXXXXXXXXXXXXXXXXXXX
 LFR4: FGXGTKLEIXKRA

(a) Consensus sequence for insertions in LFR2 segment.

LFR1: ~AVLTQPPXS!%!S!GXXVTI%C
 L1: XXSXXXXXXXXXXXXXXXXX!X
 LFR2: WYQQKXGXXPK!LLRY
 L2: X%DSDXXXXGS
 LFR3: GVPXRFSGS\$D!SGTXX%LXISX!XXEDX!XY#C
 L3: XXXXXXXXXXXXXXXXXXXX
 LFR4: FGXGTKLEIXKRA

(b) Consensus sequence for insertions in L2-LFR3.

HFR1: XVQLXXSGXXL!XPGXS!\$!SCX!SG#%F%
 H1: XXXXXXXXXXXXXXXXXXXX
 HFR2: WV\$QXPG\$XLEW!!
 H2: XIXXXXXXXXGXXXYYXXXXK!
 HFR3: \$XX!%XDXSXX%!YXXXXXSLXXXED%AXYYCXX
 H3: XXXXXXXXXXXXXXXXXXXXXXXXXXXXXXXX
 HFR4: WQGTXTVTVSS

(c) Consensus sequence for insertions in the heavy chain.

Figure 4.5: Alternate consensus sequences to be used when there are insertions in (a) LFR2 segment of Light chain (b) L2 or LFR3 in Light chain (c) Heavy chain.

4.1.5 Identifying chain type using Z-scores

Since the numbering program is applicable only to antibody sequences, the need to develop a method to differentiate antibodies from non-antibodies and further, to differentiate light and heavy chains, was realised. Deret et al. (Deret *et al.*, 1995) have described a method to assign subgroups to human antibody sequences (Johnson and Wu, 2001) based on sequence conservation in framework 1. It was initially decided to use their procedure (*SUBIM*) to classify sequences. However, the program suffers from two significant limitations:

- An inability to differentiate antibody sequences from non-antibody sequences.
- Assigning incorrect chain types in several cases.

It was then decided to develop a completely new procedure using Z-scores (described in Section 3.3). The procedure for doing this is shown in Figure 4.6 and is detailed below:

1. For every sequence in the input file, do the following steps:
2. Check the length of the input sequence. If it is less than 80 residues long, report that a chain type cannot be assigned to the sequence and proceed to the next sequence.
3. Run *ssearch33* (from the FASTA package (Pearson and Lipman, 1988)) for the query sequence against the database of human light chain kappa

class sequences. An E-value cut-off of 100000 is used so that pairwise identities between the query sequence with every sequence in the database are obtained.

4. If the length of the alignment with the top hit is less than 94 residues, then goto step 7. Some antigens tend to have high sequence similarity with antibody sequences over short stretches of alignment. This filter ensures that only sequences with similarity over the entire variable chain of an antibody are considered for further processing.
5. Calculate the mean sequence identity for the query from the set of pairwise identities. From this, calculate the Z-score for the query using:

$$Z_{query} = (\mu_{query} - \bar{\mu}_{human}) / \sigma_{human} \quad (4.1)$$

where

Z_{query} - Z-score of the query sequence.

μ_{query} - Mean percentage identity of the query sequence against the library of human sequences.

$\bar{\mu}_{human}$ - Mean percentage identity of database of human sequences calculated by averaging the mean percentage identities of all human sequences when compared with all other human sequences..

σ_{human} - Standard deviation of database of human sequences from the average from the mean percentage identities.

6. If the Z-score is less than the threshold Z-score for the database (-3.9 for Kappa, -4.5 for Lambda, and -3.1 for Heavy) assign the database type to

Chain/Class type	Z-score threshold
Lambda class	-4.4970
Kappa class	-3.8730
Heavy chain	-3.0630

Table 4.4: Table showing the Z-score thresholds for identifying chaintype. The thresholds were set after examining the Z-scores of murine and human antibodies in the Kabat database.

the sequence. Goto step 2 to process the next sequence.

7. Goto step 2 and run *ssearch33* against a different database (human lambda or heavy chain sequences).
8. If none of the Z-scores of the query is above the threshold Z-scores (see below), assign ANTIGEN type to the sequence. Go to step 2 and process the next sequence.

The threshold for length was decided after manual examination of antibody sequences in the Kabat database. Sequences that are shorter than 80 residues do not contain features typical of antibodies and it was decided to set this as the length threshold. Any antibody sequence that is less than 80 residues in length is not assigned a chain type. Similarly, the threshold for Z-scores was set after evaluating the Z-scores for mouse and human antibody sequences extracted from the Kabat database. The thresholds are shown in Table 4.4 and were decided upon based on the lowest Z-scores observed for the human and mouse antibodies for every dataset (Lambda/Kappa class light chains and heavy chains). It must be noted that the thresholds were set after considering the lowest score for a murine antibody sequence and the humanness scores of antibodies belonging to other species were not considered. However, experience suggests these thresholds are suitable

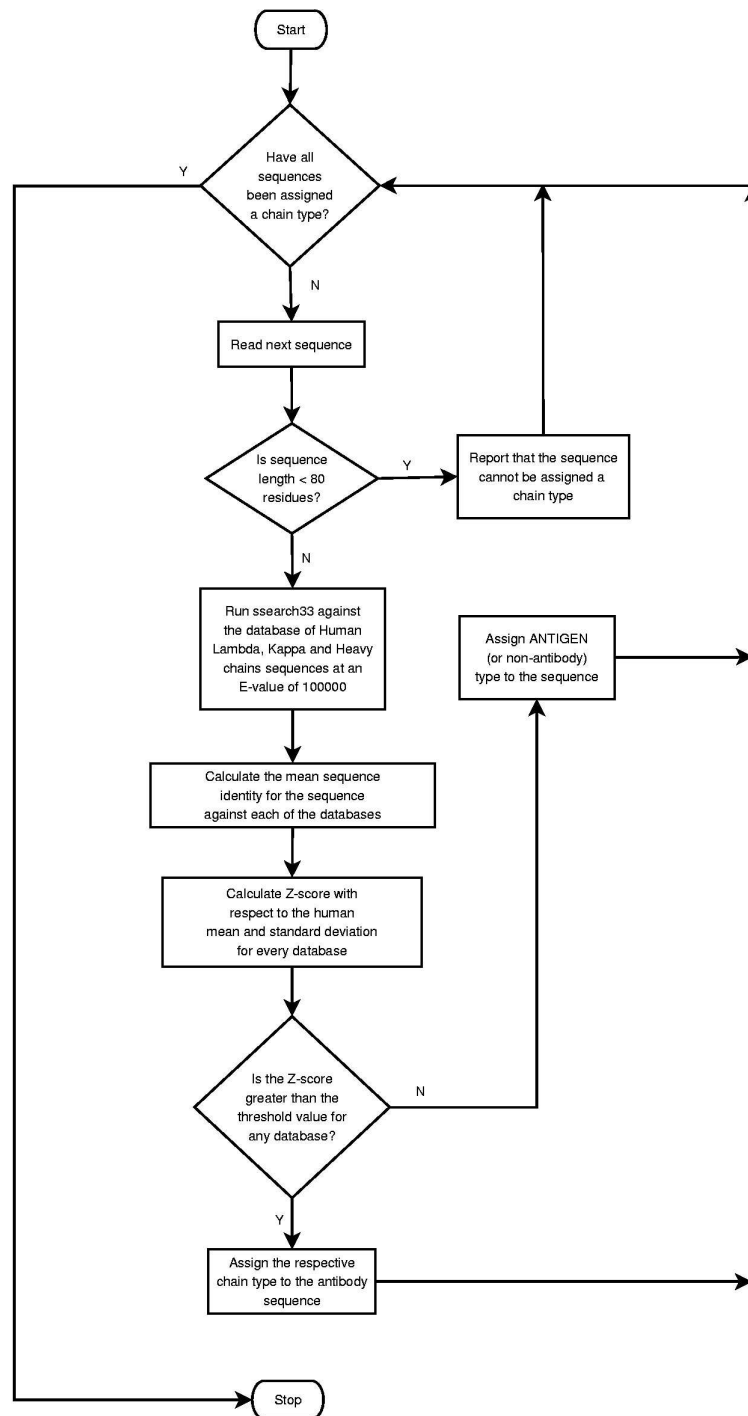


Figure 4.6: Identifying type of chain/class of an antibody sequence by calculating the Z-score with respect to the distribution of human antibody sequences.

for antibody sequences from other species.

4.1.6 How the numbering algorithm works

The overall algorithm is as shown in Figure 4.7. The first step involves the identification of the chain type (heavy chain or lambda/kappa class for light chain) using either SUBIM (Deret *et al.*, 1995) or the Z-scores procedure that has been described in Section 4.1.5. The sequence is aligned with the appropriate consensus light or heavy sequence. The alignment is checked for possible errors by examining the consensus sequence alignment for any gaps in which case it is aligned with an alternate consensus sequence.

An important problem that needed addressing was the case of light chain sequences with truncations towards the C-terminal end of the variable region. It was noticed that incorrect alignments were found particularly in the L3-LFR4 region and these had to be dealt with separately. The following section gives details of the methods developed to handle these cases.

4.1.7 Adjustments to alignments in the L3-LFR4 regions

As stated above, it was noted that the alignment was frequently incorrect and adjustments were required. The following steps were followed while adjusting the alignment in the L3-LFR4 region. Examples provided show the way the alignment changes are effected.

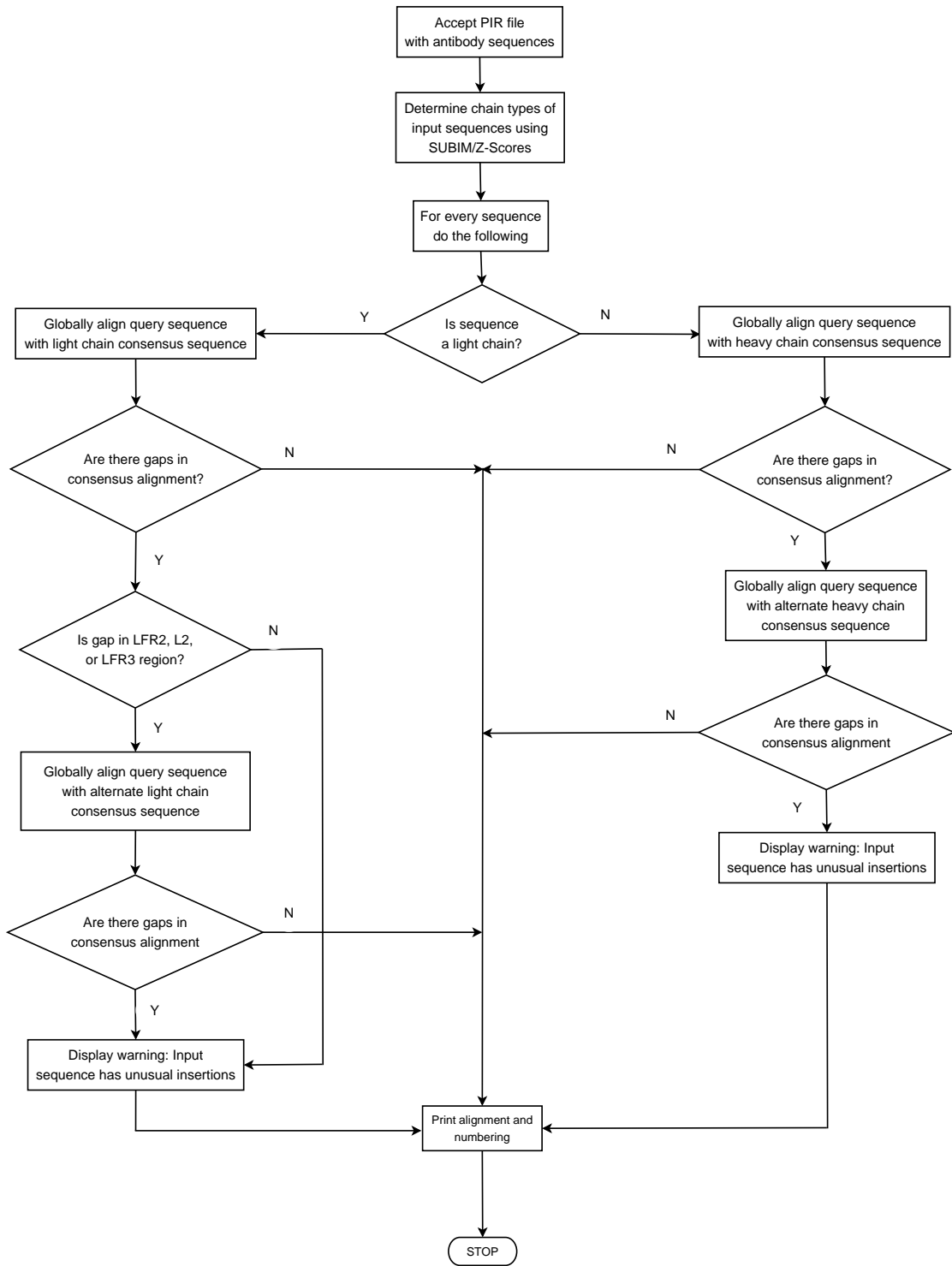


Figure 4.7: Overall algorithm for the alignment-based numbering method.

1. Extract the antibody sequence in LFR4 from the alignment with the consensus.
2. If there is no gap in the first position of LFR4, exit from the routine.
3. If LFR4 is not empty, check whether the start of LFR4 has a gap. If it does and the last residue in L3 is either of ‘T’, ‘S’, ‘P’, ‘F’, ‘L’, or ‘W’, move the last residue from L3 into the first position of LFR4 in the alignment. Having performed this, exit from the routine. The position at which the alignment is adjusted is indicated by the ‘*’ symbol.

Example:

```

                                *
DHYC      SSYTSINTWVS-----  -GGGT-----
XY#C      XXXXXXXXXXXXXXXXX  FGXGTKLEIXKRA

#####  #####
End of    L3                LFR4
LFR3

```

After adjustment, this becomes:

```

DHYC      SSYTSINTWV-----  SGGGT-----
XY#C      XXXXXXXXXXXXXXXXX  FGXGTKLEIXKRA

```

4. If LFR4 is empty, check the length of L3. If it is less than 4, then exit from the routine.
5. Pick the last 4 residues from L3 and match the following patterns of amino acids in them.
 - a) FG b) GSP c) FSP d) FDG e) FVD f) FR g) FW h) FXGG

If one of these patterns is observed in the last 4 residues of L3, then move these residues into LFR4 and exit from the routine.

Example:

```

                                *
DYYC      SSYTSISLTVLFG--      -----
XY#C      XXXXXXXXXXXXXXXX      FGXGTKLEIXKRA

#####    #####                #####

End of          L3                LFR4

LFR3

```

After adjustments, this becomes:

```

DYYC      SSYTSISLTVL----      FG-----
XY#C      XXXXXXXXXXXXXXXX      FGXGTKLEIXKRA

```

6. Check the number of Glycines in the last 4 residues of L3. If it is less than 2, exit from the routine.

7. If there are at least 2 Glycines amongst the last 4 residues of L3, examine the residue preceding the first Glycine. If it is one of 'T', 'S', 'P', 'F', 'L', or 'W', then move the segment from the residue preceding the first glycine to LFR4. Exit from the routine.

Example:

*

DYYC	QTWGTGGG-----	-----
XY#C	XXXXXXXXXXXXXXXXXX	FGXGTKLEIXKRA
####	#####	#####
End of	L3	LFR4
LFR3		

After adjustments, this becomes:

DYYC	QTWG-----	TGGG-----
XY#C	XXXXXXXXXXXXXXXXXX	FGXGTKLEIXKRA
####	#####	#####
End of	L3	LFR4
LFR3		

8. If the first residue among the last 4 residues in L3 is a Phenylalanine and the third residue is Glycine, then move the last 4 residues from L3 into LFR4. Having performed this, exit from the routine.

Example:

```

GEATAVYYVVAEVYNNYLYYGIKELGARGLLVTVSS-----
XED%AXYYCXXXXXXXXXXXXXXXXXXXXXXXXXXXXXXXXXWQGTXVTVSS
          *                               *

```

(a) Erroneous alignment in HFR3 end-H3-HFR4

```

GEATAVYYVVAEVYNNYLYYGIKEL-----GARGLLVTVSS
XED%AXYYCXXXXXXXXXXXXXXXXXXXXXXXXXXXXXXXXXWQGTXVTVSS
          *                               *

```

(b) Correct alignment

Figure 4.8: Example of an error in the alignment for an equine heavy chain sequence in the HFR3-H3-HFR4 region. The erroneous alignment (output from the numbering program) is shown in (a) and the correct alignment is shown in (b). The beginning of H3 and HFR4 are marked by the ‘*’ symbol below the alignment.

```

          *
DYHC      GADHGSGSDFVGG--      -----
XY#C      XXXXXXXXXXXXXXXX      FGXGTKLEIXKRA

####      #####              #####

End of    L3                    LFR4
LFR3

```

After adjustments, this becomes:

```

DYHC      GADHGSGSD-----      FVGG-----
XY#C      XXXXXXXXXXXXXXXX      FGXGTKLEIXKRA

```

4.1.8 Discussion

From preliminary analysis, it could be said that although the method was reasonably accurate, there was no guarantee that the numbering output from the program would be perfect owing to inherent limitations with using an alignment-based approach. It also required a large set of relatively arbitrary rules to deal with special cases. Unusual sequence features may lead to a wrong alignment and therefore wrong numbering. An example of this is shown for an equine IgE heavy chain sequence (Navarro *et al.*, 1995) in the HFR3–H3–HFR4 region in Figure 4.8. The consensus sequence for CDR-H3 contains several *X*s to represent the longest sequence that has been observed for this loop. However, this causes a wrong alignment because the start of HFR4 is unusual. HFR4 usually starts with a Tryptophan (W) whereas the start of HFR4 in this sequence is a Glycine residue (G). It was therefore decided to implement a profile-based approach to apply numbering to antibody sequences in the hope that this would be less arbitrary and more accurate.

4.2 A profile-based numbering method

This numbering algorithm uses profiles derived from the Kabat database to fix anchor points in an antibody sequence. By fixing anchor points in the sequence, it became possible to isolate the sequence of every *region* (framework region or loop) and number each of them independently.

Chain type	Sequence type	Number of sequences
Light	Complete	794
Light	Truncated	3044
Heavy	Complete	2641
Heavy	Truncated	1272

Table 4.5: Number of complete/truncated light and heavy chain sequences extracted from the Kabat database.

4.2.1 Preparation of the dataset

Using KabatMan (Martin, 1996), sequences of antibodies were extracted from the Kabat database (Johnson and Wu, 2001). For ease of benchmarking the efficiency of the algorithm, the initial set of sequences were classified as being truncated/complete light or heavy chain sequences. Any sequence with Kabat annotations for the first and last residues of the variable region (L1, L109 in the light chain and H1, H113 in the heavy chain) was regarded as being complete and all other sequences were treated as truncated sequences. Table 4.5 gives the number of complete and truncated light and heavy chain sequences extracted from the Kabat database using KabatMan.

For structural analysis, a list of antibody structures was prepared by parsing the XML file from SACS (Allcorn and Martin, 2002) and the structure files were obtained from the PDB (Berman *et al.*, 2000).

4.2.2 Creation of profile sets

The strategy adopted was to define a set of anchor points in the sequence and to fill in the numbering based around these locations. The anchor points were

Profile name	Anchor points for profile	
	Light	Heavy
FR1 Start	L1 - L6	H1 - H6
FR1 End	L18 - L23	H20 - H25
FR2 Start	L35 - L40	H36 - H41
FR2 End	L44 - L49	H44 - H49
FR3 Start	L57 - L62	H66 - H71
FR3 End	L83 - L88	H89 - H94
FR4 Start	L98 - L103	H103 - H108
FR4 End	L104 - L109	H108 - H113

Table 4.6: Kabat positions used in the profile definitions.

Chain type	Sequence type	Sequences that could not be numbered (%)
Light	Complete	1/794 (0.12%)
Light	Truncated	44/3044 (1.44%)
Heavy	Complete	2630/2641 (99.58%)
Heavy	Truncated	1260/1272 (99.05%)

Table 4.7: Number of complete/truncated light and heavy chain sequences extracted from the Kabat database that could not be numbered using just 3 profile sets (lambda, kappa, heavy).

chosen so that they would represent the start and end of every framework region. For this I extracted the propensities of each of the 20 amino acids in the first and last six positions of every framework region using KabatMan (Martin, 1996) and a Perl script to analyse results. Each set of six residues was termed a *profile* and a set of profiles representing the start and end of the four framework regions was termed a *profile set*. Table 4.6 gives the list of Kabat positions that were used to construct the profiles for the light and the heavy chain.

Initially, three profile sets were created, classified on the basis of chain– heavy chain and lambda and kappa for the light chains. However, a significant number of the sequences could not be numbered as anchor points for the start and end of the framework regions could not be fixed in the correct order (See Table 4.7).

Classification	Number of profiles
Human subgroups: Lambda class	6
Human subgroups: Kappa class	4
Human subgroups: Heavy chain	6
Species: Lambda class	6
Species: Kappa class	6
Species: Heavy chain	4

Table 4.8: Classification scheme and number of profile sets.

Additional profile sets were then created to make each more specific. Table 4.8 lists 32 profiles that were created on the basis of the following criteria:

a) Human subgroup classes as identified by Kabat. From the 1994 version of the Kabat database, sequences were divided into families based on amino acid identity where members of a family differ by 12 amino acids or fewer (Deret *et al.*, 1995). This led to the creation of 16 human sub-group-specific profiles as shown in Table 4.8.

b) Species of origin for the Lambda, Kappa and Heavy chain sequences. This resulted in a further 16 non-human species-specific profiles as shown in Table 4.8.

As will be shown later, the development of more specific profiles significantly improved the number of sequences that could be annotated using the numbering program (see Table 4.11).

4.2.3 The numbering algorithm

To number a sequence, a sliding-window protocol is applied in which each window consists of a set of six consecutive residues. The window is scored against a profile before it is moved by a single residue to span the next set of 6-residues. The score for a profile match is calculated as:

$$M = \max(S_{p,j}); (j = 0..N - 6) \quad (4.2)$$

$$S_{p,j} = \sum_{i=0}^5 \log(S_{i+j}) \quad (4.3)$$

where M represents the score and $S_{p,j}$ represents the score profile in the j 'th window of the sequence.

Once anchor points for the starts and ends of the framework regions have been fixed, the sequence for every region (framework 1, loop 2, etc) is extracted and numbered independently. However, it was noticed in several sequences that the order of the anchor points was incorrect. For example, the anchor point of the end of framework region 1 could appear after the anchor point for the start of framework region 2. While detecting out-of-order misassignments is trivial, detecting all misassignments of anchor points proved tedious requiring the design of elaborate protocols to ensure error-free assignment.

Region name	Range of lengths			
	Light		Heavy	
	Min	Max	Min	Max
Framework 1	22	23	24	29
CDR-1	7	17	6	18
Framework 2	14	16	13	14
CDR-2	5	12	10	23
Framework 3	31	40	29	34
CDR-3	5	18	2	30
Framework 4	10	15	10	12

Table 4.9: Minimum and maximum observed lengths of the 7 regions in the light and heavy chain.

A direct inference of anchor-point misassignment could be made when the order of the profiles was incorrect. In a few cases where the profile assignments were in the correct order, the separation between the profile assignments was clearly too large or too small. Such cases were detected by examining the separation between the profile assignments to see if they fell within pre-set limits shown in Table 4.9. These limits were set after the distribution of region lengths in the Kabat database was manually examined. It must be realised that it may be necessary to extend these limits in future to accommodate unusually long sequences. However, this would require cautious modification to ensure that sequences are not numbered incorrectly.

A ranking scheme was introduced to cope with profile misassignments. When a profile misassignment is detected on the basis of profile order and separation, the best seven profile set assignments are examined in turn to see if the correct match can be found. If not, it is reported that the sequence cannot be numbered. Once profile assignments are completed, the sequence of every region is extracted.

Once the anchor points for the starts and ends of the framework regions have

been fixed in the antibody sequence, the sequence of every individual region is extracted. This is shown in Figure 4.9. The boundaries for every region are set after the best profile assignments have been made and are known to be in the correct order. In some cases, the input sequence contains a leader sequence at the N-terminal end, or the constant region sequence at the C-terminal end. This process excludes extraneous residues from the N-terminal or C-terminal end of the antibody as they are not included in the alignment.

To ensure error-free assignment for the region boundaries (start and end of loop and framework regions), a final check is performed by concatenating the sequences in the individual regions and examining whether the concatenated sequence is a substring of the original sequence. This check is particularly useful when the profile representing the end of FR1 or the start of FR4 have been incorrectly assigned. An example is shown in Figure 4.10.

Numbering is applied in every region based on one of the following rules:

1. Normal numbering where deletions are made before the position of insertion – For example, the Kabat definition for region CDR-L2 is L50 to L56 giving it a standard length of 7 residues. A maximum length of 12 residues (antibody *Z84995* (Ignatovich *et al.*, 1997)) and a minimum length of 6 residues (antibody *Rer5* (Rast *et al.*, 1994)) have been observed for this region. The position of insertion according to the Kabat standard is L54 (L54A, L54B, L54C etc). Deletions are placed before the position of insertion (L54). For example, in the case of a 5-residue CDR-L2, residues L53 and L54 are deleted. This is demonstrated in Figure 4.11.

Schematic representation of an antibody sequence



Sequence to be numbered



After scanning for best profile assignments

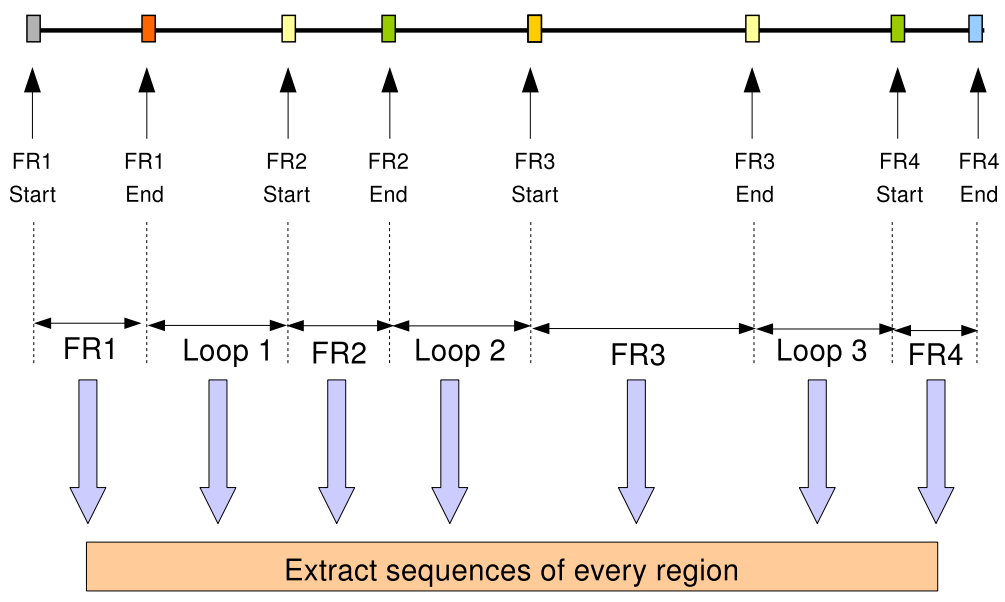
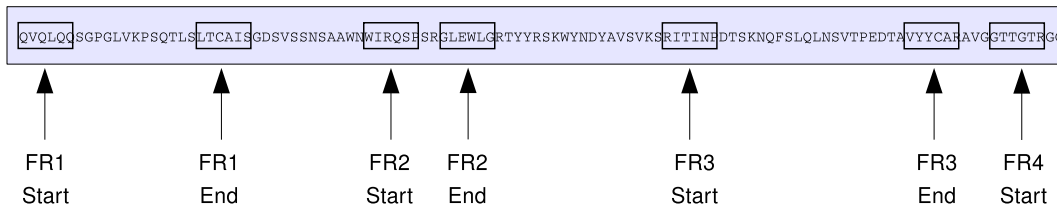


Figure 4.9: Isolating the sequence of every region from the best profile assignments. Each profile represents the start or the end of a framework region.

Sequence to be numbered

QVQLQQSGPGLVKPSQTLTCAISGDSVSSNSAAWNWIRQSPSRGLEWLGRTYYRSKWyNDYAVSVKSRITINPDTSKNQFSLQLNSVTPEDTAVYYCARAVGGTTGTRG

After best profile assignments



After extraction of the sequence in the regions

FR1: QVQLQQSGPGLVKPSQTLTCAIS
 Loop1: GDSVSSNSAAWN
 FR2: WIRQSPSRGLEWLG
 Loop2: RTYYRSKWyNDYAVSVKS
 FR3: RITINPDTSKNQFSLQLNSVTPEDTAVYYCAR
 Loop3: AVG
 FR4: GTTGTRGGMDVW

Alignment with FR4 consensus

GTTGTRGGMDVW - - - - -
 - - - - - WGQGTxVTVSS

Figure 4.10: Example showing the detection of errors through alignment with a consensus sequence pattern. In this example, the profile assignment of heavy chain framework region 4 start is incorrect as framework 4 is truncated after the first residue (W). The alignment with the framework 4 consensus is shown in the final box.

L50	L51	L52	L53	L54	L55	L56
G	T	T	-	-	R	T

(a) CDR-L2: GTTRT

L50	L51	L52	L53	L54	L55	L56
G	T	T	R	-	G	T

(b) CDR-L2: GTTRGT

L50	L51	L52	L53	L54	L54A	L55	L56
E	D	S	T	T	R	G	T

(c) CDR-L2: EDSTTRGT

Figure 4.11: Normal numbering in CDR-L2. The standard indel position is L54. Deletions are made before the position of insertion. The Kabat numbering is shown for varying lengths of CDR-L2. (a) 5 residues (GTTRT) (b) 6 residues (GTTRGT) (c) 8 residues (EDSTTRGT).

2. Reverse numbering where deletions are made after the position of insertion -
For example in CDR-L1, whose Kabat definition is L24 to L34, the standard length is 11 residues. A maximum length of 17 residues and minimum length of 7 residues have been observed in this region. Insertions are placed at position L27 according to the Kabat standard. Deletions are placed after the position of insertion (L27). For a 7-residue CDR-L1, residues L28, L29, L30, and L31 are deleted. This is shown in Table 4.12.
3. Straight numbering where residues are numbered sequentially - In the heavy chain framework region 4, residues are numbered sequentially as there are no defined indels in this region. This is shown in Figure 4.13.

In some regions, the Kabat numbering does not impose a fixed site for indels. For instance, in the heavy chain framework region 2 (HFR2) the deletion appears to be placed at the most likely position based on sequence. In these cases, an alignment

L24	L25	L26	L27	L28	L29	L30	L31	L32	L33	L34
S	A	S	V	-	-	-	Y	Y	M	Y

(a) CDR-L1: SASVYYMY (8 residues)

L24	L25	L26	L27	L28	L29	L30	L31	L32	L33	L34
S	A	S	-	-	S	V	Y	Y	M	Y

(b) CDR-L1: SASSVYYMY (9 residues)

L24	L25	L26	L27	L28	L29	L30	L31	L32	L33	L34
S	A	S	S	-	S	V	Y	Y	M	Y

(c) CDR-L1: SASSSVYYMY (10 residues)

Figure 4.12: Reverse numbering in CDR-L1. The standard Kabat indel position is L27. Table shows the Kabat numbering where deletions are made after the position of insertion (L27).

H103	H104	H105	H106	H107	H108	H109	H110	H111	H112	H113
W	G	Q	G	T	M	V	T	V	S	-

(a) HFR4 - WGQGTMTVTS (10 residues)

L98	L99	L100	L101	L102	L103
F	G	P	G	T	K
L104	L105	L106	L106A	L107	L108
V	T	A	L	S	Q
L109	L110	L111			
P	-	-			

(b) LFR4 - FGPGTKVTALSQP (13 residues)

Figure 4.13: Straight numbering in HFR4. The sequence in the region is WGQGT-MTVTS and numbering is applied sequentially to residues.

Region name	Is alignment performed for this region?	Is alignment used in numbering?	Numbering method
LFR1	Yes	No	1
L1	No	No	2
LFR2	No	No	1
L2	No	No	1
LFR3	No	No	1
L3	No	No	1
LFR4	Yes	No	3
HFR1	Yes	Yes	1
H1	No	No	2
HFR2	Yes	Yes	3
H2	No	No	2
HFR3	No	No	1
H3	No	No	1
HFR4	Yes	No	3

Table 4.10: Regions in the light and heavy chain and methods that are used to number them.

is performed between the sequence in the region and a consensus pattern for that region and numbering is applied based on the alignment. Table 4.10 summarises the numbering methods used for the different regions in the Kabat numbering scheme.

Figure 4.14 gives a flowchart of the numbering algorithm.

4.2.4 Benchmarking the numbering algorithm

In order to assess the performance of the profile-based numbering program, Ab-Num, sequences of antibodies and their Kabat numbering were extracted from the July 2000 release of the Kabat database. This was done using KabatMan and four test datasets were prepared on the basis of chain type (light or heavy chain) and nature of sequence (complete or truncated), as described in Section 4.2.1.

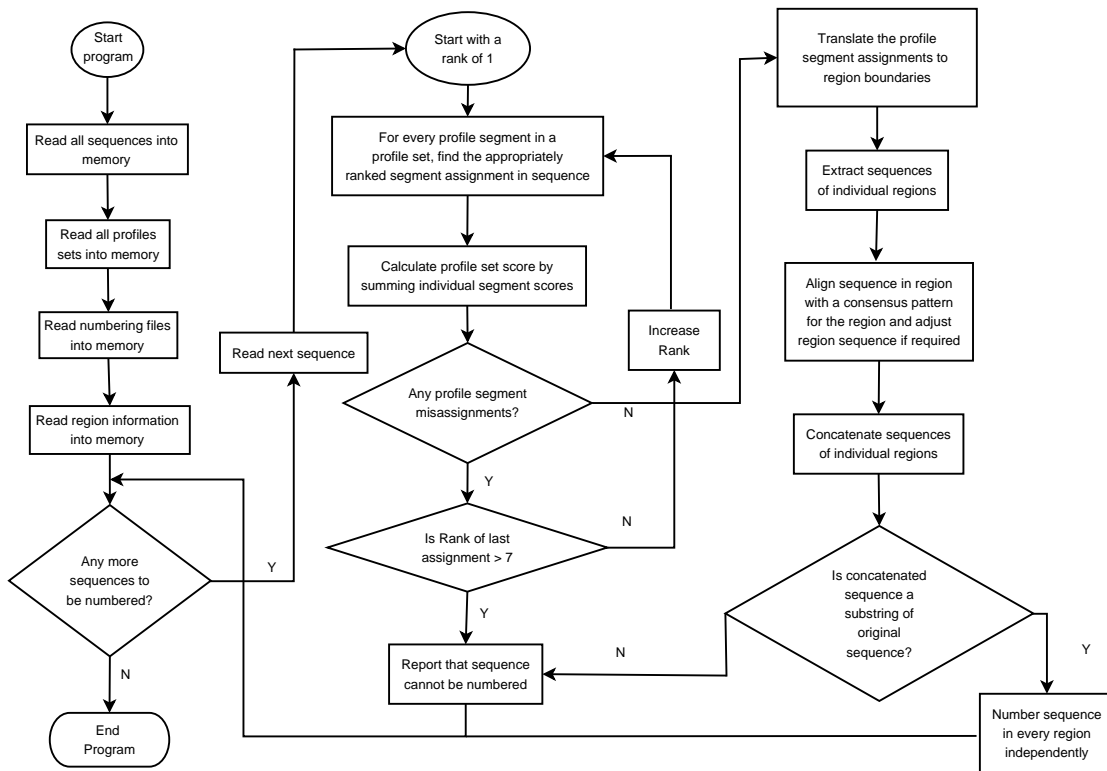


Figure 4.14: Flowchart of the numbering program. Profile segment: First or the last 6 residues in every framework region Region: Either means one of the seven framework regions (LFR1, HFR3, etc) or a loop (CDR-L1, CDR-H2, CDR-L3, etc).

Figure 4.15 gives the algorithm for benchmarking the numbering program. All sequences annotated in the Kabat database were numbered using AbNum. The numbering of AbNum was compared with the Kabat numbering. The Kabat database standard for numbering is very inconsistent in the range of L106–L111 in light chains and H100–H101 (including all residue insertions at H100: H100A, H100B, H100C, etc.) in the heavy chain. For ease of comparison, residues in these zones were excluded from examination. Sequences where the AbNum numbering matched the Kabat database numbering were regarded as being correctly numbered. For the other cases where mismatches occurred, a random sample of sequences was selected and manually examined to determine whether the error was in the AbNum numbering, or in the Kabat database. These statistics were then extrapolated to estimate the overall error percentages for the Kabat database and AbNum as shown in Formulae 4.4 and 4.5:

$$E_k = \frac{e_k \times N_m}{N_s} \times \frac{100}{N_T} \quad (4.4)$$

and

$$E_a = \left(U_a + \frac{(e_a \times N_m)}{N_s} \right) \times \frac{100}{N_T} \quad (4.5)$$

where E_k is the estimated percentage of errors in Kabat, E_a is the estimated percentage of errors in *AbNum*, e_k and e_a are the number of errors identified in Kabat and *AbNum* respectively in a sample of N_s sequences, U_a is the number of sequences that *AbNum* was unable to number, N_m is the total number of mismatches between *AbNum* and Kabat and N_T is the total number of sequences.

Chain type	Status	Total number of sequences	Numbered	Match Kabat
Light	Complete	794	793	682
Light	Truncated	3044	3014	2688
Heavy	Complete	2641	2622	2416
Heavy	Truncated	1272	1245	793

Table 4.11: Number of sequences numbered by AbNum that match the Kabat database annotations.

Table 4.11 gives the numbers of sequences that could be numbered by AbNum and agreed with manual numbering in the Kabat database.

Table 4.12 shows the results of the benchmarking study. All discrepancies in the AbNum numbering and Kabat database annotations were attributed to errors in the manual Kabat numbering. Every sequence that could be numbered by AbNum appears to have been numbered accurately.

4.3 Analysis of errors in the Kabat database

Since the manual examination of discrepancies between AbNum numbering and the Kabat database numbering seemed to suggest that all were errors in the Kabat database, I set out to examine the source of these errors. All sequences for which the AbNum numbering differed from the Kabat numbering were isolated and a region-wise distribution of these differences is shown in Table 4.13.

The following sections detail the nature of errors in each of these regions. All definitions of regions described here are Kabat standard definitions.

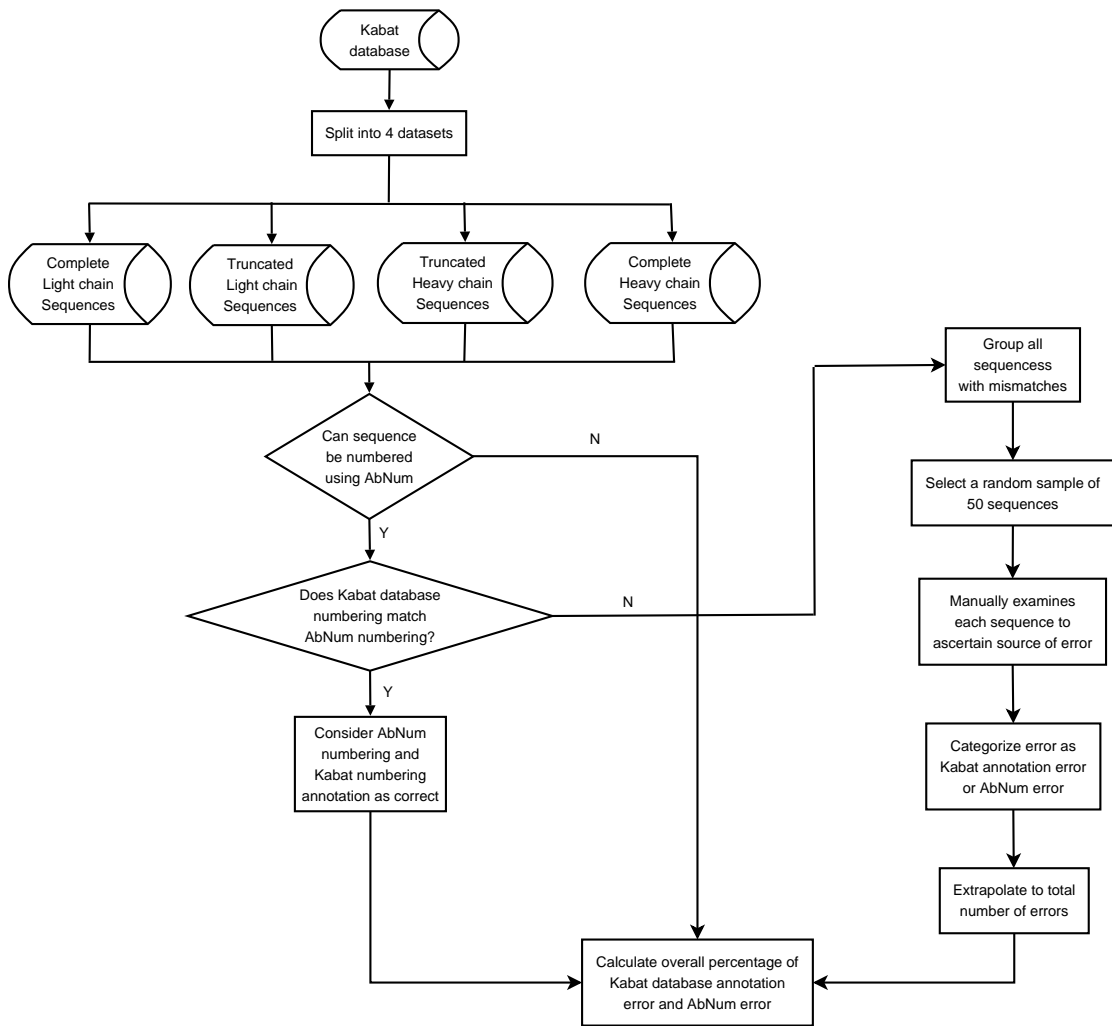


Figure 4.15: Algorithm for benchmarking the numbering program.

Chain type	Total number of sequences	Not numbered	Do not match Kabat	Sample size	Error (%)	
					Kabat	AbNum
Light chain complete	794	1	111	50	50/50 (14%)	0/50 (0.12%)
Light chain truncated	3044	30	326	40	40/40 (10.7%)	0/40 (1%)
Heavy chain complete	2641	19	206	50	50/50 (7.85%)	0/50 (0.72%)
Heavy chain truncated	1272	27	452	39	39/39 (10.7%)	0/39 (2.12%)

Table 4.12: Benchmarking the performance of AbNum: comparison with the Kabat database annotations. The percentages reported in the last two columns are estimated error percentages based on the sample set examined manually.

Chain type	Total number of mismatches	Number of errors						
		FR1	Loop1	FR2	Loop2	FR3	Loop3	FR4
Light chain complete	111	0	13	5	54	72	43	8
Light chain truncated	326	5	71	7	112	73	187	49
Heavy chain complete	206	70	4	13	71	47	92	10
Heavy chain truncated	452	294	11	2	34	34	149	73

Table 4.13: Region-wise distribution of errors in the Kabat database.

Label	L1	L2	L3	L4	L5	L6
AbNum	Q	S	A	L	T	Q
Kabat	Q	S	A	L	T	Q
Label	L7	L8	L9	L10	L11	L12
AbNum	P	A	S	-	V	S
Kabat	P	A	S	V	S	G
Label	L13	L14	L15	L16	L17	L18
AbNum	G	S	P	G	Q	S
Kabat	-	S	P	G	Q	S
Label	L19	L20	L21	L22	L23	
AbNum	I	T	I	S	C	
Kabat	I	T	I	S	C	

Figure 4.16: Kabat annotation error in LFR1. The 1-residue deletion is placed at L13 by Kabat although the Kabat standard imposes that it must instead be at L10.

Analysis of errors in the light chain

The Kabat standard assigns residues L1–L23 to LFR1. The usual length of LFR1 is 23 residues with a possible 1-residue deletion which according to the Kabat standard is at position L10. However, as the LFR1 numbering for the protein *B3* (Kalsi *et al.*, 1996) in Figure 4.16 demonstrates the position of deletion in Kabat is not consistent. Such errors have been corrected by AbNum as the position of deletions has been enforced.

Similarly, incorrect numbering has been observed in CDR-L1. The Kabat standard assigns residues L24–L34 to CDR-L1 with L27 as the indel position. A number of incorrect assignments have been observed in this region such as the one shown in Figure 4.17 for the protein *SSbPB* (Ivanovski *et al.*, 1998). In the example, the one-residue insertion must be placed at L27A (the second Serine in RASQSVSSSYLA) whereas the Kabat database places the insertion at L27F with no L27A....L27E.

Label	L24	L25	L26	L27	L27A	L27B
AbNum	R	A	S	Q	S	-
Kabat	R	A	S	Q	-	-
Label	L27C	L27D	L27E	L27F	L28	L29
AbNum	-	-	-	-	V	S
Kabat	-	-	-	S	V	S
Label	L30	L31	L32	L33	L34	
AbNum	S	S	Y	L	A	
Kabat	S	S	Y	L	A	

Figure 4.17: Kabat annotation error in L1. The one-residue serine (RASQSVSSSYLA) has been assigned L27F by the Kabat database although it should have been assigned L27A.

A different type of error has been observed to occur for the regions L1, LFR2, L2 and LFR3 as shown in Figure 4.18. The example shown is for the light chain of the antibody *SHLC5.1* (Hohman *et al.*, 1992). The end of L1 has been incorrectly annotated and the error can be seen to extend all the way up to LFR4. The example in Figure 4.19 shows a similar case where the boundaries of L3 and LFR4 have been incorrectly assigned in the Kabat database.

Analysis of errors in the heavy chain

In the heavy chain too, similar errors with respect to incorrect assignment of region boundaries have been observed. This is particularly clear in the case of the H2–HFR3 region. The Kabat numbering for HFR3 is from H66 to H94 and most sequences have a 3-residue insertion at H82 (H82A, H82B, H82C). However, my analysis of mismatches between the Kabat and AbNum numbering led me to discover a large number of discrepancies between the two annotations (nearly 30%). An example of this is shown in Table 4.20 which gives the Kabat database numbering and the AbNum numbering for CDR-H2 and HFR3. This sequence

Original sequence

DPVLTQPGSISSSPGKTVTITCTMSGGTISSYWASWYWQ
KPDSAPVFWSESDRMASGIPNRFAGSVDSSSNKMHLTI
TNVQSEDATDYYCAAAAASRSPYRSIFGSGTKLNLGSPR

AbNum assignment

LFR1: DPVLTQPGSISSSPGKTVTITC
L1: TMSGGTISSYWAS
LFR2: WYWQKPDSAPVFWWS
L2: ESDRMAS
LFR3: GIPNRFAGSVDSSSNKMHLTITNVQSEDATDYYC
L3: AAAASRSPYRSI
LFR4: FGSGTKLNLGSPR

Kabat database assignment

LFR1: DPVLTQPGSISSSPGKTVTITC
L1: TMSGGTISSYWASWY
LFR2: WQKPDSAPVFWSES
L2: DRMASGI
LFR3: PNRFAGSVDSSSNKMHLTITNVQSEDATDYYC
L3: AAAASRSPYRSI
LFR4: FGSGTKLNLGSPR

Figure 4.18: Errors in the Kabat annotation in regions L1–LFR3. *AbNum* assigns the boundaries of each of the regions correctly (marked in blue) whereas the Kabat annotation (which is wrong) is marked in red.

Original sequence

SYELTQPPSVSVPPGQTARITCSGDALPKKFAYWYQQ
KSGQAPVLVIYEDNKRPEIPERFSGSSSGTMATLTI
SGAQVEDEGDYYCYADINAKRVFGGGTKLTVLGQP

AbNum assignment

LFR1: SYELTQPPSVSVPPGQTARITC
L1: SGDALPKKFAY
LFR2: WYQQKSGQAPVLVIY
L2: EDNKRPS
LFR3: EIPERFSGSSSGTMATLTISGAQVEDEGDYYC
L3: YSADINAKRV
LFR4: FGGGTKLTVLGQP

Kabat database assignment

LFR1: SYELTQPPSVSVPPGQTARITC
L1: SGDALPKKFAY
LFR2: WYQQKSGQAPVLVIY
L2: EDNKRPS
LFR3: EIPERFSGSSSGTMATLTISGAQVEDEGDYYC
L3: YSADINAKRVFG
LFR4: GGTKLTVLGQPKA

Figure 4.19: Errors in the Kabat annotation in L3–LFR4. AbNum assigns the boundaries of each of the regions correctly (marked in blue) and the Kabat annotation (which is wrong) is marked in red.

Label	H50	H51	H52	H52A	H52B	H53	H54	H55
AbNum	R	F	H	S	G	R	N	P
Kabat	R	F	H	-	-	S	G	R
Label	H56	H57	H58	H59	H60	H61	H62	H63
AbNum	P	Q	Y	A	S	E	A	V
Kabat	N	P	P	Q	Y	A	S	E
Label	H64	H65	H66	H67	H68	H69	H70	H71
AbNum	K	G	R	V	T	A	S	T
Kabat	A	V	K	G	R	V	T	A
Label	H72	H73	H74	H75	H76	H77	H78	H79
AbNum	D	S	S	S	C	Y	M	Q
Kabat	S	T	D	S	S	S	C	Y
Label	H80	H81	H82	H82A	H82B	H82C	H83	H84
AbNum	M	N	S	L	-	-	K	T
Kabat	M	Q	M	N	S	L	K	T
Label	H85	H86	H87	H88	H89	H90	H91	H92
AbNum	E	D	T	G	I	Y	Y	C
Kabat	E	D	T	G	I	Y	Y	C
Label	H93	H94						
AbNum	E	D						
Kabat	E	D						

Figure 4.20: Kabat database error in the H2-HFR3 region of *Axo1*.

does not have the usual 3-residue insertion at H82 and this has been correctly identified by AbNum. However, since the Kabat database annotations have largely been manual and the 3-residue insert at H82 is very common, the sequence has been incorrectly annotated as having residues at H82A-C whereas the insert should have been at position H52 in CDR-H2.

4.4 Structural analysis: An alternate structure-based numbering scheme to accommodate indels in the framework regions

As described above, the two most widely used numbering schemes for antibodies are the Kabat and the Chothia schemes. The Kabat numbering scheme (Kabat *et al.*, 1983) was based on sequence alignments and placed insertions where they occurred in sequence. Chothia and co-workers (Chothia and Lesk, 1987; Al-Lazikani *et al.*, 1997) examined structures of antibodies and proposed a numbering scheme correcting the positions of insertions at the structural level rather than at the sequence level. However, only CDRs were included in this analysis and framework regions were not examined.

A list of antibody structures was extracted from SACS (Allcorn and Martin, 2002). Light chain and heavy chain sequences from 561 structures were extracted from the SEQRES records of the PDB files. These were numbered using AbNum and the numbering was patched into the PDB files using *patchpdb* (Dr. A. Martin, unpublished). The sequence of every framework region was extracted and analysed for deviations from the standard lengths described in Kabat (Wu and Kabat, 1970). Structures whose framework region lengths differed from the standard were fitted using **ProFit** (Martin, ACR, <http://www.bioinf.org.uk/software/profit/>). Where structures of variable regions were not available, four or five structures were chosen and fitted together to see if certain positions in the region are more flexible than others and therefore likely to accommodate indels.

Region Name	Kabat definition (Standard length)	Length range Min - Max	Kabat indel position	Structural ins. pos.	Structural del. pos.
LFR1	L1 - L23 (23)	22 - 23	L10	-	L10
LFR2	L35 - L49 (15)	14 - 16	-	L40	L41
LFR3	L57 - L88 (32)	31 - 40	L66	L68	L68
LFR4	L98 - L110 (12)	12 - 13	L106	L107	-
HFR1	H1 - H30 (30)	29 - 34	H6	H8	H8
HFR2	H36 - H49 (14)	13 - 14	-	-	H42
HFR3	H66 - H94 (29)	30 - 34	H82	H72	-

Table 4.14: Table comparing the Kabat indels with the structurally corrected indels.

Table 4.14 compares the results of this analysis with the Kabat standards for the positions of insertions and deletions in the framework regions. For LFR1 (Kabat definition L1 to L23) which has a standard length of 23 residues, a structure with 22 residues (PDB Code 2vit (Fleury *et al.*, 1998)) was found. 2vit also has an LFR4 (Kabat definition L98 to L110) length of 13 residues compared with the standard length of 12 residues. I fitted the LFR1 and LFR4 regions of 2vit to that of 12e8 (Trakhanov *et al.*, 1999) which has standard lengths in these regions. For the remaining regions however, no structures with unusual framework region lengths exist.

The fitted structures of light and heavy chain framework regions are shown in Figures 4.21 and 4.22 respectively indicating the Kabat indel sites and my proposed structurally correct sites.

The case of HFR3 is particularly interesting. The Kabat definition for HFR3 is from H66 to H94, a standard length of 29 residues. In most heavy chains however, there is a 3-residue insertion in HFR3 which Kabat designates as being at H82 (H82A, H82B, H82C); see Figure 4.23a. There are a small number of sequences

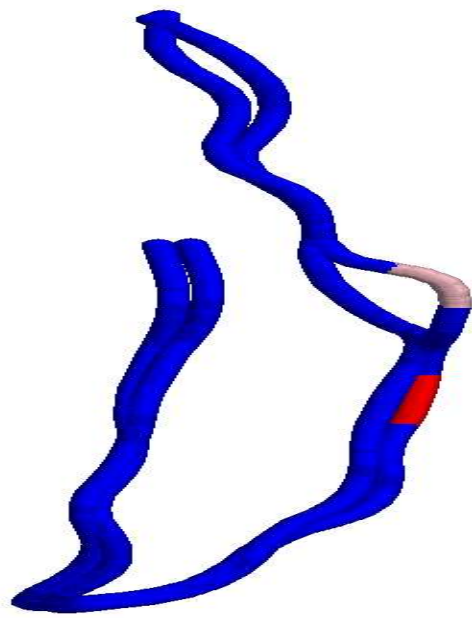
that do not contain this insertion, but because this situation is rare, the majority of these are erroneously annotated in Kabat as containing the 3-residue insertion in HFR3 whereas the residues should be inserted in CDR-H2 at position H52 (Figure 4.23b). In total, 74 sequences in Kabat were identified where the end of the CDR-H2 and the start of heavy chain framework region 3 have been annotated incorrectly.

Further analysis of HFR3 indicates that position H82 is unlikely to accommodate insertions. A pairwise sequence alignment between antibodies **axo1** (Patel and Hsu, 1997) and **mab113** (Mantovani *et al.*, 1993) as shown in Figure 4.24 suggests that H72 is the likely position of the 3-residue insertion. Figure 4.25 shows the spacefilled representation of the Fv region of an antibody. Residues that would be numbered H72 and H82 are indicated and it can be seen that H82A-C are relatively buried while H72A-C are on the surface making it more likely that these residues would be deleted. This is further corroborated by the work of Annemarie Honegger (Honegger and Plückthun, 2001) who analysed the sequences and structures of light chain and heavy chain variable regions of antibodies and suggested that the heavy chain has a 2-residue insertion with respect to the light chain at position H72.

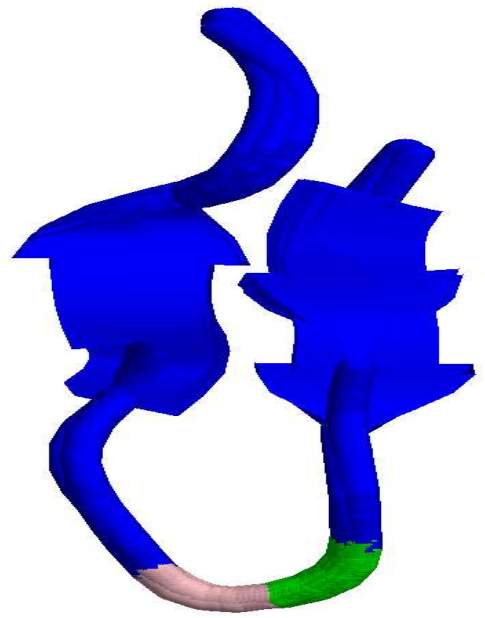
4.5 Conclusions

In this chapter, a new method that uses profiles to apply numbering schemes to antibody sequences has been described. This approach successfully numbers the

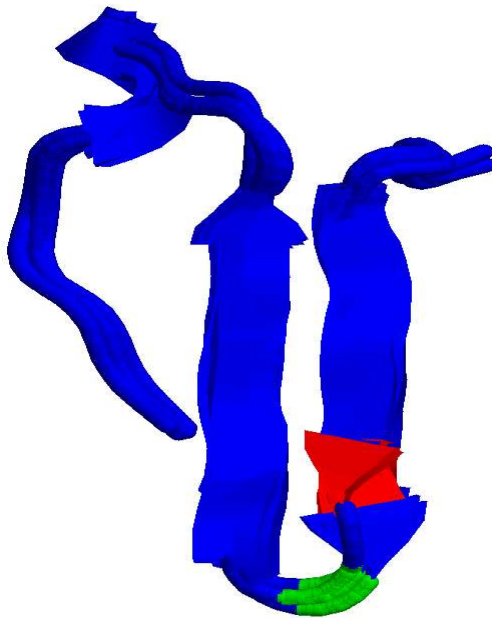
'problem' sequence described in Section 4.1.8. The analysis of manual annotations in the Kabat database shows that there is a high percentage of errors. Based on structural analysis of insertions and deletions in the framework regions of antibodies, I have extended the Chothia numbering scheme to correct the positions of insertions and deletions in the framework regions.



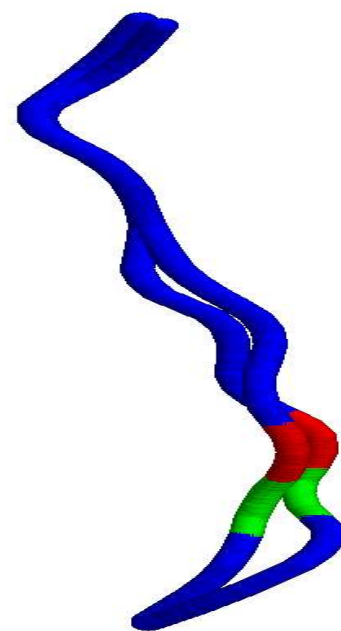
(a) LFR1



(b) LFR2



(c) LFR3



(d) LFR4

Figure 4.21: Rigid body superposition of light chain framework regions. Colour codes are: red - kabat indel position, green - structurally correct position of insertion, pink - structurally correct position of deletion.

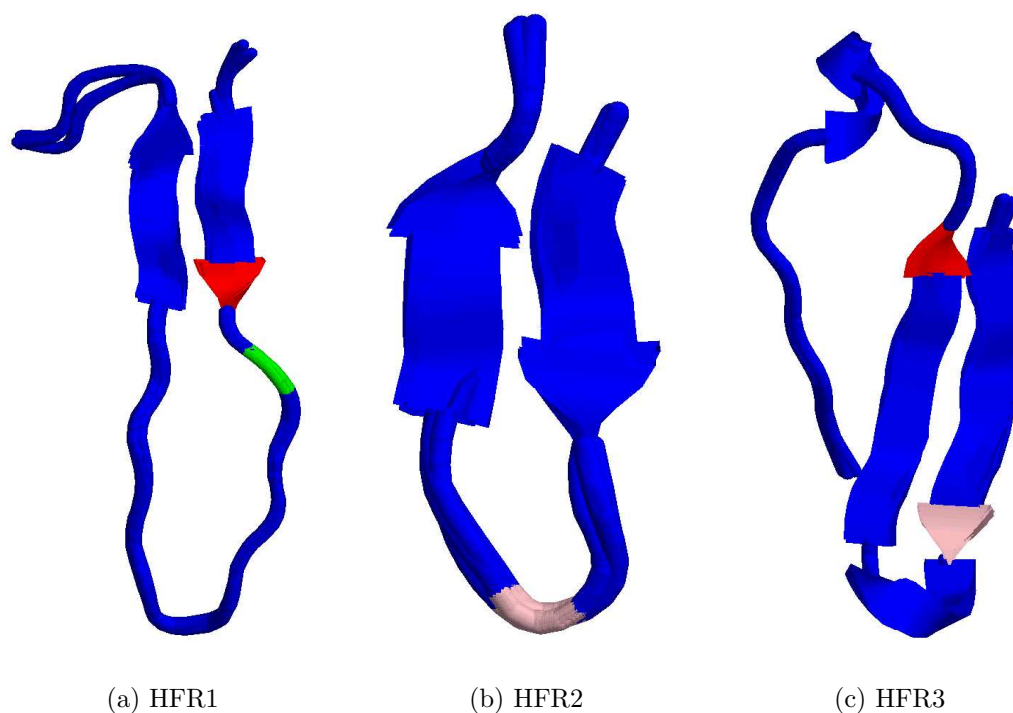


Figure 4.22: Rigid body superposition of heavy chain framework regions. Colour codes are: red - kabat indel position, green - structurally correct position of insertion, pink - structurally correct position of deletion.

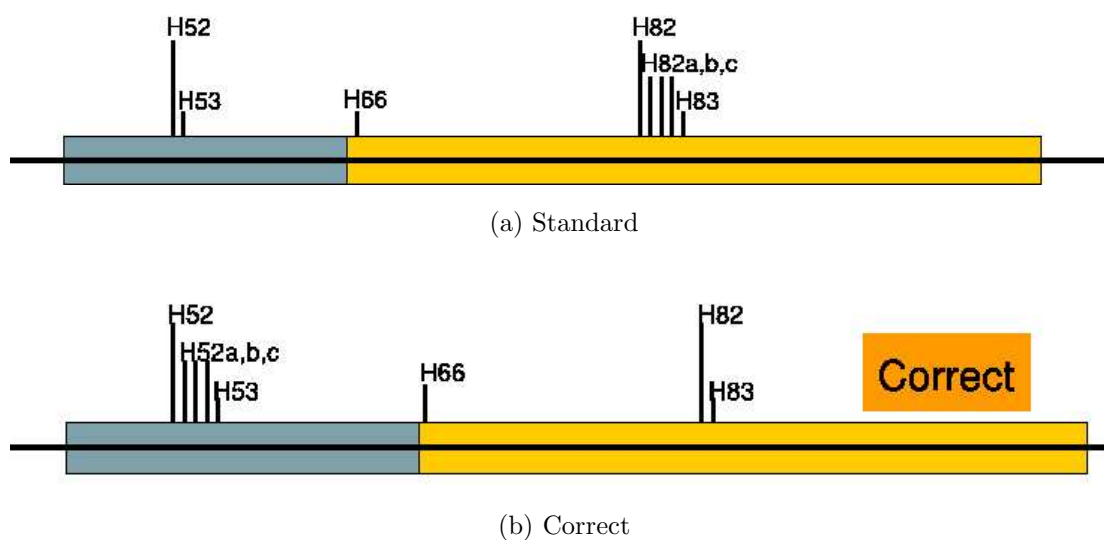


Figure 4.23: Numbering in H2-HFR3 (a) The standard numbering for H2-HFR3 in the Kabat database annotations (b) The correct numbering when the 3-residue insertion at H82 are not present.

axo1 QIVLTQSGSEVKKPGESMQLKCTVTGFNVNSYWMHWVRQAPG
mab113 QVQLVQSGAEVKRPGAPVKVSCKASGYTFTDYIMHWVQQAPG

...CDR-H2- > <- HFR3...

axo1 KGLEWVLRFHSGRNPPQYASEAVKG RVTASTDS- - SSC
mab113 QGLEWMGRINPNTGGTN- SAQKFQG RVTMTRDTSISTA
65 6789012abc345

..HFR3- >

axo1 YMQMNSLKTEDTGIYYCAR
mab113 YMELSNLRSDDTAMYSCAR
6789012345678901234

(a) Alignment if position of insertion is H72

axo1 QIVLTQSGSEVKKPGESMQLKCTVTGFNVNSYWMHWVRQAPG
mab113 QVQLVQSGAEVKRPGAPVKVSCKASGYTFTDYIMHWVQQAPG

...CDR-H2- > <- HFR3...

axo1 KGLEWVLRFHSGRNPPQYASEAVKG RVTASTDSSSCYM
mab113 QGLEWMGRINPNTGGTN- SAQKFQG RVTMTRDTSISTA
65 6789012345678

..HFR3- >

axo1 QMNSL- - KTEDTGIYYCAR
mab113 YMELSNLRSDDTAMYSCAR
9012abc345678901234

(b) Alignment if position of insertion is H82

Figure 4.24: Sequence alignment between antibodies Axo1 and mab113.

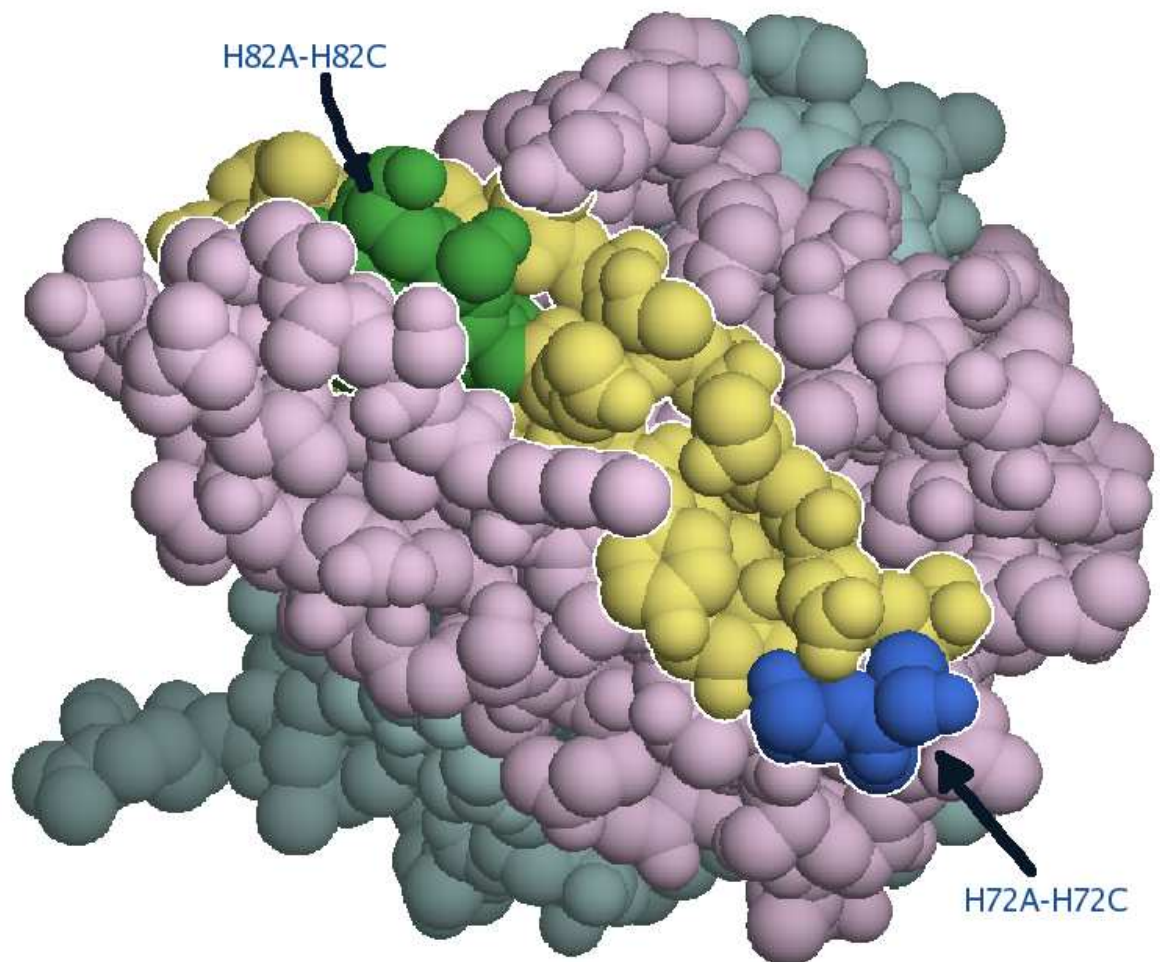


Figure 4.25: Spacefill representation of the variable domain of an antibody. The colour codes are: light chain - blue gray, heavy chain - pink, HFR3 - yellow and highlighted by the white borders. The residues coloured in blue and green are H72A-C (if insert position is H72) and H82A-C (if insert position is H82) respectively. This diagram was prepared using *QTree* (Martin, ACR, <http://www.bioinf.org.uk/software/qtree/>).

Chapter 5

Predicting the V_H/V_L interface angle from interface residues

The variability of antibodies is encoded in the Fv region which consists of two protein domains. Interactions between the light and the heavy chain contribute significantly to the stability of the variable fragment (F_v). The V_H/V_L interface between the light chain and heavy chain has been shown to affect the binding kinetics of a peptide (Chatellier *et al.*, 1996). The framework region at the V_H/V_L interface consists of two β -sheets (Poljak *et al.*, 1973), the structures of which are conserved across Fab and light chain dimers (Chothia *et al.*, 1985; Novotný and Haber, 1985). However, the contribution of residues in the framework regions to interactions with the antigen remains poorly understood. It has been demonstrated that modification of residues distant from the antigen binding site of the antibody has a small yet significant effect on the binding affinity with the

antigen (Chatellier *et al.*, 1996; Roguska *et al.*, 1996). For example, Adair and co-workers have demonstrated that modification of residue H23 significantly affects binding of the antibody with the antigen (Adair *et al.*, 1999). While this may be an impediment for predicting the affinity of engineered antibodies, it must also be emphasised that interactions at the V_H/V_L interface are crucial to maintaining stability of the F_{ab} . Understanding the influence of residues in the V_H/V_L interface on the packing angle between the two domains would help design antibodies with a definable binding site topography.

In this chapter, I present an analysis of the distribution of the V_H/V_L packing angle and a method to predict the interface angle from the nature of interface residues is described. A set of conserved residues in the framework regions of V_L and V_H were chosen and the interface angle was defined as the torsion angle between these points. The main applications of trying to predict packing angle from interface residues are in modelling studies of antibodies and in humanization protocols. The packing angle between the variable chains of antibodies has previously not been considered when modelling variable chains of antibodies (Martin *et al.*, 1991; Martin *et al.*, 1989; Whitelegg and Rees, 2000). Knowing the packing angle prior to modelling the variable region light and heavy chain may help in choosing more appropriate template structures upon which models may be based. This work also helps in identifying key residues that influence the packing angle and therefore, are instrumental in determining the topography of the paratope. The process of humanization involves grafting of murine CDRs onto human framework regions (Jones *et al.*, 1986). Further modification of residues flanking the CDRs is usually required to restore the binding affinity of the mouse antibody (Riechmann *et al.*, 1988). This could be extended by modifying residues at the V_H/V_L interface

in the humanized antibody to their murine counterparts so that the topography of the paratope would be preserved.

5.1 Preparation of the dataset

A list of F_v and F_{ab} structures was extracted from the SACS (Allcorn and Martin, 2002) XML file. This yielded a set of 561 antibody structures including 6 anti-idiotypic antibodies (PDB Codes: 1cic, 1dvf, 1iai, 1pg7, 1qfw, and 2dtg). Anti-idiotypic antibodies are antibodies derived against epitopes present in other antibodies. As every anti-idiotypic antibody structure consists of two antibodies, all anti-idiotypic antibody structures were split into two and the final dataset consisted of 567 antibody structures. This set comprised 314 structures for which the sequences of the light chain and heavy chain were distinct. Conformational changes in the antibody CDRs upon binding with the antigen have been established in several studies (Colman *et al.*, 1987; Bhat *et al.*, 1990; Herron *et al.*, 1991; Rini *et al.*, 1992; Wilson and Stanfield, 1994; Mylvaganam *et al.*, 1998). The idea behind allowing redundancy in the dataset is that it allows for variability in a given structure. Structural fitting of antibodies was performed using **ProFit** (<http://www.bioinf.org.uk/software/profit/>) which implements the McLachlan algorithm (McLachlan, 1982). The AbNum program described in the previous chapter was used to apply Chothia numbering to the structures of antibodies.

Programs for analysis were written in C and PERL. All graphs were created us-

ing GNUPLOT and GRACE (<http://plasma-gate.weizmann.ac.il/Grace/>). The program *ssearch33* from the FASTA package (Pearson and Lipman, 1988) was used in the calculation of Z-scores for chain assignment. The *Stuttgart Neural Network Simulator (SNNS)* (<http://www-ra.informatik.uni-tuebingen.de/SNNS/>) was used to make associations between packing angle and interface residues. The *GRASS* library (Team, 2006) was used for calculation of Eigen vectors and values. The *Sun gridengine* was used to distribute jobs across a grid consisting of the *C³* and the *Queen*. The *C³* is a farm consisting of 96 IBM series 335 nodes and the *Queen* is a farm consisting of 30 nodes with each node having 2 dual-core AMD Opteron processors.

The ‘interface residues’ are defined as Chothia-numbered interface positions for which there is a change in accessibility as a result of V_H/V_L interaction. As a first step, sequences of the light and heavy chain were extracted from PDB files of the antibodies. The Chothia numbering scheme (Chothia and Lesk, 1987; Al-Lazikani *et al.*, 1997) was applied to all the sequences using *AbNum*. In the case of F_{abs} , only the variable region was considered for further analysis. The Chothia numbered variable region sequences were patched back into the PDB files to yield 567 numbered F_v region structures.

Once the structure files were prepared with the Chothia numbering applied to them, the accessibility of all residues in the light and heavy chains was calculated. Simon Hubbard’s *naccess* program that implements the algorithm described by Lee and Richards (1971) was used for the calculation of accessibility. The accessibility of all residues in the V_H/V_L complex and in the individual chains was calculated. Those residues which sustained any change in the accessible surface area were

regarded as being interface residues.

5.2 Calculation of the packing angle

The packing angle was defined as the torsion angle at the V_H/V_L interface. The steps involved in the calculation of the packing angle are as described below:

1. Identify a set of residues SL and SH that are structurally conserved in the light and heavy chain respectively.
2. Extract the $C\alpha$ coordinates for the residues in SL and SH .
3. Find the centroid for each set (CL and CH).
4. For each set, compute the best-fit line passing through the centroid.
5. Identify one point on each line PL and PH on the same side relative to the respective centroid.
6. Calculate the packing angle as the torsion angle between the points PL , CL , CH , and PH .

Five antibody light and heavy chains were fitted together on all residues in the variable region using **ProFit** to identify conserved residues at the V_H/V_L interface. The backbone representations of the fitted structures are shown in Figures 5.2 and 5.3 respectively. The regions coloured in blue correspond to residues that are highly conserved across antibody structures. These are **L35-L38**, **L85-L88** in

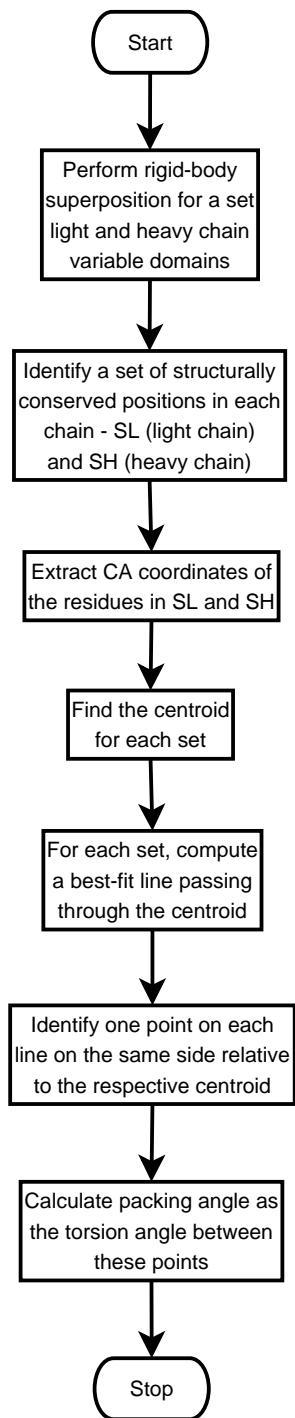


Figure 5.1: Algorithm to calculate the packing angle at the V_H/V_L interface.

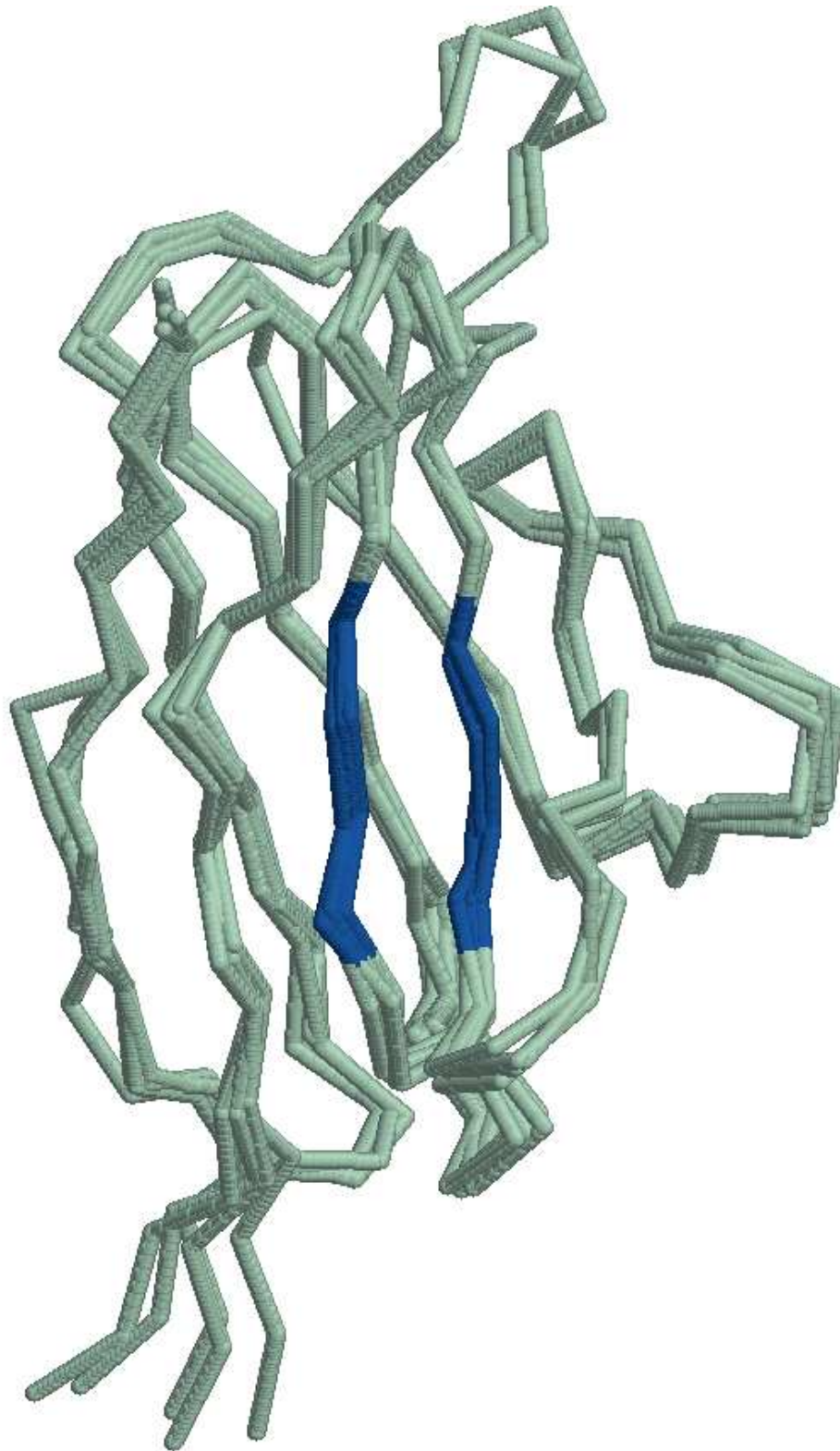


Figure 5.2: Rigid body superposition of the $C\alpha$ atoms in five structures of the light chain variable region. The structures used were: **12e8**, **15c8**, **1a0q**, **1a3l**, **1a3r**.

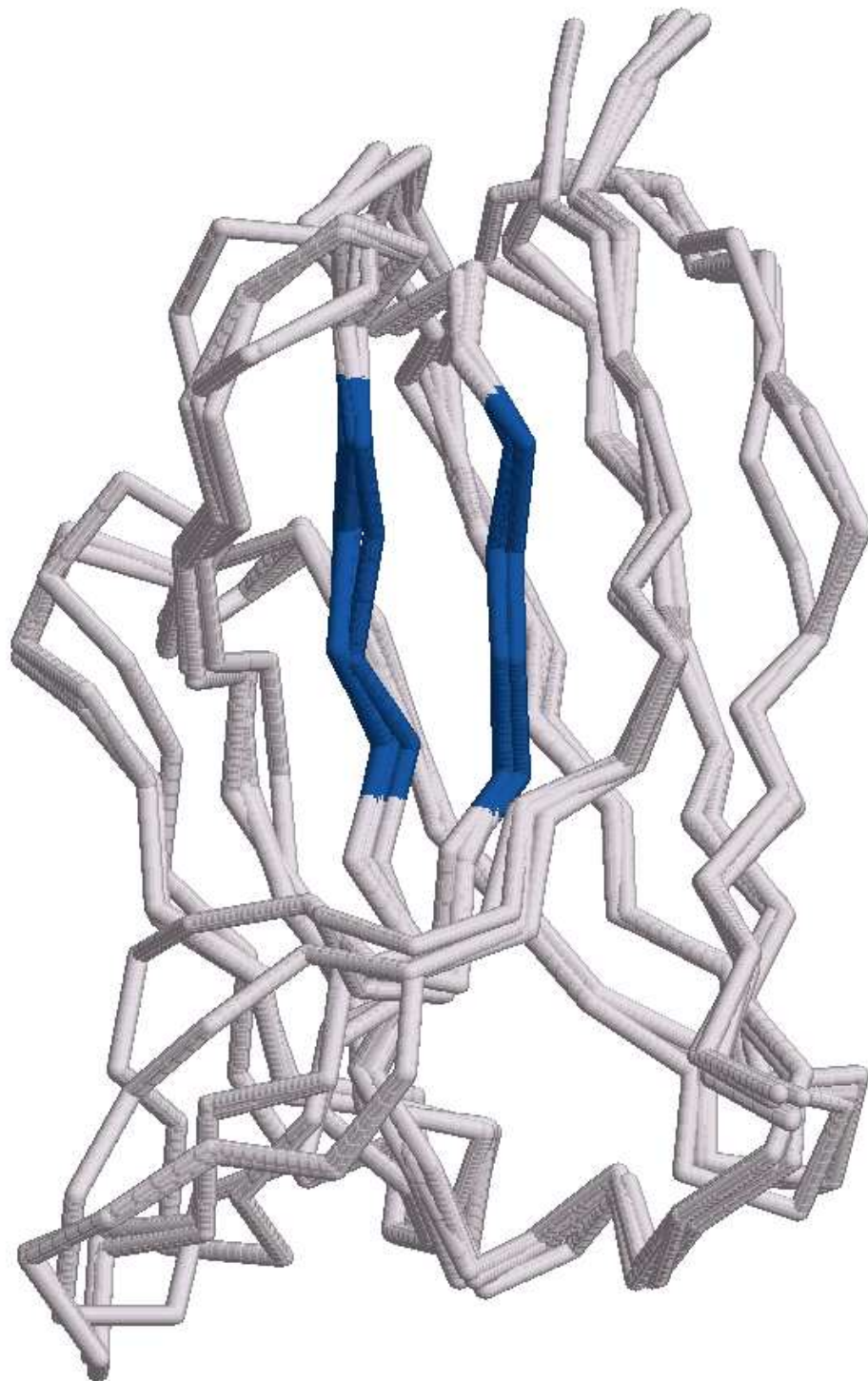


Figure 5.3: Rigid body superposition of the $C\alpha$ atoms in five structures of the heavy chain variable region. The structures used were: : **1oax**, **1yec**, **1yef**, **2ddq**, **8fab**.

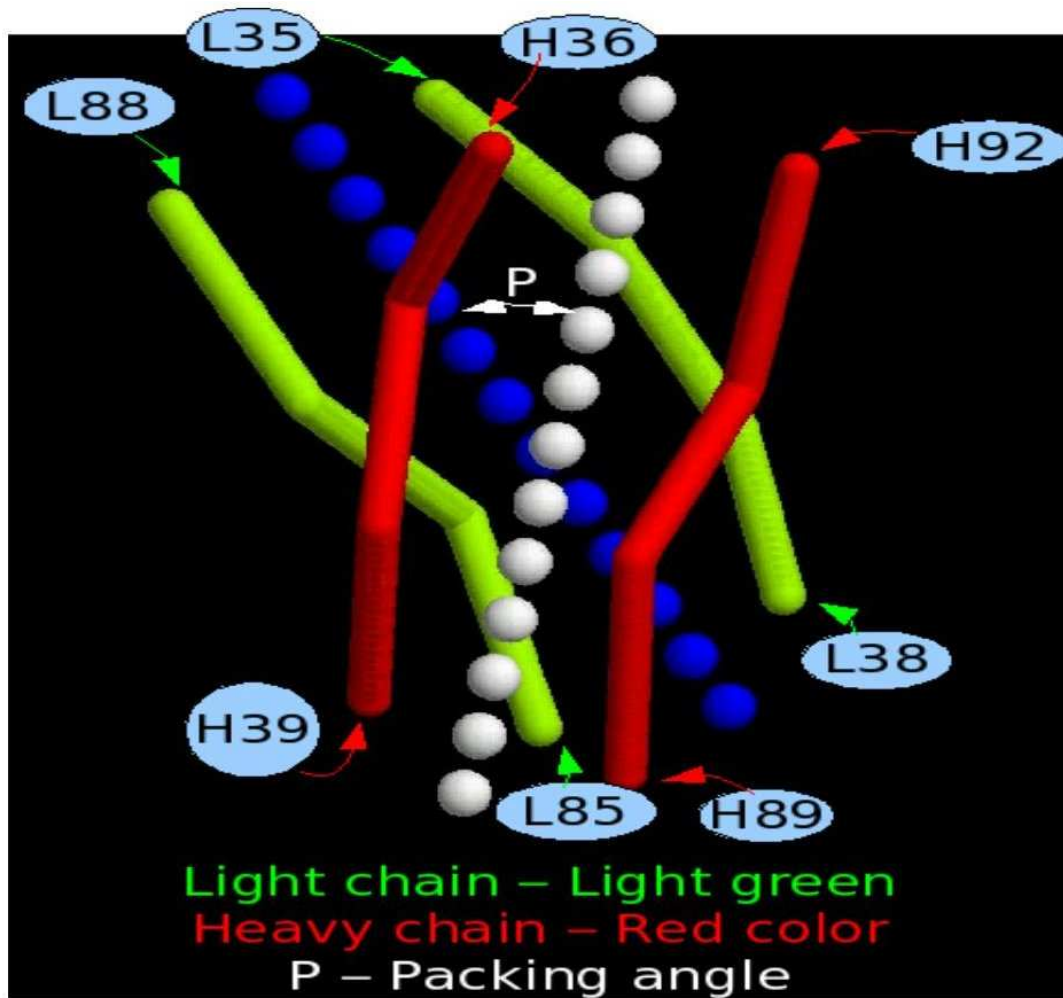


Figure 5.4: The beta strands at the V_H/V_L interface, best-fit lines, and packing angle.

the light chain and **H36-H39**, **H89-H92** in the heavy chain. These positions form part of a beta-sheet which is at the core of the interface and outside the hyper-variable loops. Figure 5.4 shows the beta sheets, the best-fit lines drawn through them, and the packing angle.

The next step was to calculate a best-fit line for the points in *SL* and *SH*. Only the coordinates of the $C\alpha$ atoms were used to compute the best-fit line. The method employed was *Principle Component Analysis (PCA)* and the calculations were performed according to the algorithm shown in Figure 5.5.

After calculation of the packing angle across the 567 structures in the dataset, their frequency distribution was plotted and this is shown in Figure 5.6. The packing angle varies quite considerably across different structures. The smallest and largest packing angles observed were 30° and 60° in the structures **1FL3** (Simeonov *et al.*, 2000) and **1BGX** (Murali *et al.*, 1998) respectively. The extreme packing angles are shown in Figure 5.7.

5.3 Identifying interface residues

Interface residues for the 567 structures were defined as described in Section 5.1. Owing to the variability in the V_H/V_L packing angle, the interface residues in any given structure will be a subset of the total set. A total of 124 positions (63 light chain and 61 heavy chain positions) were identified as contributing to the interface in at least one of 567 structures. Figure 5.8 shows the plot of the

1. For points in a set (*SL* or *SH*) calculate centroid *C* (*CL* or *CH*).
2. Compute the covariance matrix. The pseudocode for this is given below:

```

For i=0 to 3(number of dimensions)
Do
  For j=0 to 3(number of dimensions)
  Do
    Total = 0

    For start=0 to 4 (number of points in set SL or SH)
    Do

      Total+=( x[start][i] - C[i] ) *
              ( x[start][j] - C[j] )

    Done /* End of loop For start=0 to 4 */

    Covariance(i,j) = Total/(number of points in SL or SH)

  Done /* End of For j=0 to 3 */

Done /* End of For i=0 to 3 */

```

3. Perform an eigen decomposition for the covariance matrix. Calculate eigen values and eigen vectors.
4. The eigen vector represented by the largest eigen value is the best-fit line when it passes through the centroid.

Figure 5.5: Algorithm used in the calculation of the best-fit line for the light and heavy chain variable regions.

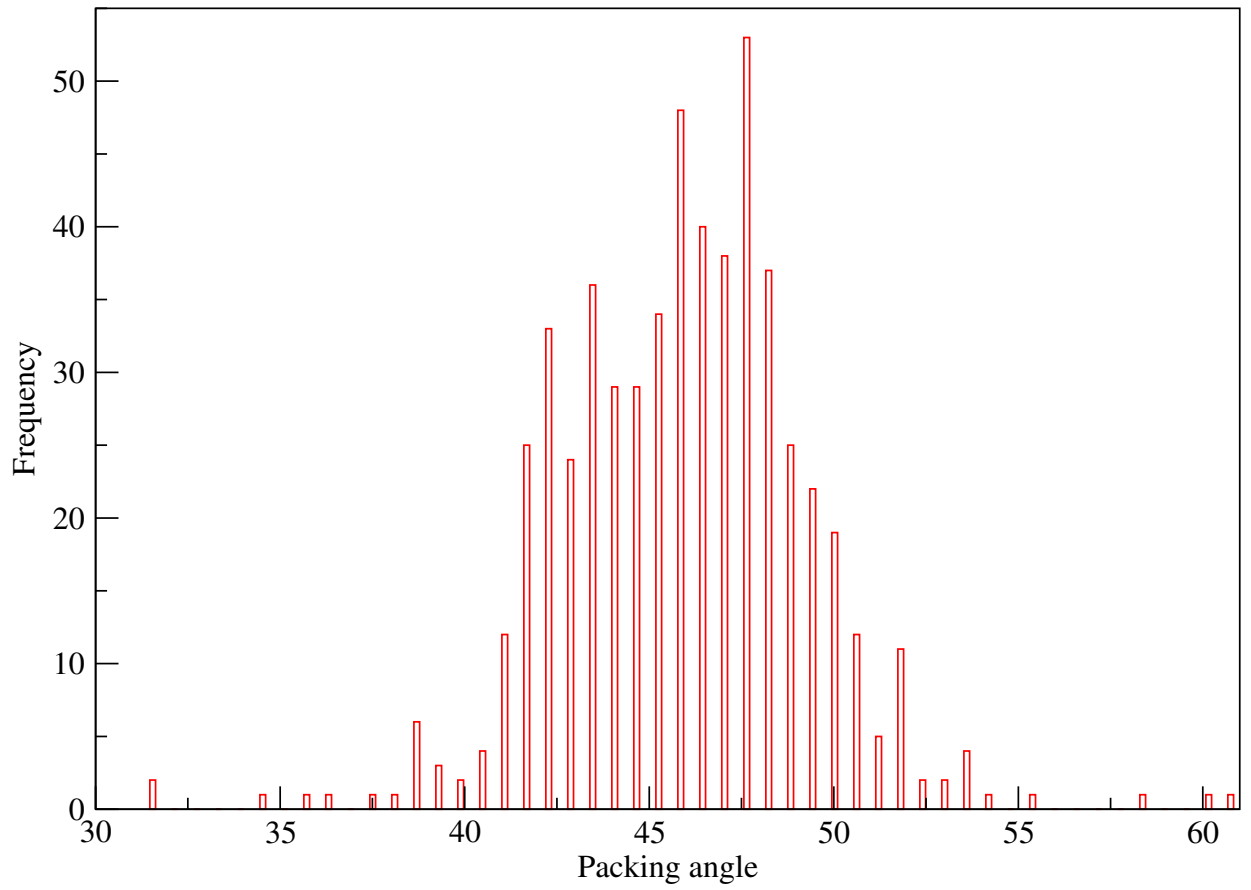
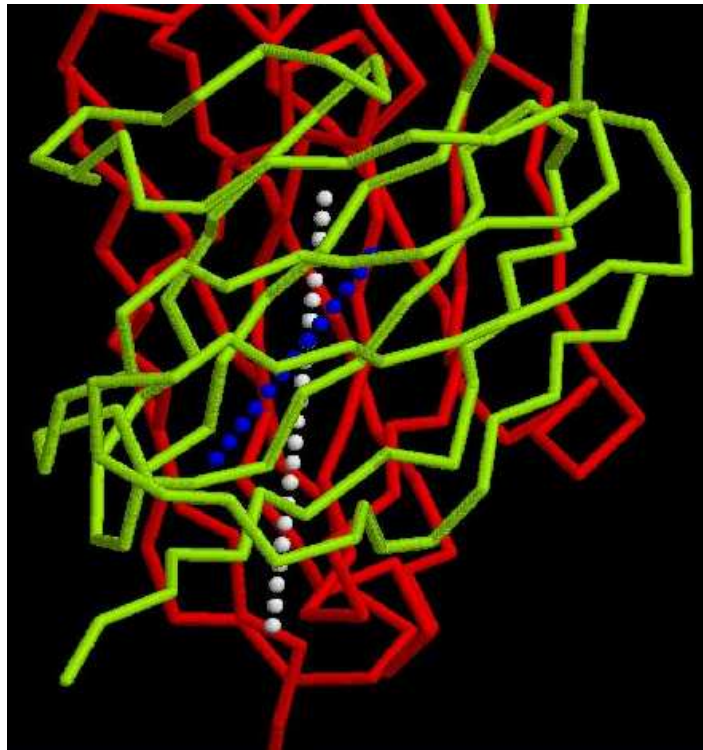
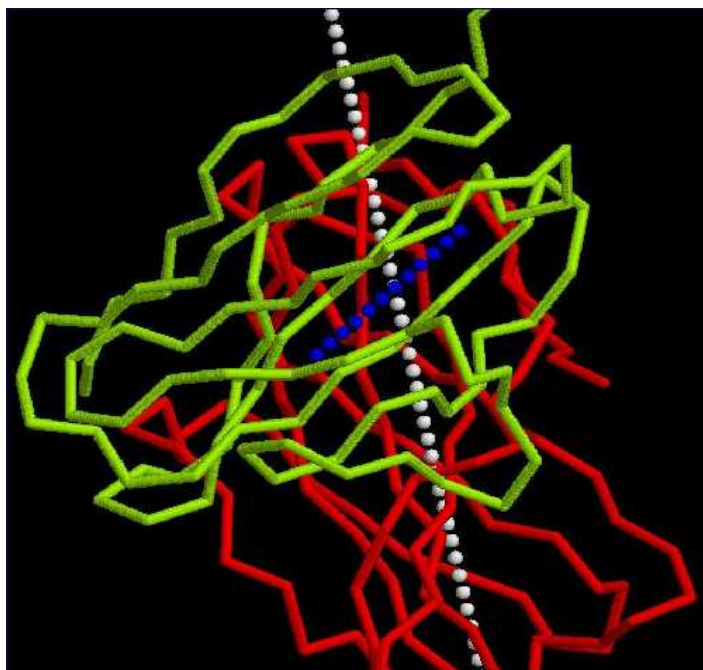


Figure 5.6: Frequency distribution of the packing angle.



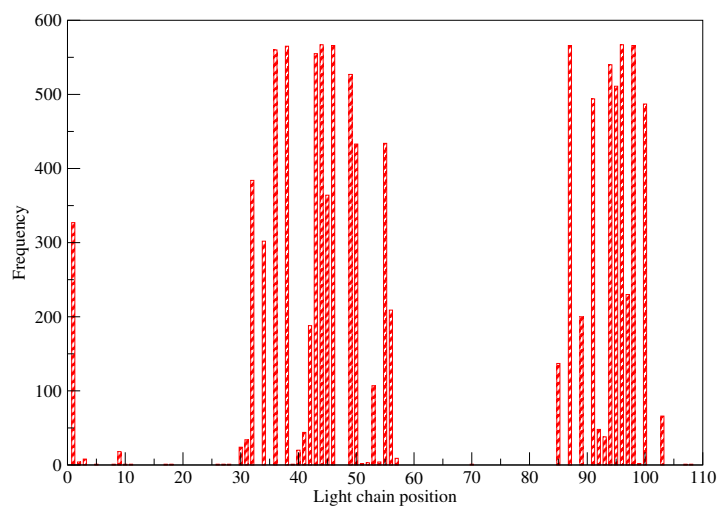
(a) 1FL3



(b) 1BGX

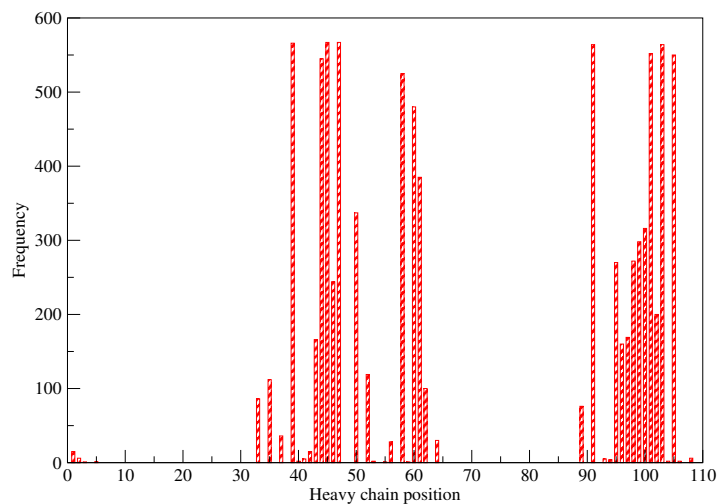
Figure 5.7: Extreme packing angles in (a) 1FL3 - 30° (b) 1BGX - 60° .

Frequency distribution at interface: light chain



(a) Light chain

Frequency distribution at interface: heavy chain



(b) Heavy chain

Figure 5.8: Frequency distribution of interface residues in (a) The Light chain and (b) Heavy chain.

frequency distribution of interface residues in the light chain and heavy chain.

5.4 Predicting packing angle from interface residues

It was decided to use a neural network to predict the packing angle from the interface residues. Amino acids representing the interface residues in different structures were used as input for the neural network and the output was the packing angle. The process of training a network involves supplying a set of input patterns and the output (the result to be predicted) values to help the neural network ‘learn’ from the data. Once the network has passed the learning phase, it is supplied with inputs for which it is expected to make predictions of the output values. The predictions of the neural network are compared with the actual values and the performance of the neural network is assessed. Here, a five-fold cross validation was performed. In this procedure, the neural network is trained on $\frac{4}{5}$ of the total data available and the quality of its training is evaluated by assessing its predictions on the remaining $\frac{1}{5}$ of the data. This is repeated on each slice of the data and the overall performance is averaged over the five folds.

The input is fed to the neural network in the form of numbers that represent the amino acids at the interface. A common method of doing this is using a 20-dimensional binary vector representing the 20 amino acids or values from a similarity matrix. The binary vector contains nineteen 0s and one 1 to indicate a specific amino acid or values from a similarity matrix. The input layer size is calculated as:

$$S_i = N_{aa} \times S_e \quad (5.1)$$

where S_i , N_{aa} , and S_e represent the Input layer size, Number of amino acids and size of the encoding vector respectively. As described above, there are a total of 124 potential interface positions. By applying equation 5.1 and using 20 numbers to represent one of the 20 amino acids, the size of the input layer would be 2480.

The total number of variables in the network is defined as:

$$N_v = (S_i \times S_h) + (S_h \times S_o) \quad (5.2)$$

where N_v is the number of variables in the network, S_i is the number of nodes in the input layer, S_h is the number of nodes in the hidden layer, and S_o is the number of nodes in the output layer. If we use 10 hidden nodes and a single output node to represent the packing angle, then the number of variables in the network would be 24810. As a rule of thumb, it is recommended to use $3N_v$ patterns to train a neural network. Hence, it would have ideally required data from about 75000 structures to train and validate the network successfully. Considering that only about 570 structures were available, I decided to restrict the number of input variables by applying the following rules:

- By using only 4 numbers to represent every amino acid instead of 20.
- By limiting the number of interface positions (used in training and validating

the neural network) to 20 instead of 124.

The four numbers used to represent every amino acid were chosen on the basis of the following physical properties:

1. Size of the amino acid, in terms of the number of atoms in the side-chain.
2. Size of the amino acid expressed as the shortest path from the C α atom to the atom farthest away from it, i.e. the length of the sidechain.
3. Hydrophobicity
4. Charge

Table 5.1 lists the numbers used to represent the 20 different amino acids. The hydrophobicity scales used were taken from the consensus values reported by Eisenberg *et al.* (1982). I decided to use a 4-dimensional encoding vector with 20 interface residues chosen as being most likely to influence the packing angle. By doing this, the input layer size was reduced to 80 nodes.

Initially, a manual selection of 20 interface residues most likely to influence the packing angle made using the following sets of criteria:

Method I Highest change in Accessible Surface Area (ASA) in any one structure.

Method II Highest average change in ASA

Method III Most frequently occurring positions with highest change in ASA

Amino acid	Size NS	Size SP	Hydrophobicity	Charge
Alanine (A)	1	1	0.250	0
Valine (V)	3	2	0.540	0
Leucine (L)	4	3	0.530	0
Isoleucine (I)	4	3	0.730	0
Proline (P)	3	4	-0.07	0
Methionine (M)	4	4	0.26	0
Phenylalanine (F)	7	5	0.610	0
Tryptophan (W)	10	6	0.370	0
Glycine (G)	0	0	0.160	0
Serine (S)	2	2	-0.26	0
Threonine (T)	3	2	-0.18	0
Cysteine (C)	2	2	0.04	0
Asparagine (N)	4	3	-0.64	0
Glutamine	5	4	-0.69	0
Tyrosine (Y)	8	6	0.02	0
Aspartate (D)	4	3	-0.72	-1
Glutamate (E)	5	4	-0.62	-1
Lysine (K)	5	5	-1.1	1
Arginine (R)	7	6	-1.8	1
Histidine (H)	6	4	-0.4	0.5

Table 5.1: Amino acid properties for size, hydrophobicity and charge. *NS*: number of side chain atoms in the amino acid; *SP*: shortest path to the atom farthest away from the $C\alpha$ atom of the residue. 0.5 was chosen as the charge for Histidine to represent the fact that it can exist in both charged and uncharged states.

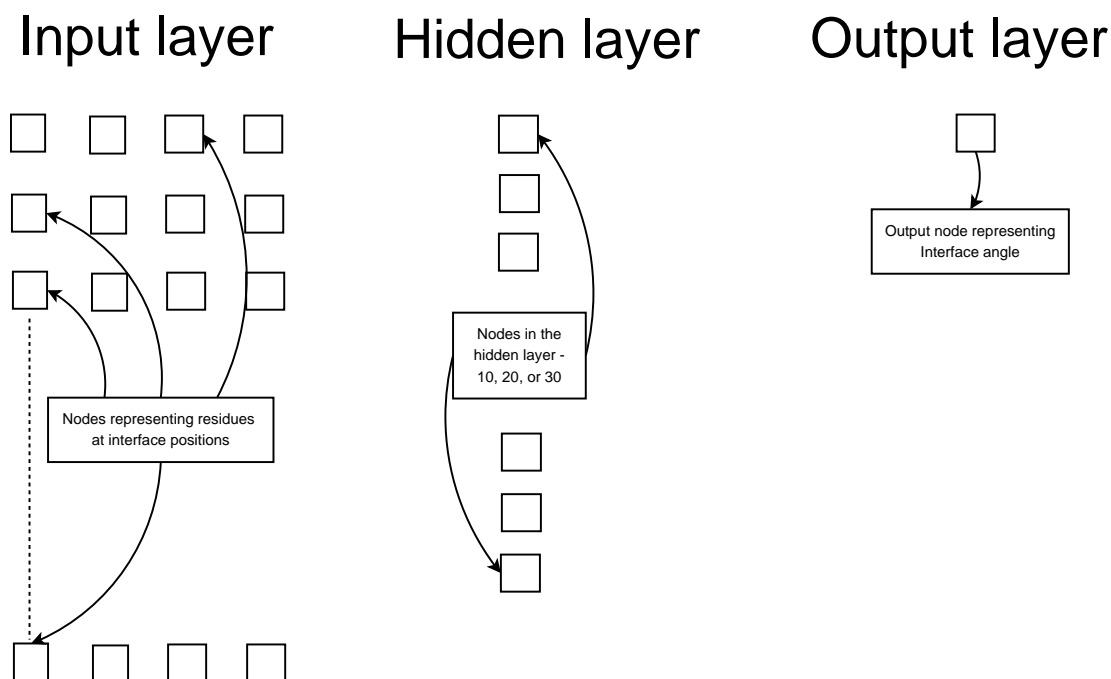


Figure 5.9: Architecture of a fully connected network. Not shown in the figure are the connections between every pair of nodes in the input layer and hidden layer and between nodes in the hidden and output layer.

Method IV Most frequently occurring positions with highest average change in ASA

The top 10 positions in each chain (light and heavy) were taken and a 5-fold cross validation was performed. Table 5.2 lists the interface positions that were manually selected. A fully connected artificial neural network was constructed with the architecture shown in Figure 5.9. Using the *Stuttgart Neural Network Simulator (SNNS)* the neural network parameters: learning function, update function, initialisation function, shuffling and number of cycles were varied and the following values were found to be most optimal for the problem:

1. Number of cycles of training - 150

Method	Interface positions
Method I	L34, L36, L44, L46, L50
	L87, L89, L91, L96, L98
	H35, H47, H91, H100B, H100C H100D, H100I, H100G, H100M, H103
Method II	L34, L36, L43, L44, L46
	L86, L87, L89, L91, L98
	H35, H47, H91, H100B, H100C H100D, H100G, H100I, H100M, H103
Method III	L32, L34, L36, L44, L46
	L50, L87, L91, L96, L98
	H45, H47, H50, H91, H99 H100, H100A, H100B, H101, H103
Method IV	L34, L36, L38, L43, L44
	L46, L87, L91, L96, L98
	H39, H45, H47, H91, H99 H100, H100A, H100B, H101, H103

Table 5.2: Manually chosen interface positions based on methods (I) Highest change in ASA, (II) Highest average change in ASA, (III) Most frequently occurring positions with highest change in ASA, and (IV) Most frequently occurring positions with highest average change in ASA.

2. Training until sum-of-squares error (SSE) becomes ≤ 1.5
3. Init function - Randomise weights
4. Learning function - RProp
5. Update function - Topological order
6. Pruning function - Magnitude pruning.
7. Shuffling - TRUE
8. Number of hidden nodes - 10.

A neural network consists of a set of ‘perceptrons’ which generate values between 0 and 1 using a sigmoid function applied to a weighted sum of the inputs:

Method	Average Pearson's coefficient over 5 folds
I	0.32
II	0.38
III	0.40
IV	0.30

Table 5.3: Results of a 5-fold evaluation over interface positions chosen manually using the four methods described in the text. The correlation coefficient reported has been averaged over the 5 folds.

$$O = f\left(\sum_{i=1}^N W_i x_i\right) \quad (5.3)$$

where O is the output of the perceptron, $f()$ is the sigmoid transfer function, x_i is an input, W_i is an weight and N is the number of inputs. I therefore decided to represent all output values (packing angles) by a value between 0 and 1. The scaling of packing angles was done according to:

$$\theta_f = \frac{\theta - \theta_{\min}}{\theta_{\max} - \theta_{\min}} \quad (5.4)$$

where θ_f is the interface angle fraction, θ is the interface angle, θ_{\max} is the maximum observed interface angle, and θ_{\min} is the minimum observed interface angle. From manual examination, it appeared that shuffling the training data (item 7 in the list of optimal SNNS parameters shown above) while training the neural network had a positive effect. However, this could not be used when training and validating the neural network through scripts as it appears that this feature is only supported by the graphical interface to SNNS.

To evaluate the performance of the neural network, the Pearson’s correlation coefficient (r) was initially used to compare the output of the neural network and the actual scaled packing angle (between 0 and 1):

$$r_{xy} = \frac{\sum_{i=1}^n (x_i - \bar{x})(y_i - \bar{y})}{(n - 1)s_x s_y} \quad (5.5)$$

where r_{xy} is the Pearson’s correlation coefficient between two variables x and y , n is the number of data points, x_i and y_i are the individual values of variables x and y , and s_x and s_y are the standard deviations of the two distributions x and y . Table 5.3 shows the result of training and validating the neural network based on the manual selection of interface positions. None of the methods to select interface residues manually worked particularly well as the Pearson’s correlation coefficient for all methods was low. However, from manual examination of correlation coefficients over single folds, correlation coefficients as high as 0.6 had been observed. I therefore decided to have the computer sample sets of interface positions to find the combination that would be most predictive of the packing angle.

5.5 Using a genetic algorithm to sample the interface-residue space

The use of a genetic algorithm (GA) for feature selection (i.e. to sample sets of interface residues and pick the most optimal set) appeared to be a potential

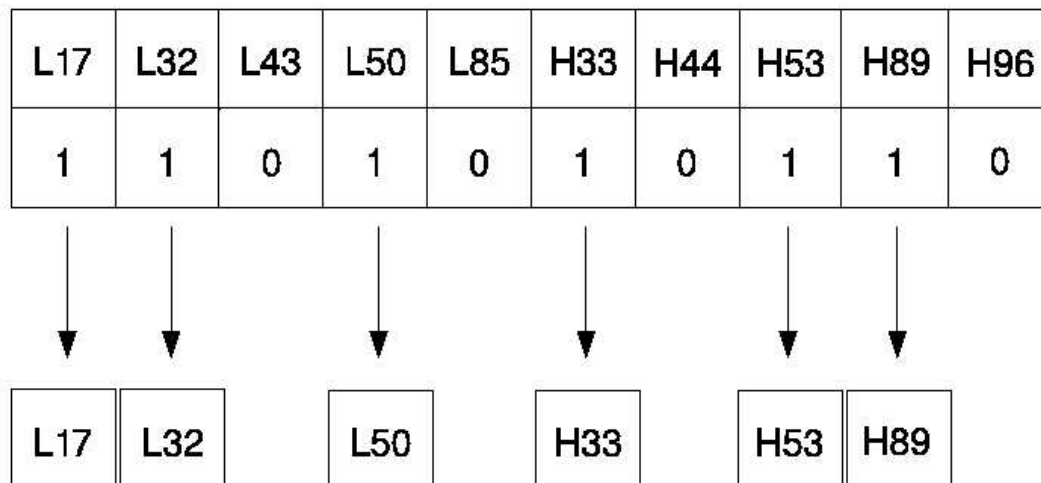


Figure 5.10: An individual to represent 10 interface positions. From the string shown, those *alleles* with a 1 imply the inclusion of the residue at the respective interface position for training and validation of the neural network.

solution to the problem of low scores of manually selected interface positions.

The overall method of the genetic algorithm developed to sample the space of interface residues is described below:

1. Create a random population of individuals where each individual represents a set of interface positions, each allele being a 1 or 0 to indicate whether a given interface position is included in training the neural net.
2. Evaluate the quality of each individual by training and validating the neural network over 5 folds (5-fold cross-validation)
3. Create a new population of individuals by crossover of high-scoring individuals.
4. Repeat the above steps for as many generations as required.

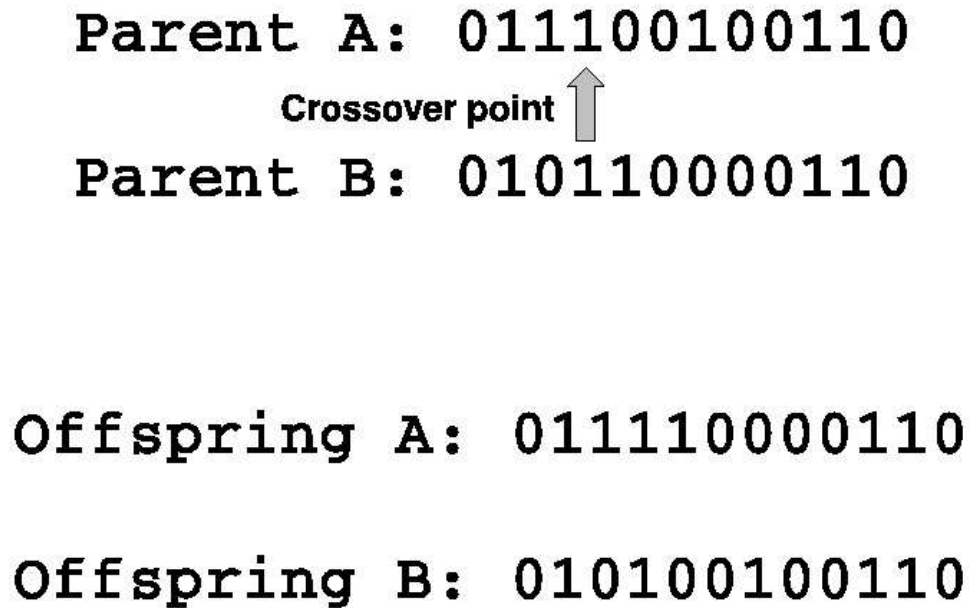


Figure 5.11: Crossover of two high-scoring individuals A and B

The first step involves the creation of a random population of individuals. Every individual is a string whose length is the number of interface positions. It consists of a set of 0s and 1s (alleles) and represents a selection of interface positions to be used to train and validate a neural network. This is demonstrated in Figure 5.10. The quality of every individual is assessed by training the neural network and averaging the Pearson's correlation coefficient over 5 folds. Initially, a random population of individuals is created and the quality of every individual is assessed. A new population of individuals is then generated by selective *crossover* of high scoring individuals which is shown in Figure 5.11. Newly created *offspring individuals* are subject to random mutations at a rate referred to as the *mutation rate* (μ). In this work, unless otherwise specified, a default mutation rate of 0.0001 has been used for Rank-based selection (See Section 5.6). Once the random mutations have been effected, the offspring individuals become *children*. These children become

the parents for the next generation. They are scored by training and validating the neural network and further generations of the genetic algorithm progress in the same way. These steps are repeated until the required number of generations have been completed or the population has converged.

5.6 Methods of selection

In the process of creating offspring through crossover, a bias is made towards the selection of parents that have high scores. There are many selection methods for choosing the parents and in this project, I primarily used **Roulette-wheel** based selection and **Rank-based** selection. These selection strategies have already been addressed in Chapter 2.

Generation	Best Pearson's r	
	Rank	Roulette-wheel
1	0.4964	0.4980
2	0.5039	0.5082
3	0.5039	0.5082
4	0.5007	0.5082
5	0.5039	0.5082
6	0.5167	0.5082
7	0.5159	0.5082
8	0.5122	0.5082
9	0.5581	0.5054

continued on next page

continued from previous page

Generation	Best Pearson's r	
	Rank	Roulette-wheel
10	0.5266	0.5082
11	0.5271	0.5082
12	0.5581	0.5054
13	0.5581	0.5054
14	0.5318	0.5082
15	0.5503	0.5082
16	0.5703	0.5082
17	0.5703	0.5054
18	0.5586	0.5082
19	0.5703	0.5082
20	0.5572	0.5082
21	0.5703	0.5054
22	0.5703	0.5082
23	0.5703	0.5082
24	0.5703	0.5082
25	0.5703	0.5082
26	0.5626	0.5082
27	0.5910	0.5082
28	0.5910	0.5082
29	0.5910	0.5054
30	0.5829	0.5082

continued on next page

continued from previous page

Generation	Best Pearson's r	
	Rank	Roulette-wheel
31	0.5870	0.5082
32	0.5910	0.5082
33	0.5910	0.5054
34	0.6006	0.5082
35	0.5910	0.5082
36	0.5946	0.5082
37	0.6149	0.5082
38	0.6006	0.5054
39	0.5910	0.5054
40	0.5910	0.5082

Table 5.4: Comparing Roulette-wheel and Rank-based selection methods. The table shows the best Pearson's r calculated over 40 generations of a GA run.

The effectiveness of a selection procedure is largely assessed by the ability of the procedure to keep the population diverse (i.e. avoid local minima) and yet achieve convergence in a reasonable time span. To decide on the method best suited for the current problem, I performed test runs of the GA on small populations of individuals for short durations using both Rank-based and Roulette-wheel based selection methods. Results from a sample run are summarised in Table 5.4. From the table, it can be seen that the initial scores were nearly equal (0.496 in Rank and

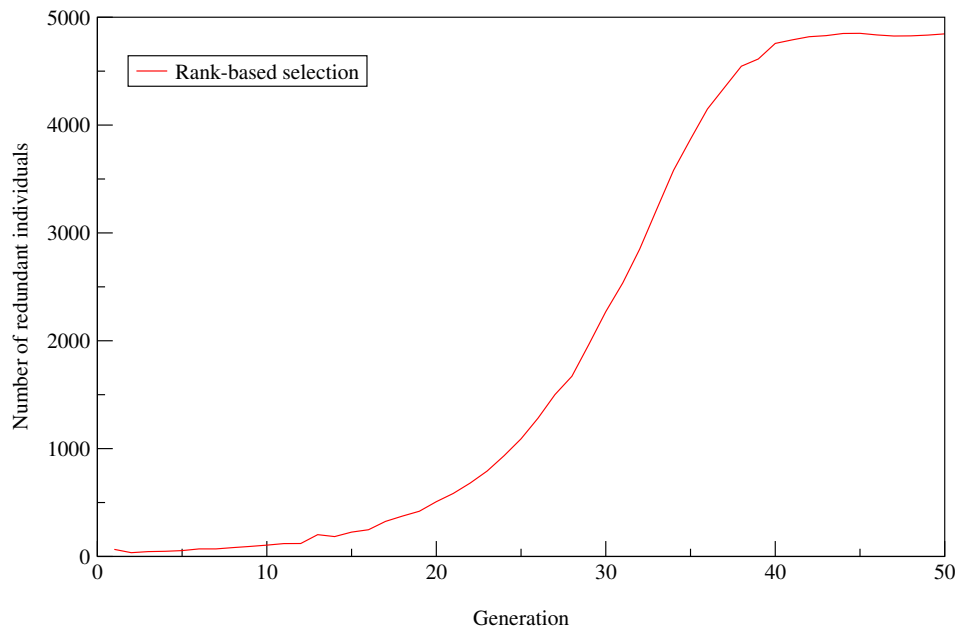
0.498 in Roulette-wheel based selection). However, there is a steady increase in best score for Rank-based selection whereas the best score remains largely static for Roulette-wheel based selection. It was therefore decided to use Rank-based selection for future runs of the GA.

5.7 Problems: Redundancy in individual population and intelligent selection

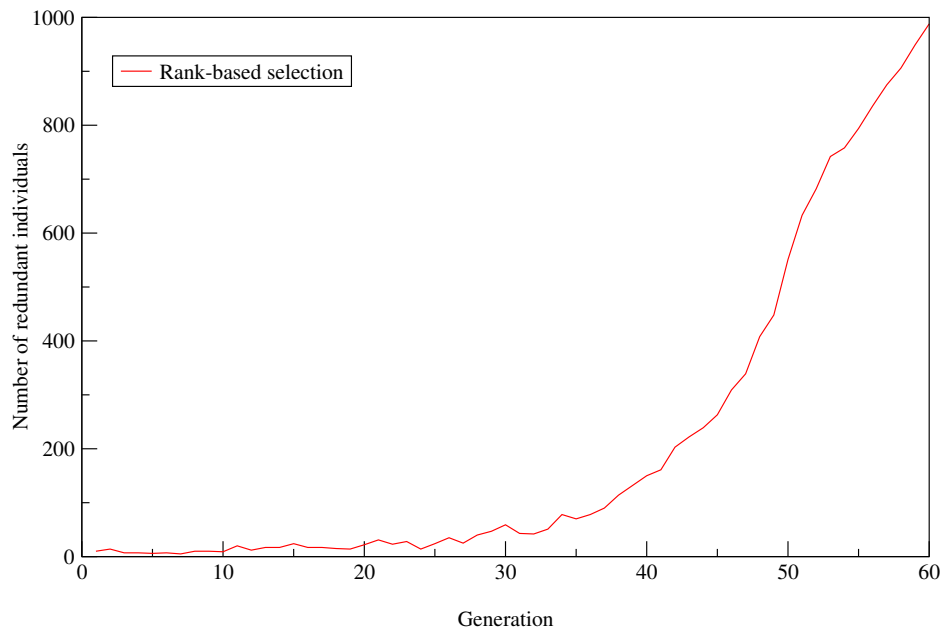
A problem with Rank-based selection that became apparent after a few tens of generations of the GA was that the population of individuals was becoming decreasingly diverse. Figure 5.12a shows a graph of a GA run where Rank selection, together with a mutation rate of 0.0001 were used. The score of the best individual at the end of 50 generations was 0.638. This could have meant either a) The genetic algorithm was converging to a globally optimal solution, or b) The GA was getting stuck in a local minimum problem.

It was assumed that the GA was getting stuck in a local minimum and, as will become clear from the following sections, this was indeed the case. I developed an alternative method to alter the mutation rate dynamically during crossover.

In Rank-based selection, the creation of new child individuals is done by biasing selection towards high-scoring parents. A *crossover* point is chosen randomly within the parents and the two parts of the parents are combined to yield offspring (Figure 5.11). When the number of redundant individuals in the population in-



(a)



(b)

Figure 5.12: Redundancy of individuals in a GA run using Rank-based selection with (a) 5000 individuals and $\mu=0.0001$ (b) 1000 individuals and $\mu=0.001$.

creases, the chances of choosing two identical individuals randomly for crossover also increases. Crossover of identical individuals would clearly yield a child identical to the parents. Since the mutation rate applied to the offspring individual is very low (0.0001), the final offspring are likely to be unchanged. However, a higher mutation rate ($\mu=0.001$) did not help curb the exponential rise in the number of redundant individuals with the passage of every generation. Figure 5.12b shows that the population of individuals quickly saturates and by the end of 60 generations, nearly the entire population of individuals is redundant.

As a solution to the problem of individual redundancy, I developed a combinatorial approach. Parent individuals are selected using Rank-based selection, but a modification to the strategy of using a standard mutation rate was made so that the mutation rate was varied dynamically, depending on how similar the parents selected for crossover are. The method, which I term *Intelligent selection*, is described below:

1. For every child individual to be created, select 2 parents P1 and P2 based on Rank Based Selection.
2. Choose a cross over point and splice P1 and P2 to create a child O_i .
3. Calculate the degree of similarity $S_{(P1,P2)}$ between the parents P1 and P2 as given by:

$$S_{(P1,P2)} = \frac{C_{(P1,P2)}}{N_{(P1,P2)}} \quad (5.6)$$

where $C_{(P1,P2)}$ is the number of active alleles common between $P1$ and $P2$

and $N_{(P1,P2)}$ is the sum of active alleles in $P1$ and $P2$. When the two parents are completely identical, the similarity is 0.5 whereas when they have no common alleles, the similarity is 0.

4. If $(0.45 \leq S_{(P1,P2)} \leq 0.5)$, then swap five 0s and 1s in O_i .
5. If $(0.35 \leq S_{(P1,P2)} < 0.45)$, then use a mutation rate of 0.01 on O_i .
6. If $(0.25 \leq S_{(P1,P2)} < 0.35)$, then use a mutation rate of 0.008.
7. if $(0.15 \leq S_{(P1,P2)} < 0.25)$, then use a mutation rate of 0.005.
8. if $(0 \leq S_{(P1,P2)} < 0.15)$, then use a mutation rate of 0.001.

I used a generational replacement strategy in which the entire population of parents was replaced by children. In addition, I maintained a record of the best parent from every generation. By using generational replacement, the interface position space can be explored better and by keeping a record of the best individual in every generation, it was possible to report the score of the best-performing individual in the entire GA run.

By varying the mutation rate, it became possible to keep the population diverse and therefore sample many different combinations of the possible ‘interface position space’. Figure 5.7 shows a comparison of the performance of Rank-based selection and Intelligent selection for similar runs of the GA using a population of 5000 individuals over 50 generations. It must also be highlighted that the best individual at the end of 50 generations in Rank selection had a Pearson’s r of 0.638 while the Pearson’s r for the best individual after 50 generations in Intelligent selection was 0.63. In the limited test of 50 generations, the intelligent selection

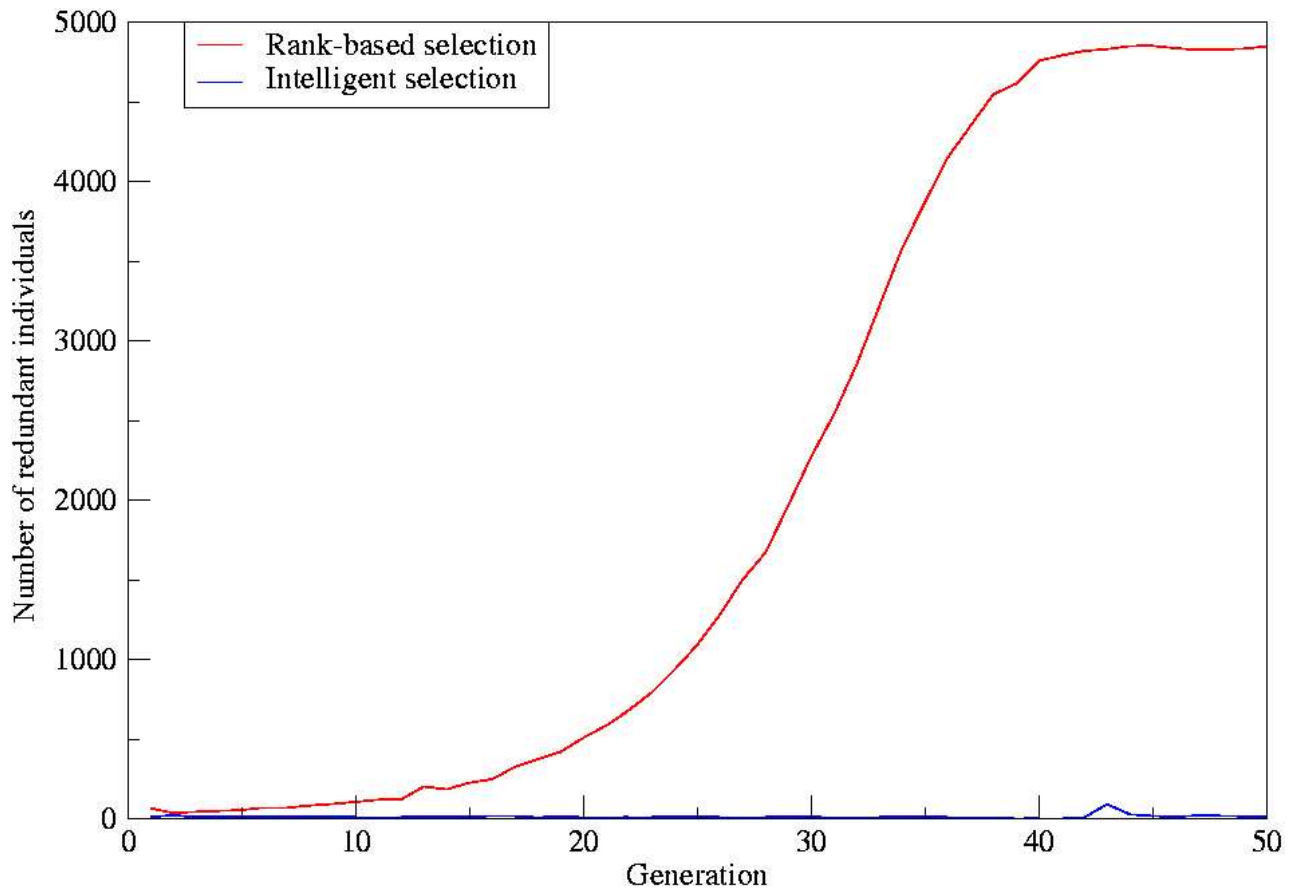


Figure 5.13: Comparing Rank and Intelligent selection strategies. Both plots correspond to GA runs with 5000 individuals over 50 generations.

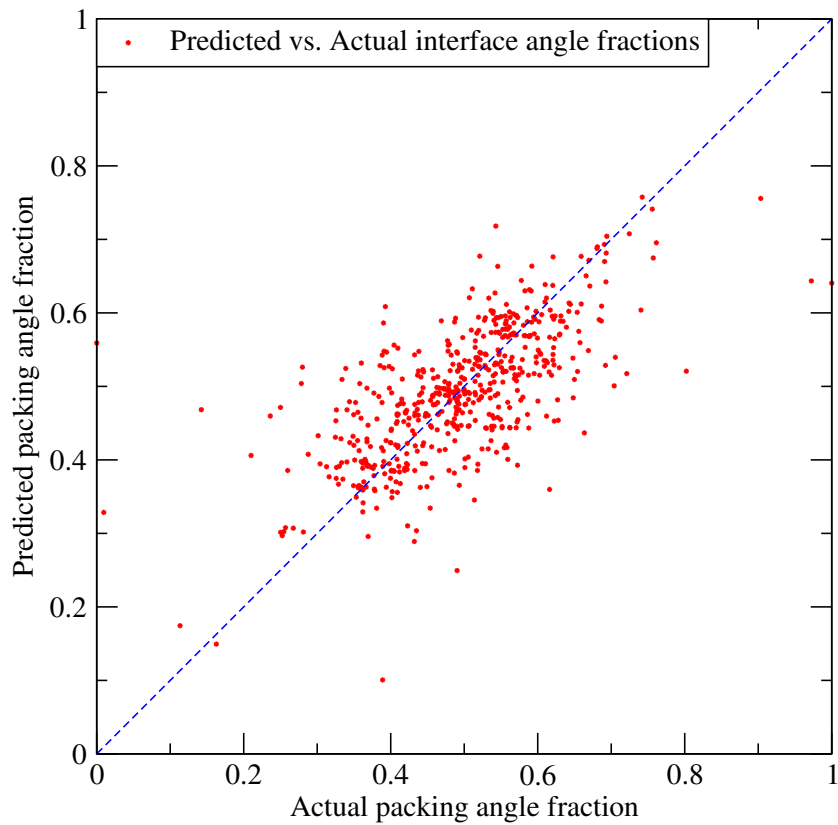


Figure 5.14: Plot of the predicted interface angle fractions vs. the actual interface angle fractions for the individual with the best Pearson's correlation coefficient (0.6442). Perfect predictions would lie on the blue dotted line.

method was able to find a best solution which was just as good as the best solution from rank-based selection but still maintained a diverse population to avoid local minima. I decided to perform all further GA runs using the intelligent selection method.

5.8 Scoring the quality of each individual

Initially, the score of all individuals was evaluated as the Pearson's correlation coefficient between the predicted and actual interface angle fractions. However, the

Pearson's r is not very reflective of the actual performance of the neural network in terms of the accuracy of predictions. This is demonstrated by the graph in Figure 5.14 which plots the actual interface angle fraction (between 0 and 1) versus the predicted interface angle fraction for the individual with the best Pearson's r (0.644). From the graph, it may be noticed that the errors (given by the distance of the data points from the blue dotted line) in predictions for very low or high interface angles is large. Despite the large error, the Pearson's r between the actual and predicted interface angle is high. I therefore also assessed the quality of every individual by means of the error difference between the predicted and actual values. For this, I used the Root mean square error which is calculated as:

$$RMSE = \sqrt{\frac{\sum_{i=1}^n (x_i - p_i)^2}{n}} \quad (5.7)$$

where $RMSE$ is the root mean square error, x_i is the actual interface angle fraction, and p_i is the predicted interface angle fraction. The score was calculated as $1 - RMSE$.

However, the RMSE was not reflective of the actual magnitude of error. Since the packing angles are scaled to a value between 0 and 1, the RMSE is indicative of the error at the scaled level and not in terms of the actual angular error in degrees. Packing angles that are either very low or very high and don't have sufficient representation in the dataset tend to be predicted with high errors. However, this is not adequately reflected in the RMSE as the overall RMSE over the entire dataset tends to be quite low owing to good predictions for a majority of the

packing angles that are sufficiently represented in the dataset. This led me to search for an alternate statistic to score the quality of predictions so that the error in extreme packing angles would be reflected.

The relative RMS error (Masters, 1993) calculates the RMS value of the error and takes the ratio of this value with respect to the sum of the actual values. This is computed as:

$$RELRMSE = \sqrt{\frac{\sum_{i=0}^n (x_i - p_i)^2}{\sum_{i=0}^n t_i^2}} \quad (5.8)$$

where $RELRMSE$ is the relative root mean square error, x_i is the actual interface angle fraction, and p_i is the predicted interface angle fraction. The Relative RMS error is calculated over five folds for every individual and the score for an individual is calculated as:

$$SCORE = 1 - RELRMSE \quad (5.9)$$

From initial performance statistics, it appeared that the RELRMSE was much more sensitive to errors in predictions of small and large packing angles than the RMSE and I decided to assess the quality of all individuals using this statistic instead of the RMSE or the Pearson's correlation coefficient r .

Parameter	Value
Neural network	
Cycles of training	150
SSE during training	≤ 1.5
Init function	Randomise weights
Learning function	RProp
Update function	Topological order
Pruning function	Magnitude pruning
Shuffling	FALSE
NH	10
Genetic algorithm	
Selection method	Intelligent selection
Scoring method	Relative RMS error

Table 5.5: Standard parameters for the Neural network and the Genetic algorithm. NH: Number of hidden nodes, SSE: Sum of square error.

5.9 Results of GA runs

5.9.1 Prediction the V_H/V_L packing angle

To summarise, a GA had been designed to perform feature selection for training the neural network to predict the V_H/V_L packing angles. The fitness function for the GA was the performance of the neural network evaluated over a five-fold cross-validation and averaging the scores calculated using the Relative RMS error over the five folds.

Once I had standardized parameters for the neural network and the genetic algorithm (summarised in Table 5.5), I initiated large scale runs of the genetic algorithm involving thousands of individuals for several thousand generations. Owing to the elaborate computations involved in this, it typically takes about 25 seconds

to perform a 5-fold cross-validation of an individual. The runs were performed on large farms over a period of several months. Problems were encountered at several stages of the GA largely owing to issues related to the Network file system (NFS). This slowed down the overall speed of execution of the GA.

Individuals were chosen to represent the following sets of interface positions:

- All interface positions.
- Interface positions that are part of the framework regions.

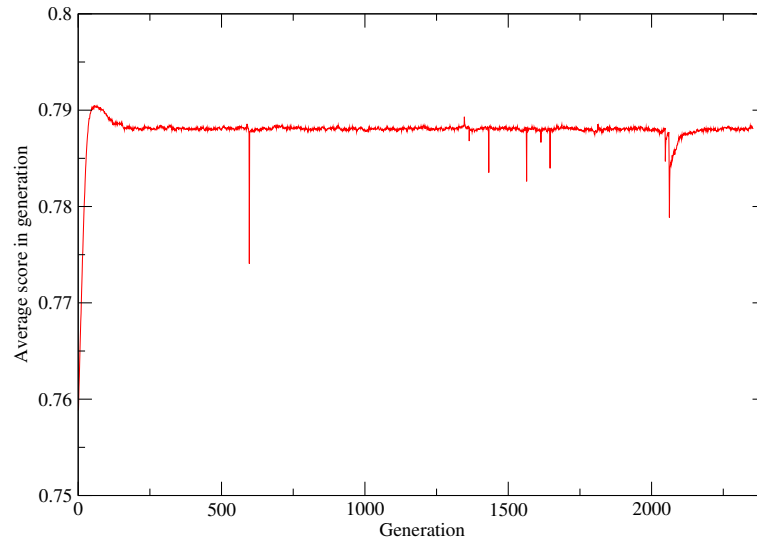
A genetic algorithm run involving all the 124 interface positions was initiated for a population of 15000 individuals. The run was initiated on the C^3 on 10th of June, 2007 and terminated on the 16th of October, 2007. Sun Gridengine was used to distribute jobs across the farm. Every job involves training and validation of a neural network on a set of interface positions which is represented by an individual in the GA.

The performance at the end of every generation was monitored and is shown as graphs in Figure 5.15. The performance in the GA is assessed by two parameters:

- The score of the best individual at the end of every generation.
- The average score of individuals in every generation.

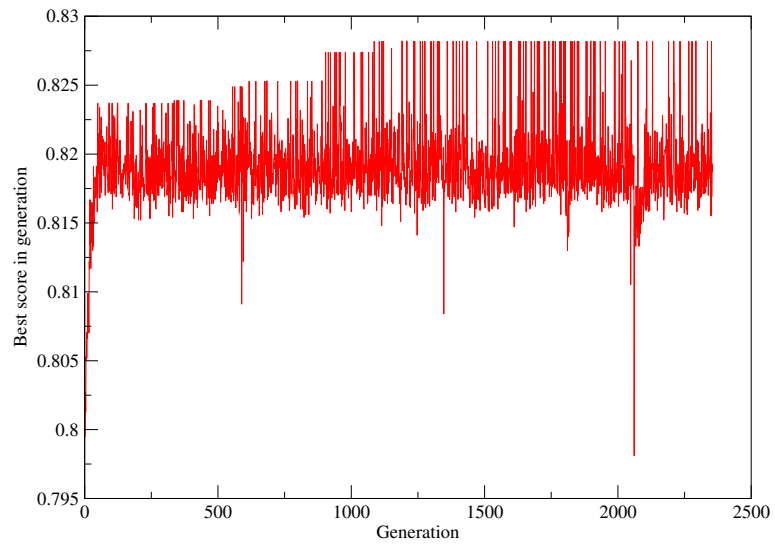
When the average score of individuals in the population increases, it is also likely

Average scores in a GA run involving all interface positions



(a) Average score in every generation

Best score in a GA run involving all interface positions



(b) Best score in every generation

Figure 5.15: GA runs involving all interface positions. Figures shown are (a) Average score in every generation (b) Best score in every generation.

GA Run type	Interface positions
All interface positions	L38
	L40
	L42
	L44
	L46
	L87
	L99
	H43
	H52A
	H55
	H64
	H100I
	H100K
	H100M
	H100O
	H106

Table 5.6: Interface positions corresponding to the best individual from a GA run involving all interface positions.

that offspring individuals produced by the crossover of high-scoring individuals will also have a high score.

From Figure 5.15a, it can be seen that the GA run registers a sharp increase in the average score initially over the first 50 generations and then flattens out over the rest of the generations. A similar trend is observed for the best scores (Figure 5.15b). The best score increases sharply for the first 50 generations from about 0.8 to a little over 0.82. However, the best score over the entire genetic algorithm run was achieved in generation 1086 (a score of 0.821 which translates to a relative RMSE of 0.172). The interface positions represented by the best individual are shown in Table 5.6.

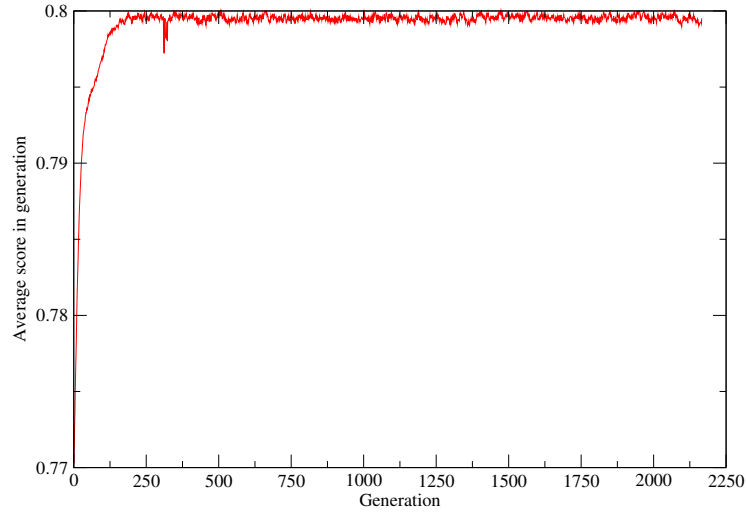
GA Run type	Interface positions
Non-CDR interface positions	L38
	L40
	L41
	L44
	L46
	L87
	H33
	H42
	H45
	H60
	H62
	H91
	H105

Table 5.7: Interface positions corresponding to the best individual from a GA run involving only non-CDR interface positions (CDRs defined according to Chothia (Al-Lazikani *et al.*, 1997)).

5.9.2 Choosing key framework interface residues

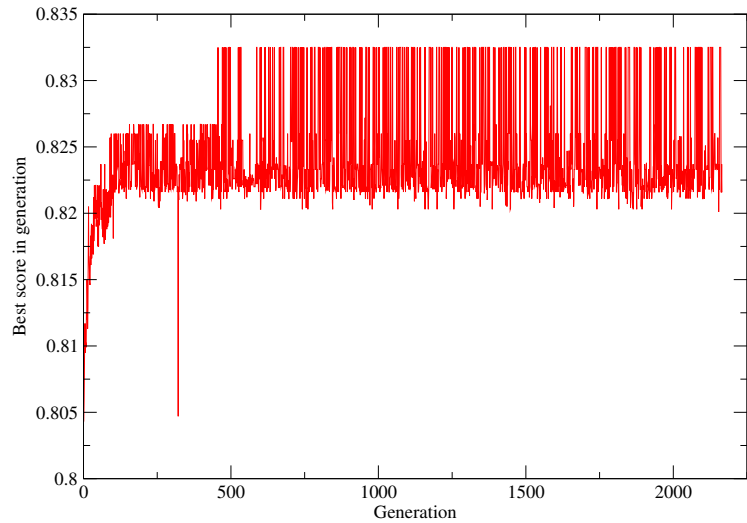
In the case of humanization of antibodies, murine CDRs are transplanted onto a human framework region. This is usually done assuming that the transfer of murine CDRs onto the human framework region would confer the same specificity of the murine antibody to the humanized antibody. However, residues in the framework regions flanking the CDRs may have to be modified in order to reinstate the binding specificity of the original murine antibody to the humanized antibody (Riechmann *et al.*, 1988). I therefore decided to explore the possibility of predicting the packing angle by using only a combination of non-CDR interface residues. Thus the main goal of this work was the identification of key residues in the framework regions that would be deterministic of the packing angle and therefore aid in the engineering of antibodies to confer appropriate antigen specificity.

Average scores in a GA run involving non-CDR interface positions



(a) Average score in every generation

Best scores in a GA run involving non-CDR interface positions



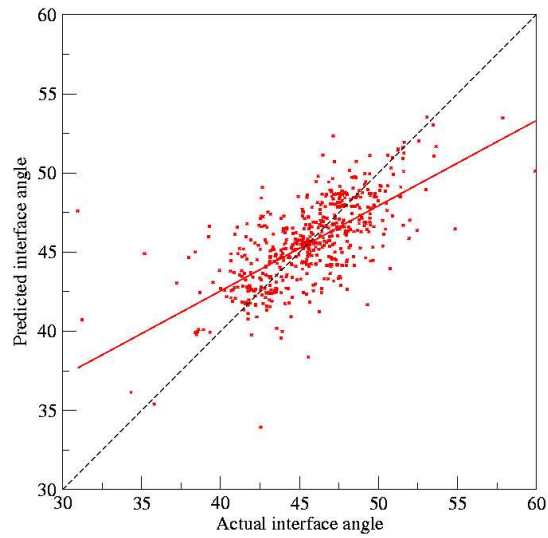
(b) Best score in every generation

Figure 5.16: GA runs involving non-CDR interface positions. Figures shown are (a) Average score in every generation (b) Best score in every generation.

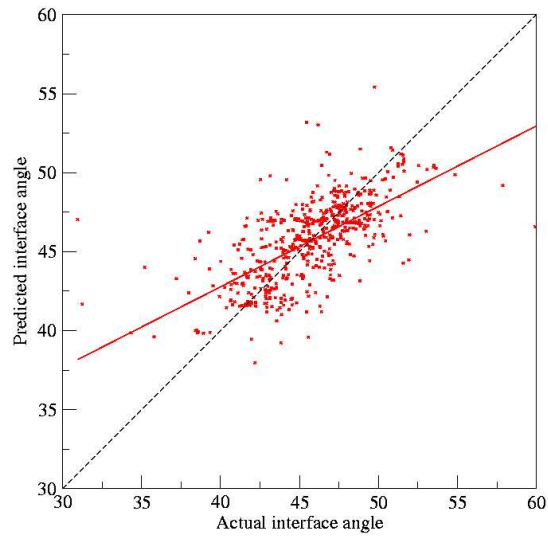
A genetic algorithm run involving 64 non-CDR interface positions was initiated on a population of 15000 individuals on the *Queen* cluster. All the 64 positions chosen are part of the framework region according to the Chothia numbering scheme. Runs were initiated on the 10th of June, 2007 and were terminated on the 4th of October, 2007. A total of 2166 generations completed in this time period. Results of the run are shown in Figure 5.16. The graphs for the average and best score in every generation are very similar in nature to the graphs involving GA runs for all interface positions. The average and best scores increase sharply for the first 150 generations and then stabilise for the remaining generations. The best score of 0.833 (a relative RMS error of 0.167) was first seen after 146 generations. The interface positions represented by the best individual are shown in Table 5.7.

5.9.3 Jackknifing and analysis of errors of the best individuals

I performed a jackknifing examination on the best individual which involved training the neural network over data from all but one structure and evaluating the quality of the training by predicting the interface angle for one structure. Results of the jackknifing run are shown in Figure 5.17. The graph plots the packing angles predicted by the neural network against the actual interface angles for the best individuals involving all interface positions (Figure 5.17a) and non-CDR interface positions (Figure 5.17b). From the figures, it can be seen that the majority of the predictions are close to the ideal line (represented by the black dotted line). It is well known that neural networks do not make good predictions on data that

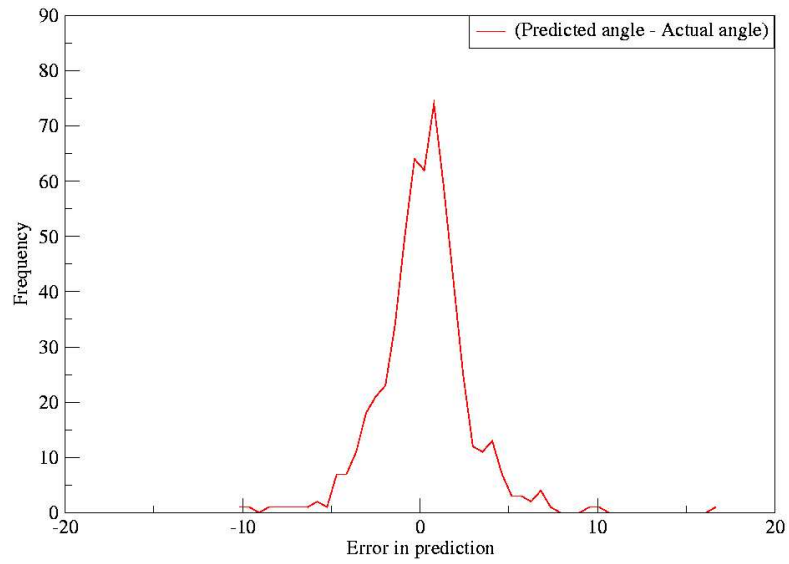


(a) All interface positions

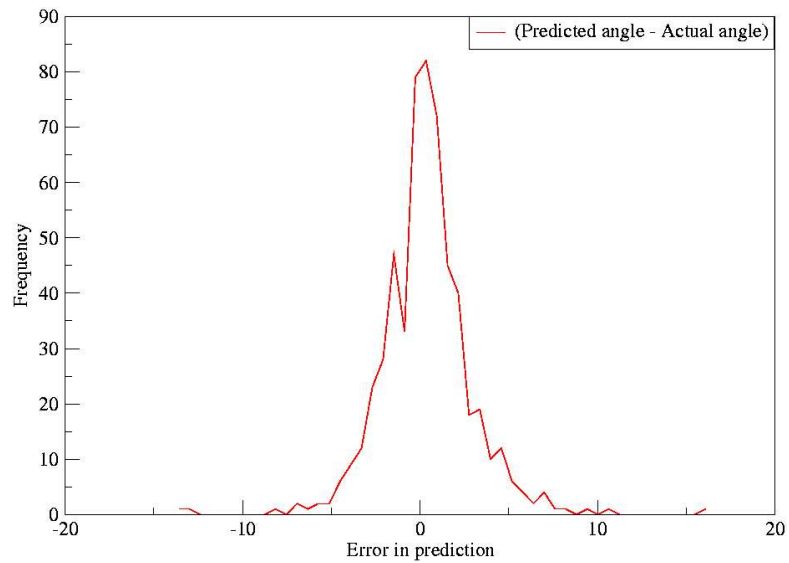


(b) Non-CDR interface positions

Figure 5.17: Predicted vs. the Actual packing angle results for jackknifing of the best individual from the GA runs for (a) All interface positions and (b) Non-CDR interface positions. Perfect predictions would lie on the black dotted line. The line in red shows the best-fit regression line for the data points.

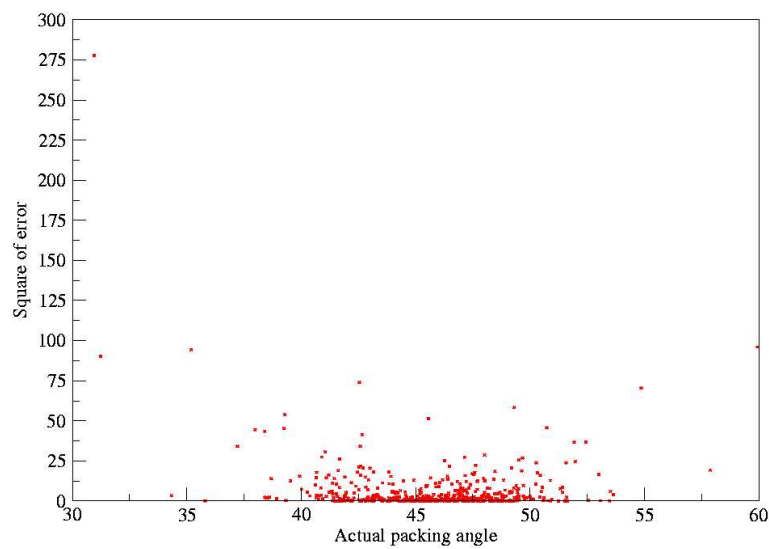


(a) All interface positions

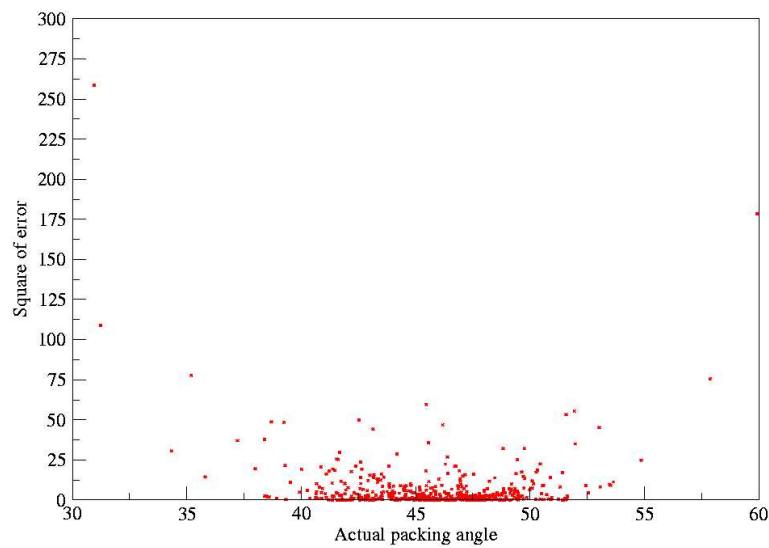


(b) Non-CDR interface positions

Figure 5.18: Frequency distribution of the error calculated as the difference between the predicted and actual interface angle for the best individual from the GA run involving (a) All interface positions and (b) Non-CDR interface positions.



(a) All interface positions



(b) Non-CDR interface positions

Figure 5.19: Plot of errors in packing angle prediction against the actual packing angle (a) involving all interface positions and (b) involving non-CDR interface positions.

are sparsely represented. This appears to be the case of predicting packing angles that are less than 43° and greater than 50° . For the remaining packing angles, the predictions of the neural network are very close to the actual packing angle. This is further corroborated by the frequency distribution plots for the errors in predictions shown in Figure 5.18. The graph approximates a normal distribution with a peak around an error value of 0.

Further, to understand the correspondence between the actual packing angle and the tendency for an error in the prediction, the square of the error for each prediction was plotted against the actual packing angle. These plots are shown in Figures 5.19a and 5.19b for the best individuals identified from GA runs involving all interface positions and non-CDR interface positions respectively. The two graphs are very similar and it may be seen that the majority of the data points lie close to the X-axis. This reinforces the conclusion from the graphs in Figure 5.18 that the majority of predictions are made with very low error rates. Further, it may also be inferred that the large errors are primarily seen for either low and high packing angles which do not have adequate representation in the repertoire of structures that constitutes the dataset.

5.10 Discussions and conclusion

In this chapter, I have defined and analysed the V_H/V_L packing angle. From the runs of the genetic algorithms, I have identified a set of interface residues (including the CDR residues) which can be used to predict the V_H/V_L packing

angle. Further, important interface residues in the framework regions have been identified which influence the packing angle and should therefore be considered during humanization of antibodies. From the analysis and discussions presented in the above sections, it seems clear that correlations exist between residues in the V_H/V_L interface and packing angle.

The results of this work can be used to model the framework regions of antibodies better by including the correct packing angle between the V_H and V_L domains. This work also has applications in humanization of antibodies. The list of interface residues in Tables 5.6 and 5.7 may be therefore critical in maintaining binding site topography. By modifying non-CDR residues in the human framework and replacing them with their counterparts in the murine antibody, there are better prospects of the humanized version retaining the binding affinity of the murine antibody. Another future application of this work will be to set up a web-interface to predict the packing angle. A sequence may be submitted to a server which would then predict an angle.

However, there are some remaining questions. The fact that the overall scores of the genetic algorithm (and also the best scores) remain the same for most of the run suggests that the GA may be caught in a local minimum despite the use of intelligent selection to sample lots of different combinations of interface positions. Another problem may be that the neural network is unable to learn adequately from the input features presented to it. Such a situation may be addressed by altering the nature of input information representing interface residues to the neural network.

The errors in the prediction of low and high interface angles are quite large even for the best individuals identified after several rounds of the genetic algorithm. In practice however, this is not an uncommon problem in the field of neural networks as the identification of a single highly precise rule that applies to all data is usually very hard. An easier solution is to identify more general ‘rules of thumb’. The procedure for doing this is called *boosting* (Haykin, 1994). In this method, different subsets of data are used to train a learning algorithm and general rules are identified for each subset. At the end of the procedure, all the general rules are combined to yield one concrete rule. There are several implementations of boosting algorithms, the most notable amongst them being *AdaBoost* (Freund and Schapire, 1996a; Freund and Schapire, 1996b).

However, despite the shortcomings, the neural network is able to predict the majority of packing angles successfully. The limitations posed by the network in predicting packing angles which are not adequately represented may be addressed by over-representation of data for the extreme packing angles.

Chapter 6

Conclusions

In this thesis, I developed tools and performed analysis of antibody sequence and structure. First, I described a method to assess the ‘humanness’ of antibodies. Next, I presented a method to number antibody sequences and a modified numbering scheme to accommodate structural insertions and deletions in the framework regions of the antibody variable region. Third, I described an analysis of the antibody packing angle at the interface of the light and heavy chain variable domains and a method to predict this angle.

6.1 Assessing humanness of antibodies

In the work to assess ‘humanness’ of antibodies, I compared mouse and human antibody sequences. Frequency distribution plots of human and mouse pairwise

sequence identities with human sequences reveals significant overlaps as shown in Figures 3.3 and 3.4. Further, Z-scores were calculated and chosen to represent how typically ‘human’ an antibody sequence is. Comparison of the mouse and human Z-score distribution showed that a significant portion of the two plots overlap (Figures 3.5 and 3.6) indicating that many mouse antibodies are more typically human-like than some mouse antibodies. Analysis of the Z-score frequency distribution of human germline genes showed that certain germline genes tend to be used more frequently than certain others (Figures 3.5 and 3.6). As a final step, I analysed the correlation between the Z-scores of therapeutic antibodies and their tendency to be immunogenic. Overall, this examination appeared to suggest no clear correlation between Z-scores and the AAR (anti-antibody response) of therapeutic antibodies. While high humanness scores in humanized antibodies appear to give low AAR, the same trend does not hold for Chimeric antibodies. Analysis of the antibody sequences for prominent T-cell epitopes using SYFPEITHI did not show significant differences between immunogenic and non-immunogenic antibodies, but further work in this area would be useful.

A potential problem with the current method of calculating humanness is that it is based on the Kabat database which may have introduced a bias towards antibodies against specific targets. However, the fact that the frequency distribution plots of pairwise identities between human antibodies roughly resemble a Gaussian distribution and further, that human germline genes tend to have high humanness scores suggests that the bias is not a major issue. As more clinical data becomes available, the idea of correlating humanness scores of therapeutic antibodies and AAR should be revisited. Future work should also extend the analysis to the larger set of sequences available in IMGT and recent work by an undergraduate

student in the lab to analyse humanness of antibodies extracted from the IMGT database indicates that the nature of the graphs are not significantly different.

Part of work from this chapter was published in Abhinandan and Martin (2007).

6.2 Analysis of antibody numbering

From the analysis of antibody variable-region structures, I found that approximately 10% of sequences in the manually annotated Kabat database have errors in the numbering. Given the fact that the publicly available Kabat data have not been updated since July 2000, the availability of reliable numbering is the key reason why people still use these data. The major alternative source of antibody sequence data (IMGT) does not provide numbered sequence files.

I have been able to suggest corrections to the positions of insertions and deletions in the framework region in comparison with the Kabat standard locations that are used in both the Kabat and the Chothia numbering schemes. I have therefore proposed a new numbering scheme (See Table 4.14) that extends the Chothia analysis to correct the positions of indels in the framework regions.

The *AbNum* numbering program has been thoroughly tested and benchmarked and can be used to apply numbering schemes to antibody sequences with a very high level of accuracy. *AbNum* was able to number 99% of sequences and we believe that in all cases, discrepancies from the manual numbering in the Kabat

database resulted from errors in the Kabat database and not in *AbNum*. By simply supplying different data files, Chothia and Kabat numbering schemes can be applied, as can my modified Chothia scheme with structurally correct indels in the framework regions. Thus the program can be used reliably to apply standard numbering schemes to sequences in IMGT thereby enhancing the usefulness of this resource.

Although most errors in the manual Kabat annotations have been corrected, there are still a number of sequences that cannot be numbered by the program *AbNum* (See 4.12). While the ranking of profiles at the start and end of the framework regions improves the performance of the numbering program, a ranking scheme for profile-sets would help improve the coverage of sequences that can be annotated automatically.

An alternative approach, which would be likely to overcome many of the problems encountered in positioning the profiles, would be to score and align the profiles against the sequence using global dynamic programming. This would have zero gap penalties applied when separation between the profiles is within the observed ranges with affine penalties applied outside this range. This approach would ensure that profiles are not positioned out of sequence and would probably simplify the code considerably.

The work has been published in (Abhinandan and Martin, 2008).

6.3 Analysis of packing angle at the V_H/V_L interface

The V_H/V_L packing angle has been defined as the torsion angle at the interface of the light and heavy chain variable region. Analysis of the packing angle has shown that it can vary by up to 30° and approximates to a normal distribution. Neural networks, together with feature selection using genetic algorithms has proved a successful approach to predicting the packing angle. This confirms the hypothesis that the interface residues are important in defining the packing angle. The best neural networks are able to predict the packing angle with an RMSE of 2.4° and a Pearson's correlation coefficient between the predicted and actual interface angle of 0.65. However, there are shortcomings in the prediction of low or high interface angles as the errors in these predictions are quite large despite several cycles of the genetic algorithm. The use of *boosting* may alleviate this problem. In addition, over-representation of data for the extreme packing angles may also help improve the quality of predictions.

During runs of the genetic algorithm, I noticed that the population of genes was becoming increasingly redundant after every generation. In order to address this problem, I developed the method of intelligent selection to maintain diversity. In addition, I used generational replacement wherein an entire parent population of chromosomes is replaced by a population of children. This was done with the intention of increasing the sampling of the interface position space. However, the performance of the genetic algorithm did not improve as significantly as might have been expected. The performance may have been better had elitist

replacement been used where the best gene from every generation of the genetic algorithm is retained (even if it is from the population of parents). It would be interesting to execute large runs of the genetic algorithm with elitist selection and analyse whether this represents a better solution of searching through the interface-position space. However, despite the shortcomings, the neural network is able to predict the majority of packing angles successfully.

In summary, the work in this thesis has developed a new method for analysing humanness of antibodies which has potential applications in selecting and designing antibodies for use *in vivo*. A new method for automatically numbering antibodies has been developed and deficiencies in the Kabat database have been highlighted. Analysis has led to the introduction of a refined chothia numbering scheme. Finally, analysis and prediction of V_H/V_L packing angles has applications in antibody modelling and the feature selection highlights interface residues that may be important in humanization.

Bibliography

- Abhinandan, K. R. and Martin, A. C. R. (2007). Analyzing the “degree of humanness” of antibody sequences. *Journal of Molecular Biology*, **369**, 852–862.
- Abhinandan, K. R. and Martin, A. C. R. (2008). Analysis and improvements to Kabat and structurally correct numbering of antibody variable domains. *Molecular Immunology*, **45**, 3832–3839.
- Adair, J. R., Athwal, D. S. and Emtage, J. S., (1999). Humanised antibodies. US patent 5,859,205.
- Al-Lazikani, B., Lesk, A. M. and Chothia, C. (1997). Standard conformations for the canonical structures of immunoglobulins. *Journal of Molecular Biology*, **273**, 927–948.
- Allcorn, L. C. and Martin, A. C. R. (2002). SACS—self-maintaining database of antibody crystal structure information. *Bioinformatics*, **18**, 175–181.
- Altschul, S. F. and Gish, W. (1996). Local alignment statistics. *Methods Enzymology*, **266**, 460–480.
- Altschul, S. F., Gish, W., Miller, W., Myers, E. W. and Lipman, D. J. (1990). Basic local alignment search tool. *Journal of Molecular Biology*, **215**, 403–410.

- Altschul, S. F., Madden, T. L., Schäffer, A. A., Zhang, J., Zhang, Z., Miller, W. and Lipman, D. J. (1997). Gapped BLAST and PSI-BLAST: a new generation of protein database search programs. *Nucleic Acids Research*, **25**, 3389–3402.
- Axelrod, R. and Dion, D. (1988). The Further Evolution of Cooperation. *Science*, **242**, 1385–1390.
- Axelrod, R., (1984). *The Evolution of Cooperation*. Basic Books.
- Baker, J. (1985). Adaptive Selection Methods for Genetic Algorithms. *Proceedings of the 1st International Conference on Genetic Algorithms*, pages 101–111.
- Bayes, T., (1763). *An Essay Towards Solving a Problem in the Doctrine of Chances*. C. Davis, Printer to the Royal Society of London.
- Berman, H. M., Bhat, T. N., Bourne, P. E., Feng, Z., Gilliland, G., Weissig, H. and Westbrook, J. (2000). The Protein Data Bank and the challenge of structural genomics. *Nature Structural Biology*, **7 Suppl**, 957–959.
- Bhat, T. N., Bentley, G. A., Fischmann, T. O., Boulot, G. and Poljak, R. J. (1990). Small rearrangements in structures of Fv and Fab fragments of antibody D1.3 on antigen binding. *Nature*, **347**, 483–485.
- Boulianne, G. L., Hozumi, N. and Shulman, M. J. (1984). Production of functional chimaeric mouse/human antibody. *Nature*, **312**, 643–646.
- Brüggemann, M., Spicer, C., Buluwela, L., Rosewell, I., Barton, S., Surani, M. A. and Rabbitts, T. H. (1991). Human antibody production in transgenic mice: Expression from 100 kb of the human IgH locus. *European Journal of Immunology*, **21**, 1323–1326.

- Bucher, P., Karplus, K., Moeri, N. and Hofmann, K. (1996). A flexible motif search technique based on generalized profiles. *Computers and Chemistry*, **20**, 3–23.
- Carter, P., Presta, L., Gorman, C. M., Ridgway, J. B., Henner, D., Wong, W. L., Rowland, A. M., Kotts, C., Carver, M. E. and Shepard, H. M. (1992). Humanization of an anti-p185HER2 antibody for human cancer therapy. *Proceedings of the National Academy of Science*, **89**, 4285–4289.
- Chatellier, J., Van Regenmortel, M. H., Vernet, T. and Altschuh, D. (1996). Functional mapping of conserved residues located at the VL and VH domain interface of a Fab. *Journal of Molecular Biology*, **264**, 1–6.
- Chothia, C. and Lesk, A. M. (1987). Canonical structures for the hypervariable regions of immunoglobulins. *Journal of Molecular Biology*, **196**, 901–917.
- Chothia, C., Lesk, A. M., Tramontano, A., Levitt, M., Smith-Gill, S. J., Air, G., Sheriff, S., Padlan, E. A., Davies, D. and Tulip, W. R. (1989). Conformations of immunoglobulin hypervariable regions. *Nature*, **342**, 877–883.
- Chothia, C., Novotný, J., Brucoleri, R. and Karplus, M. (1985). Domain association in immunoglobulin molecules. The packing of variable domains. *Journal of Molecular Biology*, **186**, 651–663.
- Clark, M. (2000). Antibody humanization: a case of the ‘Emperor’s new clothes’? *Immunology Today*, **21**, 397–402.
- Clark, M., Cobo, S., Hale, G. and Waldmann, H. (1983). Advantages of rat monoclonal antibodies. *Immunology Today*, **4**, 100–101.

- Colman, P. M., Laver, W. G., Varghese, J. N., Baker, A. T., Tulloch, P. A., Air, G. M. and Webster, R. G. (1987). Three-dimensional structure of a complex of antibody with influenza virus neuraminidase. *Nature*, **326**, 358–363.
- Couto, J. R., Blank, E. W., Peterson, J. A., Kiwan, R., Padlan, E. A. and Ceriani, R. L., (1994). *Antigen and Antibody Molecular Engineering in Breast Cancer Diagnosis and Treatment*. Plenum Press, New York.
- Dayhoff, M., Schwartz, R. and Orcutt, B. (1978). A model of evolutionary change in proteins. *Atlas of Protein Sequence and Structure*, **5**, 345–352.
- De Jong, K. (1975). An Analysis of the Behavior of a Class of Genetic Adaptive Systems, University of Michigan. *Ann Arbor, MI, Ph. D. thesis*.
- De Jong, K. and Sarma, J. (1993). Generation gaps revisited. *Foundations of Genetic Algorithms*, **2**, 19–28.
- Deret, S., Maissiat, C., Aucouturier, P. and Chomilier, J. (1995). SUBIM: a program for analysing the Kabat database and determining the variability subgroup of a new immunoglobulin sequence. *Computer Applications in the Biosciences*, **11**, 435–439.
- Dundas, J., Binkowski, T. A., DasGupta, B. and Liang, J. (2007). Topology independent protein structural alignment. *BMC Bioinformatics*, **8**, 388–388.
- Durbin, R., (1998). *Biological Sequence Analysis: Probabilistic Models of Proteins and Nucleic Acids*. Cambridge University Press.
- Dyer, M. J., Hale, G., Hayhoe, F. G. and Waldmann, H. (1989). Effects of CAMPATH-1 antibodies in vivo in patients with lymphoid malignancies: Influence of antibody isotype. *Blood*, **73**, 1431–1439.

- Edgar, R. C. (2004). MUSCLE: multiple sequence alignment with high accuracy and high throughput. *Nucleic Acids Research*, **32**, 1792–1797.
- Eisenberg, D., Weiss, R., Terwilliger, T. and Wilcox, W. (1982). Hydrophobic moments and protein structure. *Faraday Symposia of the Chemical Society*, **17**, 109–120.
- Fleury, D., Wharton, S. A., Skehel, J. J., Knossow, M. and Bizebard, T. (1998). Antigen distortion allows influenza virus to escape neutralization. *Nature Structural Biology*, **5**, 119–123.
- Fogel, L., Owens, A., Walsh, M. et al., (1966). *Artificial Intelligence Through Simulated Evolution*. Wiley New York.
- Forrest, S., (1985). *Artificial Intelligence Through Simulated Evolution*. Unpublished manuscript.
- Freund, Y. and Schapire, R. (1996a). Experiments with a new boosting algorithm. *Machine Learning: Proceedings of the Thirteenth International Conference*, **148**, 156.
- Freund, Y. and Schapire, R. (1996b). Game theory, on-line prediction and boosting. *Proceedings of the ninth annual conference on Computational learning theory*, pages 325–332.
- Gergely, J. (1967). Structural studies of igs. *Immunochemistry*, **4**, 101–107.
- Glennie, M. J. and Johnson, P. W. (2000). Clinical trials of antibody therapy. *Immunology Today*, **21**, 403–410.

GREY, H. M. and KUNKEL, H. G. (1964). H CHAIN SUBGROUPS OF MYELOMA PROTEINS AND NORMAL 7S GAMMA-GLOBULIN. *J Exp Med*, **120**, 253–266.

Gribskov, M., McLachlan, A. and Eisenberg, D. (1987). Profile analysis: detection of distantly related proteins. *Proceedings of the National Academy of Sciences*, **84**, 4355.

Haykin, S., (1994). *Neural Networks: A Comprehensive Foundation*. Prentice Hall PTR Upper Saddle River, NJ, USA.

Henikoff, S. and Henikoff, J. G. (1992). Amino acid substitution matrices from protein blocks. *Proceedings of the National Academy of Science*, **89**, 10915–10919.

Herron, J. N., He, X. M., Ballard, D. W., Blier, P. R., Pace, P. E., Bothwell, A. L., Voss, E. W. and Edmundson, A. B. (1991). An autoantibody to single-stranded DNA: comparison of the three-dimensional structures of the unliganded Fab and a deoxynucleotide-Fab complex. *Proteins*, **11**, 159–175.

Hobohm, U. and Sander, C. (1994). Enlarged representative set of protein structures. *Protein Science*, **3**, 522–524.

Hohman, V. S., Schluter, S. F. and Marchalonis, J. J. (1992). Complete sequence of a cDNA clone specifying sandbar shark immunoglobulin light chain: gene organization and implications for the evolution of light chains. *Proceedings of the National Academy of Science*, **89**, 276–280.

Holland, J., (1975). *Adaptation in natural and artificial systems*. University of Michigan press.

- Honegger, A. and Plückthun, A. (2001). Yet another numbering scheme for immunoglobulin variable domains: an automatic modeling and analysis tool. *Journal of Molecular Biology*, **309**, 657–670.
- Hopkin, M. (2006). Can super-antibody drugs be tamed? *Nature*, **440**, 855–856.
- Hulo, N., Bairoch, A., Bulliard, V., Cerutti, L., Cuče, B. A., de Castro, E., Lachaize, C., Langendijk-Genevaux, P. S. and Sigrist, C. J. A. (2008). The 20 years of PROSITE. *Nucleic Acids Research*, **36**, D245–D249.
- Hwang, W. Y. K., Almagro, J. C., Buss, T. N., Tan, P. and Foote, J. (2005). Use of human germline genes in a CDR homology-based approach to antibody humanization. *Methods*, **36**, 35–42.
- Hwang, W. Y. K. and Foote, J. (2005). Immunogenicity of engineered antibodies. *Methods*, **36**, 3–10.
- Ignatovich, O., Tomlinson, I. M., Jones, P. T. and Winter, G. (1997). The creation of diversity in the human immunoglobulin V(λ) repertoire. *Journal of Molecular Biology*, **268**, 69–77.
- Ivanovski, M., Silvestri, F., Pozzato, G., Anand, S., Mazzaro, C., Burrone, O. R. and Efremov, D. G. (1998). Somatic hypermutation, clonal diversity, and preferential expression of the VH 51p1/VL kv325 immunoglobulin gene combination in hepatitis C virus-associated immunocytomas. *Blood*, **91**, 2433–2442.
- James, L., Hale, G., Waldman, H. and Bloomer, A. (1999). 1.9 A Structure of the Therapeutic Antibody CAMPATH-1H Fab in Complex with a Synthetic Peptide Antigen. *Journal of Molecular Biology*, **289**, 293–301.

- Jerne, N. K. (1974). Towards a network theory of the immune system. *Ann Immunol (Paris)*, **125C**, 373–389.
- Johnson, G. and Wu, T. T. (2001). Kabat Database and its applications: Future directions. *Nucleic Acids Research*, **29**, 205–206.
- Johnson, S., Oliver, C., Prince, G. A., Hemming, V. G., Pfarr, D. S., Wang, S. C., Dormitzer, M., O’Grady, J., Koenig, S., Tamura, J. K., Woods, R., Bansal, G., Couchenour, D., Tsao, E., Hall, W. C. and Young, J. F. (1997). Development of a humanized monoclonal antibody (MEDI-493) with potent in vitro and in vivo activity against respiratory syncytial virus. *The Journal of Infectious Diseases*, **176**, 1215–1224.
- Jones, P. T., Dear, P. H., Foote, J., Neuberger, M. S. and Winter, G. (1986). Replacing the complementarity-determining regions in a human antibody with those from a mouse. *Nature*, **321**, 522–525.
- Junqueira, L. and Carneiro, J., (2005). *Basic histology: text & atlas*. McGraw-Hill.
- Kabat, E. A., Wu, T. T., Bilofsky, H., Reid-Miller, M. and Perry, H., (1983). *Sequences of Proteins of Immunological Interest*. National Institutes of Health, Bethesda.
- Kalsi, J. K., Martin, A. C., Hirabayashi, Y., Ehrenstein, M., Longhurst, C. M., Ravirajan, C., Zvelebil, M., Stollar, B. D., Thornton, J. M. and Isenberg, D. A. (1996). Functional and modelling studies of the binding of human monoclonal anti-DNA antibodies to DNA. *Molecular Immunology*, **33**, 471–483.

- Kolbinger, F., Saldanha, J., Hardman, N. and Bendig, M. M. (1993). Humanization of a mouse anti-human IgE antibody: a potential therapeutic for IgE-mediated allergies. *Protein Engineering*, **6**, 971–980.
- Lee, B. and Richards, F. M. (1971). The interpretation of protein structures: Estimation of static accessibility. *Journal of Molecular Biology*, **55**, 379–400.
- Lefranc, M.-P., Pommié, C., Ruiz, M., Giudicelli, V., Foulquier, E., Truong, L., Thouvenin-Contet, V. and Lefranc, G. (2003). IMGT unique numbering for immunoglobulin and T cell receptor variable domains and Ig superfamily V-like domains. *Developmental and Comparative Immunology*, **27**, 55–77.
- Low, N. M., Holliger, P. H. and Winter, G. (1996). Mimicking somatic hypermutation: Affinity maturation of antibodies displayed on bacteriophage using a bacterial mutator strain. *Journal of Molecular Biology*, **260**, 359–368.
- Macias, A., Arce, S., Leon, J., Mustelier, G., Bombino, G., Domarco, A., Perez, R. and Lage, A. (1999). Novel cross-reactive anti-idiotypic antibodies with properties close to the human intravenous immunoglobulin (IVIg). *Hybridoma*, **18**, 263–272.
- Mantovani, L., Wilder, R. L. and Casali, P. (1993). Human rheumatoid B-1a (CD5+ B) cells make somatically hypermutated high affinity IgM rheumatoid factors. *Journal of Immunology*, **151**, 473–488.
- Martin, A. C. (1996). Accessing the Kabat antibody sequence database by computer. *Proteins*, **25**, 130–133.
- Martin, A. C., Cheetham, J. C. and Rees, A. R. (1989). Modeling antibody hypervariable loops: a combined algorithm. *Proceedings of the National Academy of Science*, **86**, 9268–9272.

- Martin, A. C., Cheetham, J. C. and Rees, A. R. (1991). Molecular modeling of antibody combining sites. *Methods Enzymology*, **203**, 121–153.
- Masters, T., (1993). *Practical Neural Network Recipes in C++*. Morgan Kaufmann.
- McLachlan, A. (1982). Rapid comparison of protein structures. *Crystal Physics, Diffraction, Theoretical and General Crystallography*, **38**, 871–873.
- Mendez, M. J., Green, L. L., Corvalan, J. R., Jia, X. C., Maynard-Currie, C. E., Yang, X. D., Gallo, M. L., Louie, D. M., Lee, D. V., Erickson, K. L., Luna, J., Roy, C. M., Abderrahim, H., Kirschenbaum, F., Noguchi, M., Smith, D. H., Fukushima, A., Hales, J. F., Klapholz, S., Finer, M. H., Davis, C. G., Zsebo, K. M. and Jakobovits, A. (1997). Functional transplant of megabase human immunoglobulin loci recapitulates human antibody response in mice. *Nature Genetics*, **15**, 146–156.
- Mitchell, M., (1996). *An Introduction to Genetic Algorithms*. MIT Press.
- Mott, R. (1992). Maximum-likelihood estimation of the statistical distribution of Smith-Waterman local sequence similarity scores. *Bulletin of Mathematical Biology*, **54**, 59–75.
- Murali, R., Sharkey, D. J., Daiss, J. L. and Murthy, H. M. (1998). Crystal structure of Taq DNA polymerase in complex with an inhibitory Fab: the Fab is directed against an intermediate in the helix-coil dynamics of the enzyme. *Proceedings of the National Academy of Science*, **95**, 12562–12567.
- Mylvaganam, S. E., Paterson, Y. and Getzoff, E. D. (1998). Structural basis for the binding of an anti-cytochrome c antibody to its antigen: Crystal structures of

- FabE8-cytochrome c complex to 1.8 Å resolution and FabE8 to 2.26 Å resolution. *Journal of Molecular Biology*, **281**, 301–322.
- Navarro, P., Barbis, D. P., Antczak, D. and Butler, J. E. (1995). The complete cDNA and deduced amino acid sequence of equine IgE. *Molecular Immunology*, **32**, 1–8.
- Needleman, S. B. and Wunsch, C. D. (1970). A general method applicable to the search for similarities in the amino acid sequence of two proteins. *Journal of Molecular Biology*, **48**, 443–453.
- Neuberger, M. S., Williams, G. T. and Fox, R. O. (1984). Recombinant antibodies possessing novel effector functions. *Nature*, **312**, 604–608.
- Novotný, J. and Haber, E. (1985). Structural invariants of antigen binding: Comparison of immunoglobulin VL-VH and VL-VL domain dimers. *Proceedings of the National Academy of Science*, **82**, 4592–4596.
- O’Reilly, U. and Oppacher, F. (1995). The troubling aspects of a building block hypothesis for genetic programming. *Foundations of Genetic Algorithms*, **3**, 73–88.
- O’Connor, S. J., Meng, Y. G., Rezaie, A. R. and Presta, L. G. (1998). Humanization of an antibody against human protein C and calcium-dependence involving framework residues. *Protein Engineering*, **11**, 321–328.
- Orengo, C., Jones, D. and Thornton, J., (2003). *Bioinformatics: genes, proteins and computers*. BIOS Scientific; Distributed in the US by Springer-Verlag.
- Parker, D. (1987). Optimal Algorithms for Adaptive Networks: Second Order Back Propagation, Second Order Direct Propagation, and Second Order Hebbian

Learning. *Proceedings of the IEEE International Conference on Neural Networks*, **2**, 593–600.

Patel, H. M. and Hsu, E. (1997). Abbreviated junctional sequences impoverish antibody diversity in urodele amphibians. *Journal of Immunology*, **159**, 3391–3399.

Pearson, W. R. (1998). Empirical statistical estimates for sequence similarity searches. *Journal of Molecular Biology*, **276**, 71–84.

Pearson, W. R. and Lipman, D. J. (1988). Improved tools for biological sequence comparison. *Proceedings of the National Academy of Science*, **85**, 2444–2448.

Poljak, R. J., Amzel, L. M., Avey, H. P., Chen, B. L., Phizackerley, R. P. and Saul, F. (1973). Three-dimensional structure of the Fab' fragment of a human immunoglobulin at 2,8-Å resolution. *Proceedings of the National Academy of Science*, **70**, 3305–3310.

Porter, R. R. (1959). The hydrolysis of rabbit γ -globulin and antibodies with crystalline papain. *Biochemistry Journal*, **73**, 119–127.

Queen, C., Schneider, W. P., Seltick, H. E., Payne, P. W., Landolfi, N. F., Duncan, J. F., Avdalovic, N. M., Levitt, M., Junghans, R. P. and Waldmann, T. A. (1989). A humanized antibody that binds to the interleukin 2 receptor. *Proceedings of the National Academy of Science*, **86**, 10029–10033.

Rammensee, H., Bachmann, J., Emmerich, N. P., Bachor, O. A. and Stevanović, S. (1999). SYFPEITHI: database for MHC ligands and peptide motifs. *Immunogenetics*, **50**, 213–219.

- Rast, J. P., Anderson, M. K., Ota, T., Litman, R. T., Margittai, M., Shamblott, M. J. and Litman, G. W. (1994). Immunoglobulin light chain class multiplicity and alternative organizational forms in early vertebrate phylogeny. *Immunogenetics*, **40**, 83–99.
- Rechenberg, I., (1965). *Cybernetic Solution Path of an Experimental Problem (Royal Aircraft Establishment Translation No. 1122, BF Toms, Trans)*.
- Rechenberg, I., (1973). *Evolutionsstrategie: Optimierung technischer Systeme nach Prinzipien der biologischen Evolution*. Frommann-Holzboog Stuttgart.
- Reichert, J. M. (2001). Monoclonal antibodies in the clinic. *Nature: Biotechnology*, **19**, 819–822.
- Riechmann, L., Clark, M., Waldmann, H. and Winter, G. (1988). Reshaping human antibodies for therapy. *Nature*, **332**, 323–327.
- Riedmiller, M. and Braun, H. (1993). A direct adaptive method for faster back-propagation learning: theRPROP algorithm. *Neural Networks, 1993., IEEE International Conference on*, pages 586–591.
- Rini, J. M., Schulze-Gahmen, U. and Wilson, I. A. (1992). Structural evidence for induced fit as a mechanism for antibody-antigen recognition. *Science*, **255**, 959–965.
- Roguska, M. A., Pedersen, J. T., Henry, A. H., Searle, S. M., Roja, C. M., Avery, B., Hoffee, M., Cook, S., Lambert, J. M., Blättler, W. A., Rees, A. R. and Guild, B. C. (1996). A comparison of two murine monoclonal antibodies humanized by CDR-grafting and variable domain resurfacing. *Protein Engineering*, **9**, 895–904.

Roguska, M. A., Pedersen, J. T., Keddy, C. A., Henry, A. H., Searle, S. J., Lambert, J. M., Goldmacher, V. S., Blättler, W. A., Rees, A. R. and Guild, B. C. (1994). Humanization of murine monoclonal antibodies through variable domain resurfacing. *Proceedings of the National Academy of Science*, **91**, 969–973.

Rumelhart, D., Hinton, G. and Williams, R., (1986). *Learning internal representations by error propagation*. MIT Press Cambridge, MA, USA.

Russell, S. and Norvig, P., (1995). *Artificial intelligence: a modern approach*. Prentice-Hall, Inc. Upper Saddle River, NJ, USA.

Sato, K., Tsuchiya, M., Saldanha, J., Koishihara, Y., Ohsugi, Y., Kishimoto, T. and Bendig, M. M. (1994). Humanization of a mouse anti-human interleukin-6 receptor antibody comparing two methods for selecting human framework regions. *Molecular Immunology*, **31**, 371–381.

Schiffmann, W., Joost, M. and Werner, R. (1993). Comparison of optimized back-propagation algorithms. *Proceedings of the European Symposium on Artificial Neural Networks, ESANN*, **93**, 97–104.

Schneider, T., Stormo, G., Gold, L. and Ehrenfeucht, A. (1986). Information content of binding sites on nucleotide sequences. *Journal of Molecular Biology*, **188**, 415–431.

Schroff, R. W., Foon, K. A., Beatty, S. M., Oldham, R. K. and Morgan, A. C. (1985). Human anti-murine immunoglobulin responses in patients receiving monoclonal antibody therapy. *Cancer Research*, **45**, 879–885.

- Shawler, D. L., Bartholomew, R. M., Smith, L. M. and Dillman, R. O. (1985). Human immune response to multiple injections of murine monoclonal IgG. *The Journal of Immunology*, **135**, 1530–1535.
- Simeonov, A., Matsushita, M., Juban, E. A., Thompson, E. H., Hoffman, T. Z., Beuscher, A. E., Taylor, M. J., Wirsching, P., Rettig, W., McCusker, J. K., Stevens, R. C., Millar, D. P., Schultz, P. G., Lerner, R. A. and Janda, K. D. (2000). Blue-fluorescent antibodies. *Science*, **290**, 307–313.
- Smith, T. F. and Waterman, M. S. (1981). Identification of common molecular subsequences. *Journal of Molecular Biology*, **147**, 195–197.
- Staden, R. (1988). Methods to define and locate patterns of motifs in sequences. *Bioinformatics*, **4**, 53–60.
- Sywerda, G. (1989). Uniform crossover in genetic algorithms. *Proceedings of the third international conference on Genetic algorithms table of contents*, pages 2–9.
- Sywerda, G. (1991). A Study of Reproduction in Generational and Steady-State Genetic Algorithms. *Foundations of Genetic Algorithms*.
- Tackett, W., (1994). *Recombination, Selection, and the Genetic construction of computer programs*. PhD thesis, University of Southern California.
- Tatusov, R., Altschul, S. and Koonin, E. (1994). Detection of conserved segments in proteins: iterative scanning of sequence databases with alignment blocks. *Proceedings of the National Academy of Sciences*, **91**, 12091–12095.
- Team, G. D., (2006). *Geographic Resources Analysis Support System (GRASS) Software*. ITC-irst, Trento, Italy. <http://grass.itc.it>.

- Trakhanov, S., Parkin, S., Raffai, R., Milne, R., Newhouse, Y. M., Weisgraber, K. H. and Rupp, B. (1999). Structure of a monoclonal 2E8 Fab antibody fragment specific for the low-density lipoprotein-receptor binding region of apolipoprotein E refined at 1.9 Å. *Acta Crystallographica Section D*, **55**, 122–128.
- Valentine, R. C. and Green, N. M. (1967). Electron microscopy of an antibody-hapten complex. *Journal of Molecular Biology*, **27**, 615–617.
- Vapnik, V., (2000). *The Nature of Statistical Learning Theory*. Springer publications.
- Vaughan, T. J., Osbourn, J. K. and Tempest, P. R. (1998). Human antibodies by design. *Nature: Biotechnology*, **16**, 535–539.
- Wagener, C., Clark, B. R., Rickard, K. J. and Shively, J. E. (1983). Monoclonal antibodies for carcinoembryonic antigen and related antigens as a model system: Determination of affinities and specificities of monoclonal antibodies by using biotin-labeled antibodies and avidin as precipitating agent in a solution phase immunoassay. *Journal of Immunology*, **130**, 2302–2307.
- Whitelegg, N. and Rees, A. (2000). WAM: an improved algorithm for modelling antibodies on the WEB. *Protein Engineering Design and Selection*, **13**, 819–824.
- Whitley, D. et al. (1989). The GENITOR algorithm and selection pressure: Why rank-based allocation of reproductive trials is best. *Proceedings of the Third International Conference on Genetic Algorithms*, **1**, 116–121.
- Wilson, I. A. and Stanfield, R. L. (1994). Antibody-antigen interactions: new structures and new conformational changes. *Current Opinion in Structural Biology*, **4**, 857–867.

Winter, G., Griffiths, A. D., Hawkins, R. E. and Hoogenboom, H. R. (1994). Making antibodies by phage display technology. *Annual Review of Immunology*, **12**, 433–455.

Wu, T. T. and Kabat, E. A. (1970). An analysis of the sequences of the variable regions of Bence Jones proteins and myeloma light chains and their implications for antibody complementarity. *Journal of Experimental Medicine*, **132**, 211–250.

Yazaki, P. J., Sherman, M. A., Shively, J. E., Ikle, D., Williams, L. E., Wong, J. Y. C., Colcher, D., Wu, A. M. and Raubitschek, A. A. (2004). Humanization of the anti-CEA T84.66 antibody based on crystal structure data. *Protein Engineering Design and Selection*, **17**, 481–489.

Yi, T. and Lander, E. (1994). Recognition of related proteins by iterative template refinement (ITR). *Protein Science*, **3**, 1315.